Chapter 6

Radiometer Systems

Radiometers are highly sensitive receivers designed to measure thermal electromagnetic emission by material media. In Chapter 4, the theory of radiative transfer was used to relate the electromagnetic properties of the scene observed by an antenna to the power delivered by the antenna to the receiver, $P_A' = kT_A' B$. The antenna temperature T_A' incorporates the intensity of radiation incident upon the antenna (weighted by the antenna directional pattern) as well as self-emission by the antenna structure itself. The function of a radiometer is to measure T_A'. However, T_A' represents the average value of a fluctuating noiselike signal. Hence, strictly speaking, a radiometer provides an *estimate* of T_A'; therefore, not only is the radiometer transfer function (relating T_A' to the output voltage V_{out}) of interest, but so is the precision with which T_A' can be estimated. The latter, often referred to as the radiometer sensitivity or radiometric resolution ΔT, is the key quantity characterizing the performance of a microwave radiometer.

This chapter covers four major topics. The first topic, which is a brief treatment of the methodology used to characterize the noise properties of individual devices and multidevice receiver systems, provides the background for discussing the operation and performance characteristics of the several different types of radiometers considered in Sections 6-7 to 6-14. Receiver noise characterization also is relevant to the detection of radar signals (Chapter 8). The third and fourth topics are radiometer calibration techniques and imaging considerations.

6-1 EQUIVALENT NOISE TEMPERATURE

According to thermodynamics, electrons in a conductor are always in a state of random motion and the kinetic energy of an electron is proportional to T, the temperature of the conductor. These random motions of the electrons produce fluctuations in electric charge, which in turn produce voltage fluctuations. If we were to measure the voltage V_n across a conductor of resistance R through an ideal rectangular filter of bandwidth B, we would observe an output similar

Fawwaz T. Ulaby, Richard K. Moore, and Adrian K. Fung,
Microwave Remote Sensing: Active and Passive,
Vol. I: Microwave Remote Sensing Fundamentals and Radiometry ISBN 0-201-10759-7

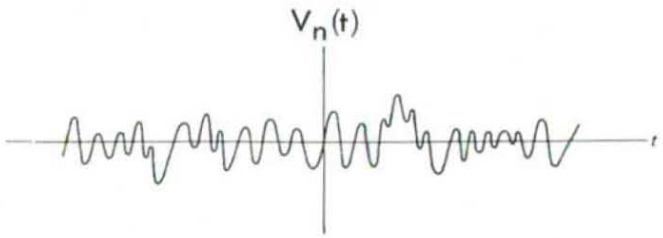

Fig. 6.1 Random variation of noise voltage across a resistor.

to that shown in Fig. 6.1. Sources that emit incoherent energy usually are referred to as noise sources. Hence, the voltage V_n usually is called the noise voltage generated by the resistor. Moreover, since V_n is related to the temperature of the conductor, the noise thus generated is called *thermal* noise. As one might expect, the average, or mean, value of V_n is zero. Its rms value, however, is not zero. Nyquist (1928) showed that

$$V_{rms}^2 = \langle V_n^2(t) \rangle = 4R\mathrm{k}TB, \tag{6.1}$$

where k is Boltzmann's constant and B, often called the *noise bandwidth*, is the bandwidth of the rectangular filter.

The thermal noise power delivered by a *noisy* resistor at a temperature T usually is determined by replacing the noisy resistor with an equivalent circuit consisting of a voltage generator V_{rms} in series with a noise-free resistance R and a reactance X as shown in Fig. 6.2. The reactance X accounts for the self-inductance of the resistor and the capacitance between its ends. The power transferred from the equivalent voltage generator to a load Z_L is maximum when Z_L is matched to the generator impedance $Z = R + jX$—that is, when $Z_L = Z^* = R - jX$. Under this condition, the average noise power dissipated in R_L is

$$P_n = \frac{V_{rms}^2}{4R} = \mathrm{k}TB. \tag{6.2}$$

We recognize the above result as being identical to the power delivered by a lossless antenna placed inside a chamber of constant temperature T. We may extend the similarity further by stating that the average power delivered by any antenna, lossless or not, to a matched load (Fig. 6.3) is equal to the average power delivered by a resistor to a matched load if the temperature of the resistor is identical to the antenna radiometric temperature T_A'. This equivalence between the antenna and the resistance provides a convenient tool for calibrating microwave receivers, as will be discussed later in Section 6-16.1.

Thermal-noise generation is a universal characteristic of matter at temperatures above absolute zero, but it is not the only source of random-noise generation. Other types of noise include quantum noise, shot noise, and flicker noise. Quantum noise, which arises from the discrete nature of electron energy,

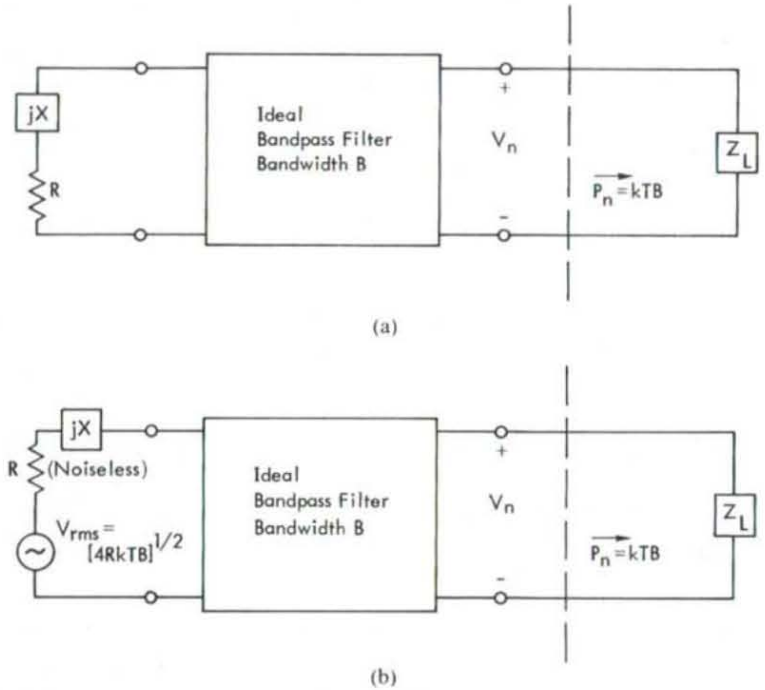

Fig. 6.2 (a) Noisy resistor connected to a matched load, and (b) its equivalent circuit.

is insignificant in comparison with thermal noise unless the frequency is very high or the temperature is very low; that is, quantum noise may be neglected as long as the Rayleigh-Jeans approximation holds (Section 4-3.3). Shot noise arises from the discrete nature of current flow in electronic devices such as diodes and transistors, and flicker noise arises from surface irregularities in cathodes and semiconductors.

According to (6.2), the thermal noise power per unit bandwidth is dependent only on the physical temperature of the resistor and is independent of the operating frequency and of the resistance R. This property of thermal-noise

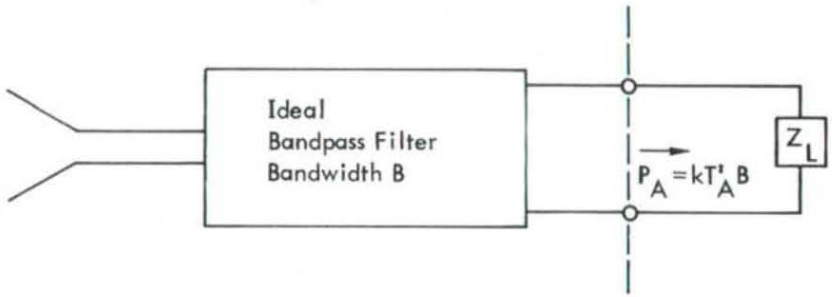

Fig. 6.3 Power delivered to a matched load by an antenna with radiometric antenna temperature T'_A is $P'_A = kT'_A B$.

sources has been extended to define an *equivalent output noise temperature** T_{Eo} for any noise source, regardless of the mechanism responsible for the generated noise. If $P_{no}(f)$ is the output noise power of a nonthermal noise source over a narrow bandwidth Δf centered at f, its equivalent output noise temperature is defined as

$$T_{Eo}(f) = \lim_{\Delta f \to 0} \frac{P_{no}(f)}{k\,\Delta f}. \tag{6.3}$$

In practice, however, most systems and devices are configured so that $P_{no}(f)$ is approximately constant over the operating frequency range (of bandwidth B) so that the output noise may be defined as

$$P_{no} = kT_{Eo}B, \tag{6.4}$$

where T_{Eo} represents an effective value of $T_{Eo}(f)$ over the bandwidth B. The above concept of equivalent noise temperature also has been used to define an *equivalent input noise temperature* T_{Ei} for two-terminal devices, which facilitates the quantification of the overall noise performance of a system consisting of several devices in terms of the T_{Ei}'s of the individual devices, as will be shown in the next section. Note that (6.4) applies *only* for a matched load.

6-2 CHARACTERIZATION OF NOISE

6-2.1 Noise Figure

The *noise figure* F of a linear two-port device (or system) is a measure of the degradation in signal-to-noise ratio between the input and output ports of the device, due to noise addition by the device. For the device shown in Fig. 6.4(a),

$$F = \frac{P_{si}/P_{ni}}{P_{so}/P_{no}}, \tag{6.5}$$

where P_{si} = available input signal power, W,
P_{ni} = available input noise power = kT_0B, W,
P_{so} = available output signal power, W,
P_{no} = available output noise power, W.

F is defined for a specific input noise power, namely that power which would be provided by a resistor matched to the input port of the device and whose temperature is $T_0 = 290$ K. If, over the bandwidth B, the average power gain of

*Conforming to the notation adopted in previous chapters, if the first subscript of T is lowercase, then T is a physical (thermometric) temperature, and if it is uppercase, then T is equivalent radiometric or noise temperature.

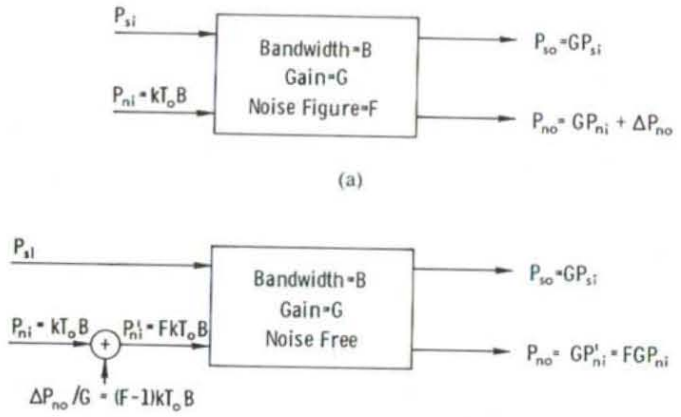

Fig. 6.4 A noisy device can be replaced by a noise-free device if the input noise is increased by the noise figure of the device: (a) noisy device; (b) equivalent representation of (a) in terms of a noise-free device.

the device is G, then

$$P_{so} = GP_{si} \tag{6.6}$$

and

$$P_{no} = GP_{ni} + \Delta P_{no}, \tag{6.7}$$

where ΔP_{no} is the noise power generated by the device. Hence,

$$F = \frac{P_{si}}{P_{so}} \cdot \frac{P_{no}}{P_{ni}} = \frac{1}{G} \cdot \frac{GkT_0B + \Delta P_{no}}{kT_0B}$$
$$= 1 + \frac{\Delta P_{no}}{GkT_0B}. \tag{6.8}$$

The noise figure F is always larger than or equal to 1; for an ideal noise-free device ($\Delta P_{no} = 0$), $F = 1$. Occasionally, F is expressed in decibels:

$$F(\text{dB}) = 10 \log F. \tag{6.9}$$

From (6.8), ΔP_{no} is given by

$$\Delta P_{no} = (F-1)GkT_0B, \tag{6.10}$$

and therefore the output noise power is, from (6.7), given by

$$P_{no} = GkT_0B + (F-1)GkT_0B$$
$$= FGkT_0B. \tag{6.11}$$

Thus, the noise performance of the device shown in Fig. 6.4(a) is equivalent to that of an ideal noise-free device with input noise temperature equal to $T_0 + (F-1)T_0 = FT_0$ (Fig. 6.4(b)).

6-2.2 Effective Noise Temperature

For a linear two-port device, the internally generated noise power ΔP_{no} should be independent of both the signal and the noise at the device input. But according to (6.10), ΔP_{no} is a function of T_0, the input noise temperature. This "apparent" dependence on T_0 follows from the form of the definition of the noise figure F. A closer look would show that for a given device, $(F-1)\,T_0$ is a constant. That is, when the noise figure is used to describe the noise performance of a device (or network) it is necessary to specify the value of T_0 at which F is measured. To avoid confusion, the definition of noise figure has been standardized by choosing $T_0 = 290$ K (room temperature).

The *equivalent input noise temperature* T_{Ei} is an alternative concept for describing the noise performance of a device. Its attractive feature is that it depends only upon the parameters of the device. T_{Ei} is defined on the basis of the equivalence of the two networks shown in Fig. 6.5. If ΔP_{no} is the noise generated by the device with its input connected to a noise-free termination (fictitious resistor at absolute zero temperature), T_{Ei} is defined as the temperature of a thermal resistor that, if placed at the input of an equivalent noise-free device, would produce the same noise power ΔP_{no} at the output terminals of the device. Thus,

$$\Delta P_{no} = GkT_{Ei}B, \tag{6.12}$$

where G is the power gain of the device. *It is important to remember that** $T_{Ei} \triangleq T_E$ *is referred to the input terminals of the device.* The corresponding equivalent (or effective) input noise power, denoted P_E, is $P_E = kT_EB$.

If the actual noise power available at the input to the device, P_{ni}, is characterized by a noise temperature $T_I (= P_{ni}/kB)$, then the total input noise temperature of the equivalent noise-free device is $T_I + T_E$, and the noise power available at the output (Figure 6.5(c)) is

$$P_{no} = G(P_{ni} + P_E) = Gk(T_I + T_E)B. \tag{6.13}$$

The effective input noise temperature T_E can be related to the noise figure F by equating (6.10) to (6.12). The result is

$$T_E = (F-1)T_0. \tag{6.14}$$

Although both quantities, F and T_E, describe the same property of a device or

*Most of the material that follows in this chapter is discussed in terms of the equivalent input noise temperature of devices. Hence, for brevity, the second subscript (i for input) will be dropped, but the subscript o will be retained when referring to output noise temperature.

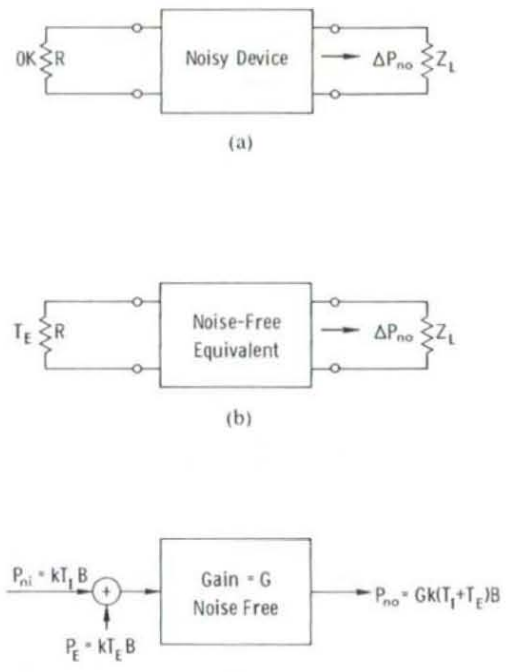

Fig. 6.5 Definition and representation of equivalent input noise temperature T_E: (a) noisy device with input connected to a fictitious resistor at 0-K temperature; (b) equivalent noise-free device with input connected to a fictitious resistor at temperature T_E; (c) device-generated noise referred to its input terminals.

network, F has been used more commonly for describing the noise performance of conventional receivers, whereas T_E has been preferred for low-noise devices and systems.

6-3 NOISE OF A CASCADED SYSTEM

The concepts used to characterize the noise performance of an individual device or system now will be extended to relate the noise behavior of a system consisting of N subsystems to the noisiness of the individual subsystems (or stages). We shall consider first two subsystems in cascade, each with the same noise bandwidth B, but with different equivalent input noise temperatures and available gain (Fig. 6.6). G_1 and T_{E1} are the available gain and equivalent input noise temperature of the first subsystem, and G_2 and T_{E2} are similar quantities for the second subsystem. From the definition of equivalent input noise temperature, each noisy subsystem can be replaced by a noise-free subsystem with an input noise source whose available power is $P_{E1} = kT_{E1}B$ for subsystem 1 and $P_{E2} = kT_{E2}B$ for subsystem 2, as shown in Fig. 6.6(b). The total available

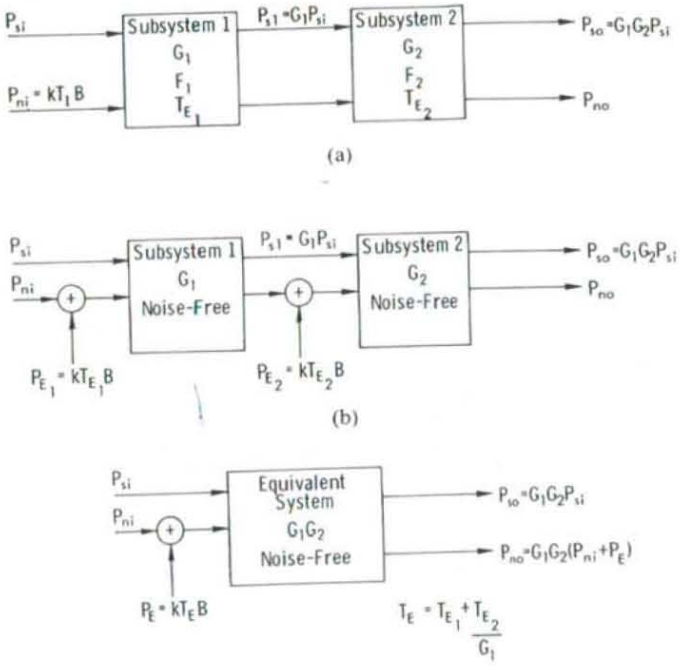

Fig. 6.6 Effective input noise temperature of two systems in cascade: (a) two noisy subsystems in cascade; (b) equivalent representation of (a) in terms of noise-free subsystems; (c) equivalent single-system representation of (b).

noise power at the output of the cascade is

$$P_{no} = G_1G_2P_{ni} + G_1G_2P_{E1} + G_2P_{E2}$$
$$= G_1G_2k\left(T_I + T_{E1} + \frac{T_{E2}}{G_1}\right)B, \tag{6.1}$$

where T_I is the input noise temperature. For the equivalent system shown Fig. 6.6(c),

$$P_{no} = G_1G_2(P_{ni} + P_E)$$
$$= G_1G_2k(T_I + T_E)B, \tag{6.1}$$

where T_E is the equivalent input temperature of the overall system. Compari (6.15) with (6.16), we see that the equivalent input noise temperature T_E of t cascade is given by

$$T_E = T_{E1} + \frac{T_{E2}}{G_1}. \tag{6.}$$

From (6.14), the overall noise figure of the cascade is

$$\begin{aligned} F &= 1+\frac{T_E}{T_0} \\ &= 1+\frac{T_{E1}}{T_0}+\frac{T_{E2}}{G_1T_0} \\ &= 1+(F_1-1)+\frac{F_2-1}{G_1} \\ &= F_1+\frac{F_2-1}{G_1}, \end{aligned} \tag{6.18}$$

where F_1 and F_2 are the noise figures of subsystems 1 and 2, respectively.

The above results may be generalized into a system consisting of N subsystems,

$$T_E = T_{E1}+\frac{T_{E2}}{G_1}+\frac{T_{E3}}{G_1G_2}+\cdots+\frac{T_{EN}}{G_1G_2\cdots G_{N-1}} \tag{6.19a}$$

and

$$F = F_1+\frac{F_2-1}{G_1}+\frac{F_3-1}{G_1G_2}+\cdots+\frac{F_N-1}{G_1G_2\cdots G_{N-1}}. \tag{6.19b}$$

6-4 NOISE CHARACTERIZATION OF AN ATTENUATOR

Consider an attenuator of physical (ambient) temperature T_p and loss factor L. The attenuator is shown in Fig. 6.7 with matched impedances (maintained at the same temperature T_p) on both sides. The loss factor L is the inverse of power gain G,

$$L = \frac{1}{G} = \frac{P_i}{P_o}, \tag{6.20}$$

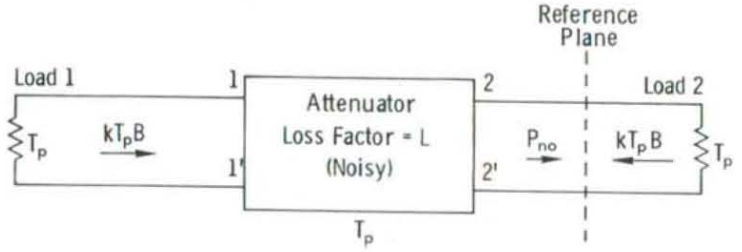

Fig. 6.7 Noise generated in an attenuator of loss L and physical temperature T_p.

where P_i and P_o are, respectively, the attenuator input and output power. Since the network is in thermodynamic equilibrium, the flow of power into load 2 (crossing the reference plane from the left) should be equal to the flow of power from load 2 (crossing the reference plane from the right). The former is designated P_{no} and the latter is equal to kT_pB. Hence,

$$P_{no} = kT_pB \tag{6.21}$$

where P_{no} is the available power at terminals 2–2′ of the attenuator. P_{no} consists of the noise power flowing into terminals 1–1′ (due to load 1) towards terminals 2–2′, attenuated by the loss factor L as it passes through the attenuator, plus noise generated internally by the attenuator and denoted ΔP_{no}:

$$P_{no} = \frac{1}{L}kT_pB+\Delta P_{no}. \tag{6.22}$$

Equating (6.21) to (6.22) gives

$$\Delta P_{no} = \left(1-\frac{1}{L}\right)kT_pB. \tag{6.23}$$

This internally generated noise power at the attenuator output (terminals 2–2′) is equal to the noise power that would appear at the output of an equivalent noise-free attenuator with an input noise power P_E given by

$$P_E = L\Delta P_{no} = (L-1)kT_pB, \tag{6.24}$$

which is equivalent to an effective input noise temperature T_E given by

$$T_E = (L-1)T_p \tag{6.25a}$$

and

$$T_{E0} = \frac{T_E}{L} = \left(1-\frac{1}{L}\right)T_p. \tag{6.25b}$$

From (6.14), the noise figure of an attenuator is

$$F = 1+(L-1)\frac{T_p}{T_0} \tag{6.26}$$

which reduces to $F=L$ for $T_p=T_0$.

The variation of T_{E0} with L(dB) ($=10\log L$) is shown in Fig. 6.8 for $T_p=T_0=290$ K. It is noted that the magnitude of L may have a significant effect on the performance of a system. Consider for example a transmission line of loss L connecting an antenna to a low-noise receiver with equivalent input noise temperature T_{REC}, as shown in Fig. 6.9. The overall noise performance of the transmission-line and receiver combination can be characterized by the effective input noise temperature T'_{REC} at the antenna terminals

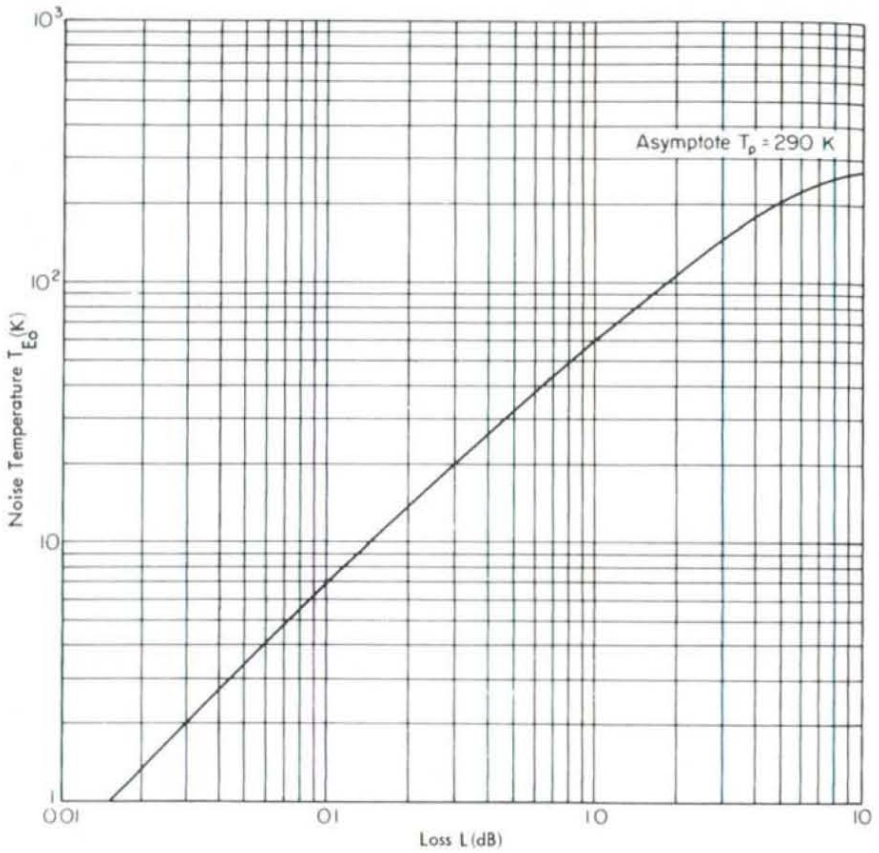

Fig. 6.8 Output noise generated by a matched attenuator.

(thereby treating the transmission line and receiver as noise-free). For a two-stage system, T'_{REC} is given by

$$T'_{REC} = T_{E1} + \frac{T_{E2}}{G_1}. \tag{6.27}$$

In this case, T_{E1} is the equivalent input noise temperature of the transmission

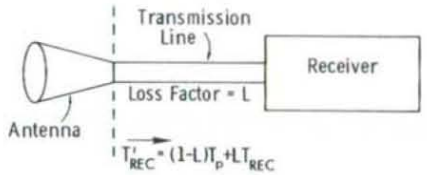

Fig. 6.9 T'_{REC} is the equivalent input noise temperature of an equivalent noise-free transmission line and receiver combination. T_{REC} is the receiver input noise temperature, and T_p is the physical temperature of the transmission line.

line (given by 6.25(a)), $T_{E2} = T_{REC}$, and $G_1 = 1/L$. Hence,

$$T'_{REC} = (L-1)T_p + LT_{REC}. \tag{6.28}$$

If the low-noise receiver is characterized by $T_{REC} = 50$ K and if $T_p = 290$ K and $L = 0.5$ dB, $T'_{REC} = 91.5$ K. Thus, even a loss factor as low as 0.5 dB can degrade the noise performance of the overall receiver system by approximately a factor of 2 (below a receiver connected to the antenna directly). Had the receiver been of the conventional type, with a typical noise temperature $T_{REC} = 1000$ K, the noise added by the transmission line would have been of minor significance, since in this case $T'_{REC} = 1155$ K, an increase of only 11.5 percent.

6-5 EQUIVALENT NOISE TEMPERATURE OF A SUPERHETERODYNE RECEIVER

Consider the *single-sideband** superheterodyne receiver shown in Fig. 6.10(a). The available input noise power P_{ni} is the noise delivered by the antenna via a transmission line, and P_{no} is the noise power available at the output. We wish to replace the noisy receiver with an equivalent noise-free receiver as shown in Figure 6.10(b) by referring the internally generated receiver noise to its input terminals. Specifically, we wish to relate its equivalent input noise temperature T_{REC} to the parameters characterizing its individual subsystems through the use of the results obtained previously for the cascaded system.

The superheterodyne receiver is characterized by the following parameters:

G_{RF} = radio-frequency (RF) amplifier power gain,
F_{RF} = RF amplifier noise figure,
T_{RF} = RF amplifier equivalent input noise temperature $= (F_{RF} - 1)T_0$,
G_M = mixer-preamplifier RF-to-IF power gain,
F_M = mixer-preamplifier noise figure,
T_M = mixer-preamplifier equivalent input noise temperature $= (F_M - 1)T_0$,
G_{IF} = intermediate-frequency (IF) amplifier power gain,
F_{IF} = IF amplifier noise figure,
T_{IF} = IF amplifier equivalent input noise temperature $= (F_{IF} - 1)T_0$,
$T_0 = 290$ K.

The noise parameters of the stages following the IF amplifier were not included in the above list because, as we will see below, the noise performance of the receiver is governed primarily by the stages at its front end. Applying (6.19a), we have

$$T_{REC} = T_{RF} + \frac{T_M}{G_{RF}} + \frac{T_{IF}}{G_{RF}G_M} + \cdots. \tag{6.29}$$

*See Problem 6.3.

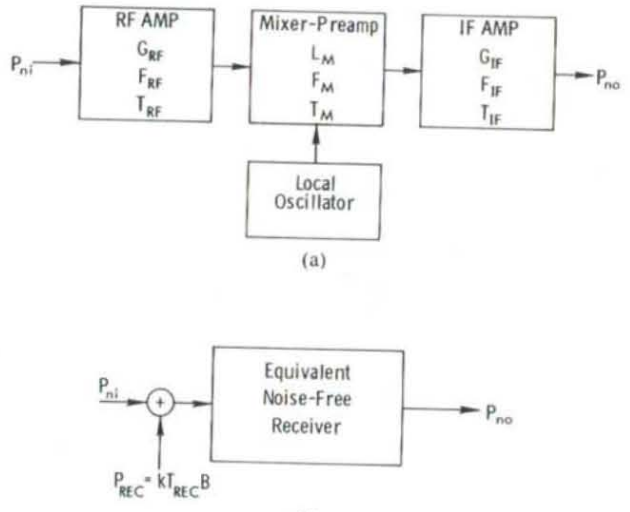

Fig. 6.10 A superheterodyne receiver may be represented by noise-free devices if its nternally generated noise is properly represented by an input noise temperature T_{REC}: (a) 'ront-end elements; (b) equivalent representation.

For a typical receiver operating at a center frequency of 1.5 GHz, $F_{RF}=2.3$ IB, $G_{RF}=30$ dB, $G_M=23$ dB, $F_M=7.5$ dB, $G_{IF}=30$ dB, and $F_{IF}=1.2$ dB. Hence,

$$T_{RF}=(F_{RF}-1)T_0=(1.7-1)290=203\text{ K},$$

$$T_M=(F_M-1)T_0=(5.62-1)290=1340\text{ K},$$

$$T_{IF}=(F_{IF}-1)T_0=(1.32-1)290=92\text{ K},$$

where the noise figures have been converted from dB to natural numbers. Employing the above noise temperatures in (6.29), we have

$$T_{REC}=203+\frac{1340}{1000}+\frac{92}{1000\times 200}+\cdots$$

$$=203+1.34+4.6\times 10^{-4}+\cdots$$

$$\simeq 204.34\text{ K}.$$

For all practical purposes, the receiver equivalent input noise temperature is equal to the equivalent input noise temperature of the first stage, the RF amplifier. Thus, with regard to noise performance, the first stage of a receiver s the most critical, if its gain is much larger than 1.

6-6 EQUIVALENT-SYSTEM NOISE POWER AT THE ANTENNA TERMINALS

Now we shall consider the total-system equivalent input noise power P_{SYS} referred to the antenna terminals of Fig. 6.11. P_{SYS} consists of P'_A, the noise power delivered by the antenna, and P'_{REC}, the equivalent input noise power of the transmission-line–receiver combination. For an antenna with a radiation efficiency η_l and physical temperature T_p, the antenna noise temperature T'_A is given by (4.61),

$$T'_A=\eta_l T_A+(1-\eta_l)T_p, \tag{4.61}$$

where T_A is the antenna radiation temperature of the scene observed by a lossless antenna (see (4.53)). The antenna noise power is

$$\begin{aligned}P'_A&=kT'_AB\\&=k\left[\eta_l T_A+(1-\eta_l)T_p\right]B,\end{aligned} \tag{6.30}$$

where B, the bandwidth, usually is the effective bandwidth of the IF amplifier. The equivalent input noise temperature of the transmission-line–receiver combination (referred to the input terminals of the transmission line) is given by (6.28). Hence,

$$\begin{aligned}P'_{REC}&=kT'_{REC}B\\&=k\left[(L-1)T_p+LT_{REC}\right]B,\end{aligned} \tag{6.31}$$

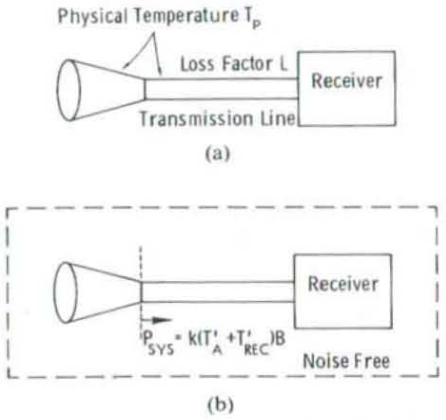

Fig. 6.11 Equivalent input system noise power incorporates noise generated by the receiver, transmission line, antenna self-emission and emission by the scene observed by the antenna: (a) "Noisy" antenna of radiation efficiency η_l connected to a receiver via a transmission line; (b) equivalent noise-free configuration with equivalent input system noise power P_{SYS}.

and therefore,

$$P_{SYS} = P'_A + P'_{REC}$$
$$= k\{\eta_l T_A + (1-\eta_l)T_p + (L-1)T_p + LT_{REC}\}B. \quad (6.32)$$

Setting $P_{SYS} = kT_{SYS}B$, where T_{SYS} is defined as the system input noise temperature, the following expression is obtained from (6.32):

$$T_{SYS} = \eta_l T_A + (1-\eta_l)T_p + (L-1)T_p + LT_{REC}. \quad (6.33)$$

For a radiometer receiver, P_{SYS} represents the "signal" at the input terminals of an equivalent noise-free receiving system (transmission line and receiver). That is, the receiver output voltage is proportional to P_{SYS}. By comparing the output voltage due to P_{SYS} with the output voltage due to a matched load (in place of the antenna) of known physical temperature, a radiometer receiver provides an estimate of T_A, the antenna temperature of the scene under observation (provided T_p and η_l are known). Details of the technique and the precision associated with the estimate of T_A are given in future sections.

In the case of a radar receiver, P_{SYS} represents the effective noise power at the input to the receiving system, while the input signal is the received power P_r given by the radar equation (Chapter 7). The input signal-to-noise ratio, with the noise added by the receiving system taken into account, is $S_n = P_r/P_{SYS}$. This ratio is used to establish the transmitter power and antenna parameters required for a given performance specification. If, through the application of signal-processing techniques, the signal-to-noise ratio at the receiver output is better than the input ratio, then the effective input signal-to-noise ratio is S_n multiplied by the improvement factor. Considerations of radar-system design and performance are given in Volume II.

6-7 RADIOMETER OPERATION

The function of a radiometer is to measure the antenna radiometric temperature T'_A, which represents the radiation power delivered by the antenna to the receiver. The measurement process is characterized by two important attributes: (1) accuracy and (2) precision.

6-7.1 Measurement Accuracy

Conceptually, the transfer function of the radiometer receiver is established by measuring the output voltage as a function of the noise temperature of a noise source connected to the receiver input terminals in place of the antenna. Alternatively, calibration is achieved through the use of a switch placed at a point as close to the antenna as possible. The scheme is shown in Fig. 6.12(a). Also, if the radiometer employs square-law detection, which most radiometers do, its output voltage is linearly related to the noise temperature of the input

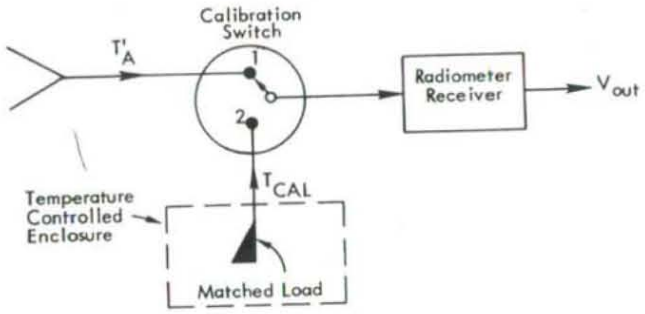

(a) Calibration Configuration

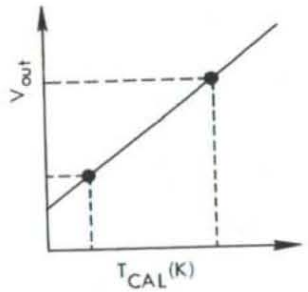

(b) Calibration Line

Fig. 6.12 Calibration of a microwave radiometer: (a) configuration; (b) calibration line.

source. Therefore, it is sufficient to measure the output voltage corresponding to each of two input noise temperatures to establish the calibration line (Fig. 6.12(b)). This calibration line then is used for converting the output voltage measured by the receiver (when connected to the antenna) to antenna temperature values. Assuming that the calibration measurements are made with a high degree of measurement precision, the absolute accuracy of T'_A then is dictated by the accuracy with which the absolute values of the calibration noise temperatures are known. If a passive device, such as a matched load (resistor), is used as a calibration source, its noise temperature accuracy may be maintained within 1 K or better by controlling the temperature of its environment. In practice, however, other sources of error also contribute to the absolute measurement accuracy of T'_A, as discussed in Section 6-16.

6-7.2 Measurement Precision

In radiometric terminology, the *radiometric sensitivity* (or *radiometric resolution*) ΔT is defined as the smallest change in T'_A that can be detected by the radiometer output. A more formal definition, in the statistical sense, is given below.

Consider the total-power radiometer system shown in Fig. 6.13(a). The antenna is connected to a superheterodyne receiver of bandwidth B and total power gain G, followed by a detector and a low-pass filter. The power delivered by the antenna usually is broadband noise extending over a wider bandwidth than the receiver bandwidth B. The function of the RF amplifier is to filter the input signal by amplifying the frequency components contained in the bandwidth B centered at the RF frequency of interest, f_{RF}. The mixer and IF amplifier translate the RF band of signals of bandwidth B to the same bandwidth at the IF and provide further amplification. In practice, the RF amplifier usually has a wider bandwidth than that of the IF amplifier, and therefore the predetection bandwidth B is effectively determined by the IF amplifier bandpass characteristics. Such a system consisting of RF-to-IF translation of a single band of width B is called a *single-sideband* receiver (see Problem 6.3).

Without an RF amplifier (or with a very wideband amplifier), the IF signal band contains signals from two RF bands centered at frequencies f_1 and f_2, where

$$f_1 = f_{LO} - f_{IF},$$
$$f_2 = f_{LO} + f_{IF}.$$

Because the input signal at each RF frequency, f_1 and f_2, is of bandwidth B, the total input power for such a *double-sideband* receiver is twice the input power received by a single-sideband receiver, since in the latter, one of two RF bands is rejected by the RF amplifier. Although the signal power is larger by a factor of 2 (assuming that the antenna temperature T'_A is about the same at f_1 and f_2), the absence of a low-noise RF amplifier usually results in an increase in receiver noise temperature by a much larger factor (see Fig. 6.26). Furthermore, if the total available frequency band is fixed, the single-sideband receiver can be designed to use the entire bandwidth, while in the double-sideband receiver, part of the available bandwidth is not used. This consideration is particularly pertinent in microwave radiometry. To avoid the threat of interference from radio transmitters, radiometric observations usually are made in the "protected" frequency bands allocated for radio-astronomy observations (Table 1.3). As will be shown later, the radiometric measurement sensitivity (resolution) improves with increasing bandwidth B. Hence, to take full advantage of the relatively narrow width of a protected band, single-sideband receivers are preferred.

A representation equivalent to Fig. 6.13(a) is shown in Fig. 6.13(b), in which the antenna is replaced by a noise source with output power $P'_A = kT'_A B$ and the receiver (including transmission line) is replaced by a combination of a noise-free receiver and an input noise source with output power given by $P'_{REC} = kT'_{REC} B$, where T'_{REC} is the equivalent input noise temperature of the transmission-line–receiver combination. The total system input noise power is

$$P_{SYS} = P'_A + P'_{REC} = kT_{SYS} B, \tag{6.34}$$

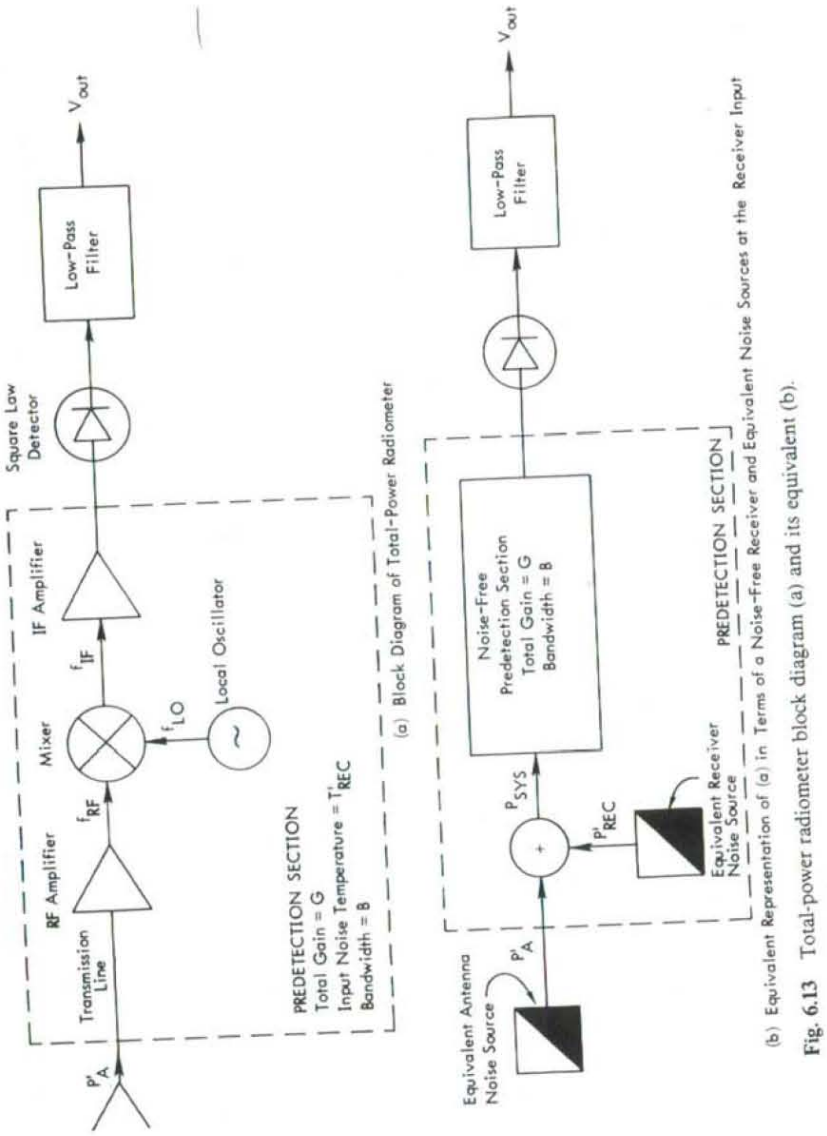

Fig. 6.13 Total-power radiometer block diagram (a) and its equivalent (b).

where

$$T_{SYS} = T'_A + T'_{REC}. \tag{6.35}$$

The IF amplifier (average) output power P_{IF} is given by

$$P_{IF} = GkT_{SYS}B. \tag{6.36}$$

Figure 6.14 illustrates the voltage waveforms and corresponding power spectra at several points between the RF input and the final output. Since the input power consists of thermal noise, the instantaneous IF voltage is described by a Gaussian probability distribution with zero mean, and, as shown in Section 6-2.3, its envelope is Rayleigh distributed. Thus,

$$p(V_e) = \begin{cases} \dfrac{V_e}{\sigma^2} e^{-V_e^2/2\sigma^2}, & V_e \geq 0, \\ 0, & V_e \leq 0, \end{cases} \tag{6.37}$$

where σ is the standard deviation of the Gaussian distribution. The mean value

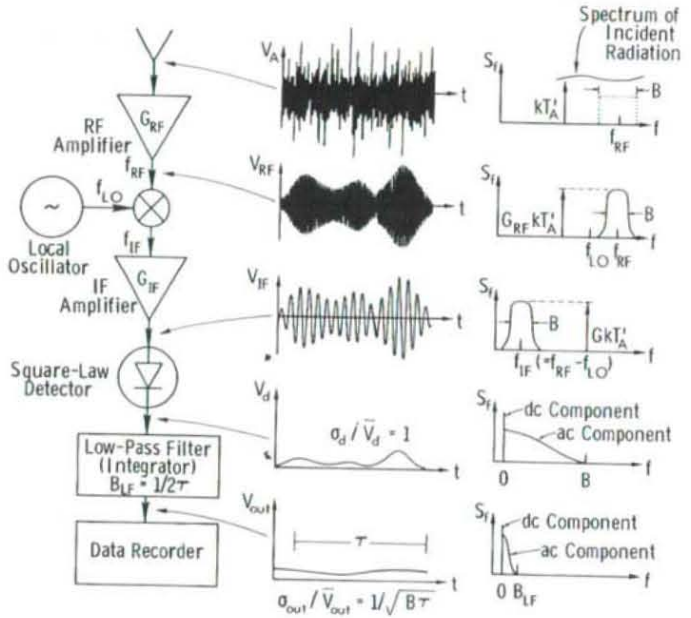

G = Power gain of predetection section (between RF amplifier input and IF amplifier output).

S_f = Power spectral density, W Hz^{-1}

Fig. 6.14 Total-power radiometer with a superheterodyne receiver. The signal voltage and corresponding spectrum are shown at various stages.

of V_e^2 can be easily shown to be given by

$$\overline{V_e^2} = 2\sigma^2. \tag{6.38}$$

Without loss of generality, we assume that the IF power is developed across a 1-ohm resistor, which leads to

$$P_{IF} = \overline{V_e^2} = 2\sigma^2. \tag{6.39}$$

The output of the square-law detector, V_d, is related to its input, V_e, via the relation

$$V_d = C_d V_e^2, \tag{6.40}$$

where C_d is the square-law detector power-sensitivity constant (volts per watt). The average value of V_d is given by

$$\begin{aligned} \overline{V}_d &= C_d \overline{V_e^2} = 2C_d\sigma^2 = C_d P_{IF} \\ &= C_d GkBT_{SYS} \end{aligned} \tag{6.41}$$

and represents the average value of the input noise power, P_{SYS} (except for multiplicative constants).

Using (6.40), the Rayleigh distribution given by (6.37) may be converted to a distribution for V_d from

$$p(V_d)dV_d = p(V_e)dV_e,$$

which leads to the exponential distribution

$$p(V_d) = \frac{1}{\overline{V}_d} e^{-V_d/\overline{V}_d}, \tag{6.42}$$

whose mean value is given by (6.41). The variance of V_d is σ_d and is obtained through

$$\sigma_d^2 = \overline{V_d^2} - \overline{V}_d^2, \tag{6.43}$$

which can be shown to lead to

$$\sigma_d^2 = \overline{V}_d^2, \tag{6.44}$$

or

$$\frac{\sigma_d}{\overline{V}_d} = 1. \tag{6.45}$$

In terms of the input power P_{SYS}, $\overline{V}_d$ (the dc value of V_d) represents its average value and σ_d (the rms value of the ac component) represents the statistical uncertainty associated with the measurement of P_{SYS} (through $\overline{V}_d$). Certainly, such a high level of uncertainty as given by (6.45) is not an acceptable result. The solution to this problem is to filter out the high-frequency fluctuations of the detected voltage, which is equivalent to averaging V_d over some interval of time τ. This is precisely the function of the low-pass filter (integrator) shown in Fig. 6.14.

The voltage V_{out} at the output of the low-pass filter consists of a dc component $\overline{V}_{out}$ and an ac component V_{ac}:

$$V_{out}(t)=\overline{V}_{out}+V_{ac}(t). \tag{6.46}$$

According to the results of Section 7-2.4, integrating a random signal of bandwidth B over a time τ leads to a reduction of its variance (normalized to the square of its mean value) by the factor $N=B\tau$. That is, the ratio $\sigma_{out}^2/\overline{V}_{out}^2$ at the low-pass filter output (where σ_{out} is the standard deviation of V_{out}) is related to $\sigma_d^2/\overline{V}_d^2$ at the filter input by

$$\frac{\sigma_{out}^2}{\overline{V}_{out}^2}=\frac{\sigma_d^2}{\overline{V}_d^2}\cdot\frac{1}{B\tau}. \tag{6.47}$$

Using (6.45), we have

$$\frac{\sigma_{out}}{\overline{V}_{out}}=\frac{1}{\sqrt{B\tau}}. \tag{6.48}$$

The dc output voltage $\overline{V}_{out}$ is directly related to the average input power P_{SYS} (and therefore to the radiometric temperature T_{SYS}) through

$$\begin{aligned}\overline{V}_{out}&=g_{LF}\overline{V}_d\\&=g_{LF}C_dGkT_{SYS}B\\&=G_ST_{SYS},\end{aligned} \tag{6.49}$$

where g_{LF} is the voltage gain of the low-pass filter, and G_S, termed the *system gain factor*, is an abbreviation for

$$G_S=g_{LF}C_dGkB. \tag{6.50}$$

Assuming that all the system parameters in (6.49) are constant, (6.48) is equivalent to

$$\frac{\Delta T_{SYS}}{T_{SYS}}=\frac{1}{\sqrt{B\tau}}, \tag{6.51}$$

where ΔT_{SYS} is the standard deviation associated with the measured (estimated) value of T_{SYS}.

From an observation standpoint, ΔT_{SYS} may be viewed as the minimum change in T_{SYS} that is necessary to produce a detectable change at the radiometer output, where detectable change is defined as a change in the dc level of the output voltage equal to the standard deviation of the ac component. Recalling that $T_{SYS}=T'_A+T'_{REC}$ and that T'_{REC} (the receiver input noise temperature) is independent of the radiation incident upon the antenna, (6.51) may be rewritten as

$$\Delta T\triangleq\Delta T_{SYS}=\frac{T_{SYS}}{\sqrt{B\tau}}=\frac{T'_A+T'_{REC}}{\sqrt{B\tau}}, \tag{6.52}$$

where ΔT is regarded as the minimum detectable change in the radiometric antenna temperature T'_A of the observed scene. The above equation defines the radiometric sensitivity (or resolution) of an *ideal* total-power radiometer with no gain fluctuations. As will be discussed in the next section, this assumption is not always valid. To emphasize the importance of this assumption, ΔT will be denoted ΔT_{IDEAL}, and (6.52) rewritten in the form

$$\Delta T_{IDEAL}=\frac{T_{SYS}}{\sqrt{B\tau}}. \tag{6.53}$$

In the above derivation, the low-pass filter was characterized as having an integration time τ. We shall now relate τ to the filter power transfer function $G_{LF}(f)$.

The effective bandwidth B_{LF} of a low-pass filter is defined as the bandwidth of an equivalent ideal filter with a rectangular passband extending from zero to B_{LF} hertz and of constant gain equal to the maximum gain G_{max} of the actual filter. In practice, $G_{max}=G_{LF}(0)$. Thus,

$$B_{LF}=\frac{\int_0^\infty G_{LF}(f)\,df}{G_{LF}(0)}. \tag{6.54}$$

An *ideal integrator* of integration time τ relates the output voltage V_{out} to the input voltage V_d through

$$V_{out}(t)=\frac{1}{\tau}\int_{t-\tau}^{t}V_d(t')\,dt'. \tag{6.55}$$

If we define the ideal integrator (low-pass filter) by the rectangular time function

$$h(\tau-t')=\begin{cases}1/\tau & \text{for } t-\tau<t'<t,\\ 0 & \text{otherwise,}\end{cases} \tag{6.56}$$

then (6.55) may be rewritten as

$$V_{out}(t)=\int_{-\infty}^{\infty} h(\tau-t')V_d(t')\,dt', \tag{6.57}$$

which we recognize as a convolution integral. Since convolution in the time domain corresponds to multiplication in the frequency domain, the power-frequency transfer function of an ideal integrator is the square of the magnitude of the Fourier transform of $h(\tau-t')$:

$$G_I(f)=|\mathfrak{F}\{h(\tau-t')\}|^2. \tag{6.58}$$

The Fourier transform of a rectangular function is a sinc function, thereby leading to the result

$$G_I(f)=\frac{\sin^2(\pi f\tau)}{(\pi f\tau)^2}. \tag{6.59}$$

The equivalent bandwidth B_{LF} of an ideal integrator may now be obtained by inserting (6.59) into (6.54) and performing the integration. The result is

$$B_{LF}=\frac{1}{2\tau}. \tag{6.60}$$

The above result now may be used to define the equivalent ideal integration time of any low-pass filter as

$$\tau=\frac{G_{LF}(0)}{2\int_0^{\infty} G_{LF}(f)\,df}. \tag{6.61}$$

It is interesting to note that an ideal integrator is not the same as an ideal low-pass filter; an ideal integrator is described by a rectangular function in the time domain, while an ideal filter is characterized by a rectangular passband in the frequency domain. In terms of smoothing (filtering) out ac fluctuations, however, the two are equivalent if the integration time of the ideal integrator is equal to the reciprocal of twice the bandwidth of the ideal filter.

One of the main objectives of this section has been to derive the radiometer sensitivity equation given by (6.53). The treatment was based on Gaussian noise statistics and essentially consisted of tracking the dc and ac components of the noise voltage from the IF amplifier output to the low-pass filter output. An alternate, equivalent approach would be to perform the tracking in the frequency domain, as shown by Tiuri (1964) and by Evans and McLeish (1977). Tiuri's derivation conveniently leads to the following definition for the

equivalent predetection bandwidth B of a nonrectangular power-transfer function $G(f)$:

$$B=\frac{\left[\int_0^{\infty} G(f)\,df\right]^2}{\int_0^{\infty} G^2(f)\,df}. \tag{6.62}$$

Figure 6.14 shows the power spectra at different stages in the radiometer receiver, adapted in part from Tiuri (1964), to whom the reader is referred for details.

6-8 EFFECTS OF RECEIVER GAIN VARIATIONS

As we stated earlier, the expression for ΔT given by (6.52) accounts only for the measurement uncertainty due to noise fluctuations and does not incorporate receiver gain fluctuations. For convenience, (6.52) is repeated below in the form

$$\Delta T_N=\frac{T_{SYS}}{\sqrt{B\tau}}, \tag{6.63a}$$

where the subscript N denotes *noise*-caused uncertainty.

The output voltage of the total-power radiometer is directly proportional to several system factors (see (6.49)) that were assumed to be constant in the derivation leading to (6.52). In practice, this is a fair assumption for the postdetection stages, but may not be valid for the predetection power gain G. Gain variations in the predetection section arise primarily from the RF amplifier and secondarily from the mixer and IF amplifier.

Since V_{out} is linearly related to the product $G_S T_{SYS}$, an increase in G_S by ΔG_S will be misinterpreted by the output as an increase in T_{SYS} by $\Delta T_{SYS}=T_{SYS}(\Delta G_S/G_S)$. Long-term (slow) variations of G_S, with periods of the order of minutes, may be factored out approximately by calibrating the radiometer output voltage against known input noise sources as frequently as is practicable. However, calibration does not eliminate short-term (fast) gain variations that occur over intervals smaller than the period between successive calibrations. Statistically, the rms uncertainty in T_A' due to system gain variations may be defined as

$$\Delta T_G=T_{SYS}\left(\frac{\Delta G_S}{G_S}\right), \tag{6.63b}$$

where G_S is the average system power gain and ΔG_S is the effective value (rms) of the detected power gain variation (ac component).

Since the noise uncertainty ΔT_N and the gain uncertainty ΔT_G are caused by unrelated mechanisms, they may be considered statistically independent, in which case the total rms uncertainty is given by

$$\Delta T = \left[(\Delta T_N)^2 + (\Delta T_G)^2\right]^{1/2}$$

$$= T_{SYS}\left[\frac{1}{B\tau} + \left(\frac{\Delta G_S}{G_S}\right)^2\right]^{1/2}. \tag{6.64}$$

The above expression defines the radiometer sensitivity of the total-power radiometer, incorporating the effects of both noise and gain variations.

To gain an appreciation for the relative significance of the two sources of measurement uncertainty, let us consider the following example. A total-power radiometer operating at a center frequency of 1.4 GHz is characterized by the following parameters: $T'_{REC} = 600$ K, $B = 100$ MHz, $\tau = 0.01$ s, and $\Delta G_S/G_S = 10^{-2}$. For an antenna temperature T'_A in the neighborhood of 300 K, the above values lead to the following conclusions:

$$\Delta T_N = 0.9 \text{ K},$$
$$\Delta T_G = 9 \text{ K},$$
$$\Delta T = 9.05 \text{ K}.$$

That is, the radiometer sensitivity is governed effectively by gain variations. The desired sensitivity in remote-sensing observations usually is of the order of 1 K or less. To reduce ΔT of the above radiometer to 1 K, the product $T_{SYS}(\Delta G_S/G_S)$ has to be reduced by a factor of 20. Since $T_{SYS} = T'_{REC} + T'_A$, the smallest possible value it can have is $T_{SYS} = T'_A$, which corresponds to an ideal noise-free receiver. T'_A may vary between a few kelvins and 330 K for natural (terrestrial) scenes. Hence, even with a noise-free receiver, the desired resolution of 1 K cannot be achieved without improving the gain variation factor $(\Delta G_S/G_S)$. Typically, the gain variation factor for low-noise microwave amplifiers is between 10^{-2} and 10^{-3}; therefore they would not be readily suitable for use in total-power radiometers. Gain variations may be reduced by an order of magnitude or better by controlling the sources that cause these variations, namely, power-supply voltages and environmental temperature variations. This may provide an acceptable solution for a total-power radiometer operating in the centimeter wavelength range, but at millimeter wavelengths it is difficult to construct highly stable receivers with $\Delta G_S/G_S \leq 10^{-4}$.

One possible solution to the gain variations problem is to use a receiver with no RF amplifier. In this case, the receiver noise temperature T'_{REC} may be as large as 3000 K or more, but without the RF amplifier, values of $\Delta G_S/G_S$ as low as 10^{-4} to 10^{-5} are achievable (Hersman and Poe, 1981), and therefore the product $T_{SYS}(\Delta G_S/G_S)$ may be reduced to about 0.1 K. Other approaches are discussed in the following sections.

6-9 DICKE RADIOMETER

Although a limited number of studies have been conducted to evaluate the nature of system-gain fluctuations (Steinberg, 1952; Colvin, 1961; Yaroshenko, 1964; Hersman and Poe, 1981), it is generally observed that: (1) the power spectral density of G_S (fluctuation spectrum) decreases with increasing frequency as $1/f$ or faster, (2) the bulk of the fluctuation spectrum lies at frequencies below 1 Hz, and (3) practically no fluctuations with frequencies above 1 kHz exist. Through the example cited in the previous section, it was concluded that gain variations are often the limiting factor to achieving high radiometric resolutions (small values of ΔT). In 1946, the gain-variation problem was alleviated by Dicke (1946) through the use of modulation techniques for reducing the effects of gain fluctuations in a radiometer.

A block diagram of the Dicke radiometer is shown in Fig. 6.15. It is basically a total-power radiometer with two additional features: (1) a switch, which has become known as a "Dicke" switch, connected at the receiver input (at a point as close to the antenna as possible) and used to *modulate* the receiver input signal, and (2) a *synchronous demodulator* (also called synchronous detector) placed in between the square-law detector and the low-pass filter (integrator). The predetection section consists of the RF amplifier, mixer, and IF amplifier and is characterized by a predetection power gain G and bandwidth B.

The modulation consists of periodically switching the receiver input between the antenna and a constant (reference) noise source (Figure 6.15) at a switching rate higher than the highest significant spectral component in the gain variation spectrum. That is, the switching rate f_s is chosen so that over a period of one switching cycle (typically between 1 and 20 ms) the system gain G_S essentially is constant, and therefore *identical* for the half-cycle during which the receiver is connected to the antenna and the half-cycle during which the receiver is connected to the reference source. For square-wave modulation, the detected dc outputs corresponding to the antenna and comparison-source powers are, respectively,

$$\bar{V}_{d\,ANT} = C_d G k B (T'_A + T'_{REC}) \quad \text{for} \quad 0 \leq t \leq \tau_s/2, \tag{6.65a}$$

$$\bar{V}_{d\,REF} = C_d G k B (T_{REF} + T'_{REC}) \quad \text{for} \quad \tau_s/2 \leq t \leq \tau_s, \tag{6.65b}$$

where T_{REF} is the reference-source noise temperature and τ_s $(= 1/f_s)$ is the period of one switching cycle. The receiver noise temperature T'_{REC} includes noise contributions from the input switch, which typically are between 7 and 75 K (Section 6-15.1).

Superimposed on the dc voltages are ac components due to noise and gain fluctuations. The synchronous demodulator (Figure 6.15) consists of a switch that operates in synchronism with the input Dicke switch, followed by two unity-gain amplifiers (in parallel), with opposite polarity, one to receive

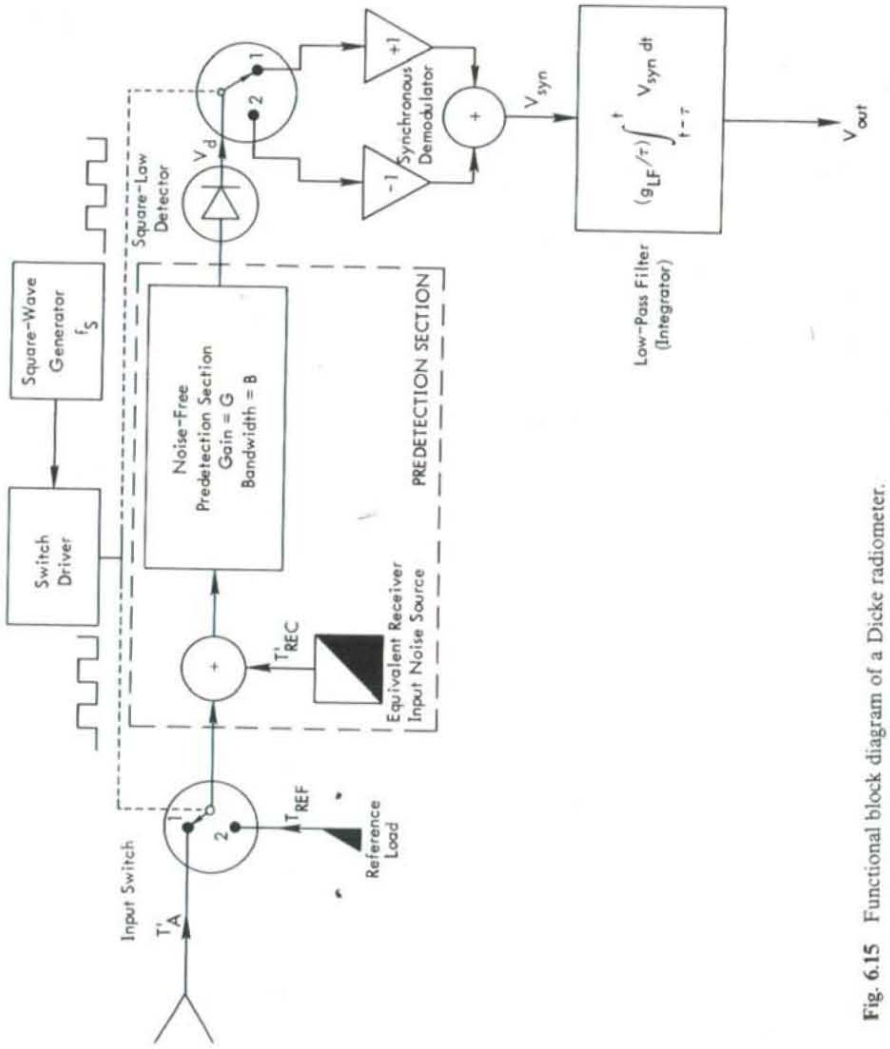

Fig. 6.15 Functional block diagram of a Dicke radiometer.

$V_{d\,ANT}(t)$ and the other to receive $V_{d\,REF}(t)$. The unity-gain amplifier outputs are then summed and fed into the low-pass filter (integrator). Accordingly, the dc output of the synchronous demodulator is

$$\begin{aligned}\overline{V}_{syn} &= \tfrac{1}{2}(\overline{V}_{d\,ANT} - \overline{V}_{d\,REF}) \\ &= \tfrac{1}{2}C_d G k B (T'_A - T_{REF}).\end{aligned} \tag{6.66}$$

With an integration time τ, the output of the low-pass filter is effectively equal to

$$V_{out}(t) = \frac{g_{LF}}{\tau}\left[\int_0^{\tau/2} V_{d\,ANT}(t)\,dt - \int_{\tau/2}^{\tau} V_{d\,REF}(t)\,dt\right]. \tag{6.67}$$

With most of the ac fluctuations removed by the integration, the output voltage consists of a dc component, $\overline{V}_{out}$, and a relatively very small ac component with rms value σ_{out}. From (6.66), $\overline{V}_{out}$ is given by

$$\begin{aligned}\overline{V}_{out} &= \tfrac{1}{2}g_{LF}C_d G k B (T'_A - T_{REF}) \\ &= \tfrac{1}{2}G_S(T'_A - T_{REF}).\end{aligned} \tag{6.68}$$

In addition to filtering out most of the fluctuating component of $V_{syn}(t)$, the low-pass filter also filters out the ac components at f_s and its higher harmonics (due to the square-wave modulation). That is, the switching rate f_s must be much larger than the low-pass filter bandwidth B_{LF}. The relationship between f_s and B_{LF} also may be considered from the viewpoint of the sampling theorem. B_{LF} represents the range of frequencies of the fluctuating component of the input signal that is retained in the output voltage, and f_s represents the frequency at which the input signal is sampled. To satisfy the sampling theorem, $f_s \geq 2B_{LF}$.

According to (6.68), the dc output voltage is proportional to the difference between T'_A and T_{REF}, and is independent of the receiver noise temperature T'_{REC}.

Next, we shall derive an expression for the radiometric resolution ΔT of the Dicke radiometer. We start by rewriting (6.68) in the following form:

$$\overline{V}_{out} = \tfrac{1}{2}G_S\left[(T'_A + T'_{REC}) - (T_{REF} + T'_{REC})\right]. \tag{6.69}$$

The ac component of $V_{out}(t)$ consists of three contributions:

1. Gain variations, which from (6.66) lead to a gain uncertainty

$$\Delta T_G = (T'_A - T_{REF})(\Delta G_S / G_S). \tag{6.70}$$

2. Noise variations of $T'_A + T'_{REC}$, which upon integration for a period $\tau/2$ (antenna is observed during only half of the integration time τ) lead to a

noise uncertainty (see (6.63a))

$$\Delta T_{NANT} = \frac{T'_A + T'_{REC}}{\sqrt{B\tau/2}} = \frac{\sqrt{2}\,(T'_A + T'_{REC})}{\sqrt{B\tau}}. \tag{6.71}$$

. Noise variations of $(T_{REF} + T'_{REC})$, which, similarly, lead to

$$\Delta T_{NREF} = \frac{\sqrt{2}\,(T_{REF} + T'_{REC})}{\sqrt{B\tau}}. \tag{6.72}$$

Assuming that the above three uncertainties are statistically independent, the otal radiometric resolution is given by

$$\Delta T = \left[(\Delta T_G)^2 + (\Delta T_{NANT})^2 + (\Delta T_{NREF})^2\right]^{1/2}, \tag{6.73}$$

vhich reduces to

$$\Delta T = \left[\frac{2(T'_A + T'_{REC})^2 + 2(T_{REF} + T'_{REC})^2}{B\tau} + \left(\frac{\Delta G_S}{G_S}\right)^2 (T'_A - T_{REF})^2\right]^{1/2}. \tag{6.74}$$

For reasons that will become obvious later, the above expression will be referred to as the radiometric resolution (sensitivity) of the *unbalanced* Dicke radiometer. Examples of satellite Dicke radiometers operating in the unbalanced mode are the 19.35-GHz Nimbus 5 and the 37-GHz Nimbus 6 electrically scanning microwave radiometer (ESMR) systems; parameters of the Nimbus 5 ESMR are summarized in Table 6.1.

Before we proceed further, let us compare ΔT of the unbalanced Dicke radiometer with that of the total-power radiometer considered earlier. For $B = 100$ MHz, $\tau = 1$ s, $T'_{REC} = 700$ K, and $\Delta G_S/G_S = 10^{-2}$, Eq. (6.64) gives the values

$$\Delta T(\text{Total Power}) \simeq \begin{cases} 7 \text{ K} & \text{for } T'_A = 0 \text{ K}, \\ 10 \text{ K} & \text{for } T'_A = 300 \text{ K}. \end{cases}$$

If we choose the reference noise temperature $T_{REF} = 300$ K, (6.74) gives

$$\Delta T(\text{unbalanced Dicke}) \simeq \begin{cases} 3 \text{ K} & \text{for } T'_A = 0 \text{ K}, \\ 0.2 \text{ K} & \text{for } T'_A = 300 \text{ K}. \end{cases}$$

Overall, the radiometric resolution of the unbalanced Dicke radiometer is superior to that of the total-power radiometer. Of particular significance, however, is the condition $T'_A = T_{REF}$, because when this condition is met, the

TABLE 6.1
Nimbus 5 Electrically Scanning Microwave Radiometer (ESMR) Flight Model Parameters[a]

Antenna:	
Antenna type	Phased array
Aperture size	83.3 cm × 85.5 cm
Half-power beamwidth	1.4° × 1.4° (at nadir)
Beam efficiency	90–92.7%
Beam scan angle	±50°
Antenna loss	1.7 dB
Polarization	Horizontal
Radiometer:	
Center frequency	19.35 GHz
Predetection bandwidth	200 MHz
Mixer noise figure	6.5 dB
ΔT_{min}[b]	1.5 K
Absolute accuracy	2 K
Dynamic range	50–330 K
Calibration	
(a) Reference load	338 K
(b) Ambient load	Local ambient
(c) Sky horn antenna	3 K

[a] From *Nimbus 5 User's Guide* (NASA, 1972).
[b] For 47-ms integration time.

second term inside the square brackets of (6.74) goes to zero, thereby eliminating the effects of gain variations altogether. When $T'_A = T_{REF}$, the radiometer is said to be *balanced*, in which case (6.74) reduces to

$$\Delta T = \frac{2(T'_A + T'_{REC})}{\sqrt{B\tau}} \qquad \text{(balanced Dicke radiometer)}$$
$$= 2\,\Delta T_{IDEAL}, \tag{6.75}$$

or twice the theoretical sensitivity of an ideal total-power radiometer (free of gain variations). The factor of 2 comes about from the fact that T'_A is observed for only half the time.

Techniques used for continuously maintaining the Dicke radiometer in a balanced state are discussed in the next section.

Sometimes, practical considerations dictate that the square wave at the output of the square-law detector be amplified prior to feeding it into the synchronous demodulator. A video amplifier is used for this purpose. To preserve the square-wave shape of the detected signal, the video amplifier must be capable of providing equal amplification to all of the major harmonics of the square-wave signal, which means that the bandpass of the video amplifier should extend from below f_s to at least $5f_s$, and preferably to as high as $10f_s$. A square wave consists of only odd harmonics, with the amplitude of the first

harmonic equal to $4/\pi$ times the amplitude of the square wave, and the amplitude of the nth harmonic equal to $1/n$ times the amplitude of the first harmonic. This places an additional requirement on the necessary dynamic range of the video amplifier and makes it vulnerable to noise saturation. To avoid this problem, some Dicke radiometers employ a narrow-bandpass amplifier tuned to f_s, but whose bandwidth exceeds the bandwidth of the low-pass filter, B_{LF}. With only the first harmonic of the square wave reaching the synchronous demodulator, the dc output of the synchronous demodulator is smaller than when the full square wave is used, which leads to a reduction in radiometric sensitivity (larger ΔT) by a factor of $(\pi\sqrt{2}/4)=1.11$, or approximately 11 percent (Tiuri, 1964). The simplification in system design and specification brought about by the sinusoidal demodulation, with a relatively small cost in terms of loss in radiometric sensitivity, has made the square-wave-modulated, sine-wave-demodulated Dicke radiometer a popular choice. The merits of other modulation and demodulation waveforms have been considered also (Colvin, 1961; McGillem and Seling, 1963) but in terms of the radiometric sensitivity ΔT, using square-wave modulation and demodulation gives the best results.

6-10 BALANCING TECHNIQUES

A Dicke radiometer is said to be *balanced* if

$$\overline{V}_{dANT} - \overline{V}_{dREF} = 0, \tag{6.76}$$

where $\overline{V}_{dANT}$ is the dc component of the detected voltage during the half cycle that the receiver input switch is connected to the antenna, and a similar definition applies to $\overline{V}_{dREF}$. In the balanced condition, $\overline{V}_{syn}=0$ and consequently $\overline{V}_{out}=0$. With reference to (6.65), the balanced condition may be realized by either: (1) adjusting T_{REF} to equal T_A' (or vice versa) prior to the input switch, or (2) controlling the predetection gain of $\overline{V}_{dANT}$ and $\overline{V}_{dREF}$ separately, in such a manner that the two voltages are made equal. Some examples of feedback configurations, proposed to realize automatically balanced operations in a Dicke radiometer, are discussed next.

6-10.1 Reference-Channel Control Method

Figure 6.16 is a block diagram of a null-balancing Dicke radiometer employing the reference-channel method (Machin et al., 1952). A feedback loop is used to control the magnitude of T_{REF} so that it continuously balances the antenna temperature T_A'. This is realized by feeding the integrator output into a control circuit that applies the necessary voltage (or current) to an electronically controlled variable attenuator to maintain a null at the integrator output. In this case, the control voltage V_c becomes the output voltage to be recorded.

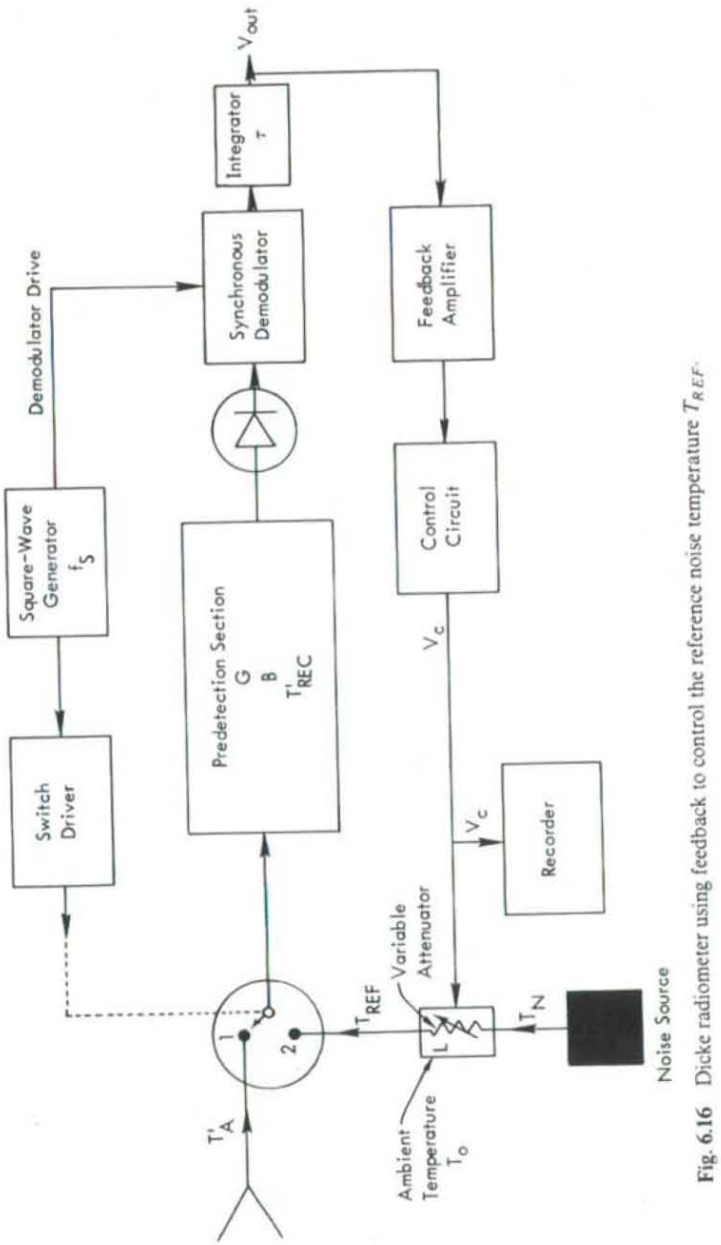

Fig. 6.16 Dicke radiometer using feedback to control the reference noise temperature T_{REF}.

since it is related to T_{REF}, which, in the balanced condition, is equal to T_A'. The radiometer is calibrated by measuring V_c as a function of the noise temperature T_{CAL} of a calibration noise source put in place of the antenna (or through the use of a calibration switch as shown in Fig. 6.12). In general, the calibration curve may be nonlinear, thereby necessitating that V_c be measured over a wide range of values of T_{CAL}.

Returning to Fig. 6.16, the reference noise temperature T_{REF} is in part due to the noise generated by the noise source and in part due to self-emission by the attenuator,

$$T_{REF} = \frac{T_N}{L} + \left(1 - \frac{1}{L}\right) T_0, \tag{6.77}$$

where T_N is the noise temperature of the source, L is the loss factor of the attenuator, and T_0 is its physical temperature. As a function of L, the limiting values of T_{REF} are $T_{REF} = T_N$ for $L = 1$ (no attenuation) and $T_{REF} = T_0$ for L very large. Conceptually, T_N and T_0 can be specified so that the range between them covers the range of values over which T_A' is expected to vary. In practice, however, this specification cannot be realized with passive noise sources unless cryogenic cooling is used (the use of active "cold" sources is discussed below). To illustrate with an example, consider a radiometer system specified to operate over the range $50\ \text{K} \leq T_A' \leq 300\ \text{K}$. The upper limit of T_A' can be accommodated easily by maintaining the environmental temperature of the front end of the radiometer, including the attenuator, at $T_0 = 300$ K, which for L very large, gives $T_{REF} = T_A' = 300$ K. To accommodate the lower limit of T_A', T_N has to be assigned a value of 50 K (or lower). If a matched load is used as the noise source, it has to be physically cooled to the desired noise temperature. Moreover, for real, variable attenuators, the loss factor L cannot be reduced all the way to unity, and therefore the temperature of the matched load has to be lower than 50 K in order to compensate for the noise power generated by the attenuator. Cryogenic techniques sometimes are used in ground-based radiometer systems to reduce the receiver noise temperature and certainly may be used to cool the matched load of the radiometer system under discussion. However, in airborne and spaceborne operations, cryogenic cooling usually is avoided because of the large amounts of power required to maintain the cryogenic fluids at the desired temperature.

Traditionally, active noise sources have been used to provide noise temperatures in excess of their ambient temperatures, thereby relying on cryogenically-cooled matched loads for low noise-temperature sources. Recent advances in FET technology, however, have led to the development of an active circuit that behaves like a noise source with an output noise temperature that is much smaller than its ambient temperature; Frater and Williams (1981) have developed the theory for such a "cold" FET device, which they call a COLDFET, and have demonstrated that a noise temperature as low as 50 K can be achieved at 1.4 GHz. Future developments will undoubtedly extend the use of the COLDFET to higher microwave frequencies.

If, instead of controlling the input noise temperature of the reference channel to equal the noise temperature of the antenna channel, the reverse is done, the cryogenic refrigeration problem associated with the use of passive devices can be alleviated. This approach is discussed next.

6-10.2 Antenna-Channel Noise-Injection Method

The configuration shown in Fig. 6.17 was proposed by Goggins (1967) to achieve null balancing through the use of noise injection into the line connecting the antenna to the input switch. The front end of the radiometer—including the reference load, the variable attenuator, and the directional coupler (as well as other RF devices)—is enclosed in a constant-temperature chamber at a temperature T_0 slightly higher than the highest specified value for T_A' (for reasons that will become obvious later). In other words, when the input switch is connected to terminal 2 (Fig. 6.17), the input noise temperature is $T_{REF} = T_0 = \text{constant}$. To balance the reference load, a sufficient amount of noise power is injected into the antenna port through a directional coupler so that the input noise temperature T_A'' appearing at the input switch (terminal 1 in Fig. 6.17) is equal to T_{REF},

$$T_A'' = T_{REF} = T_0. \tag{6.78}$$

The amount of injected power is controlled by the variable attenuator, which itself is controlled by a feedback network. The noise temperature T_A'' is related to the antenna noise temperature T_A' through

$$T_A'' = \left(1 - \frac{1}{F_c}\right) T_A' + \frac{T_N'}{F_c}, \tag{6.79}$$

where F_c (≥ 1) is the coupling factor of the directional coupler. T_N' is the noise temperature of the injected noise at the input to the directional coupler and is given by

$$T_N' = \frac{T_N}{L} + \left(1 - \frac{1}{L}\right) T_0. \tag{6.80}$$

Combining the above three expressions leads to

$$L = \frac{T_N - T_0}{(F_c - 1)(T_0 - T_A')}. \tag{6.81}$$

The radiometer output indicator is the attenuator control voltage V_c. If V_c is scaled and linearized so that $V_c = 1/L$, then (6.81) becomes a linear relationship between V_c and T_A':

$$V_c = \frac{F_c - 1}{T_N - T_0}(T_0 - T_A'). \tag{6.82}$$

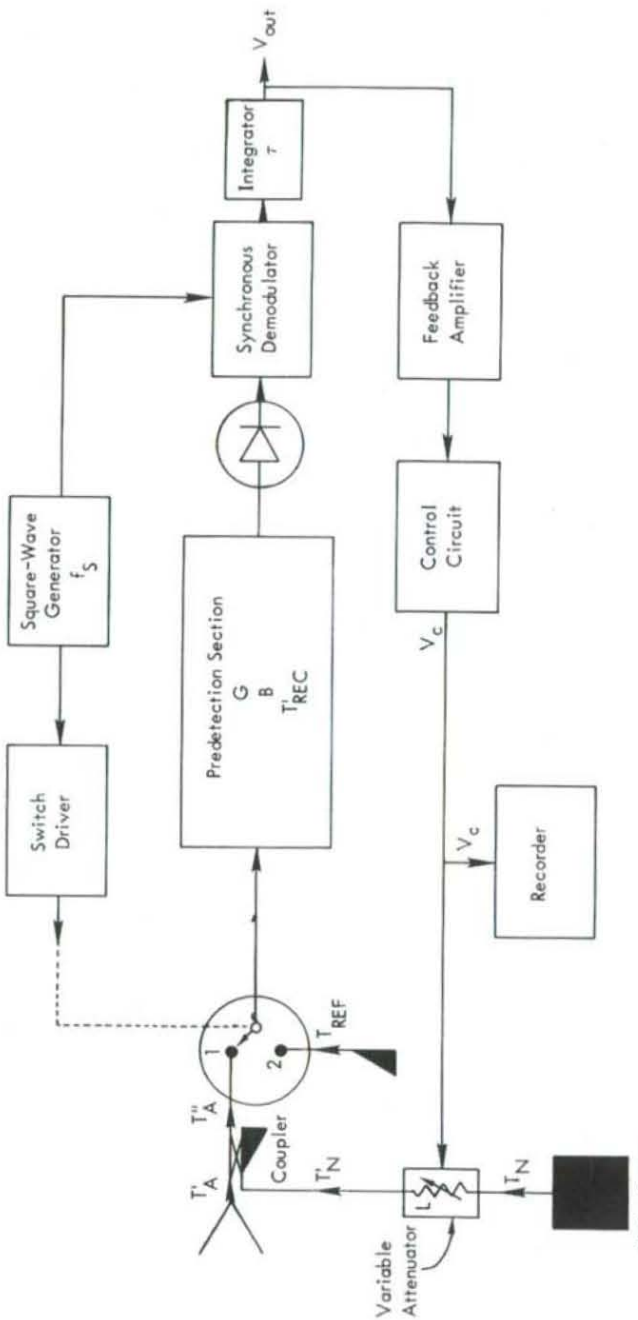

Fig. 6.17 Balanced Dicke radiometer using feedback to control the level of the injected noise temperature T'_N to maintain the condition $T''_A = T_{REF}$.

Suppose that the radiometer is specified to operate over the range 50 K $\leq T'_A \leq$ 300 K. Let us choose $T_0 = 310$ K, and let us use a 20-dB directional coupler ($F_c = 100$) and an avalanche noise diode having an output power noise temperature T_N of 50,000 K. From (6.81), L has to vary between 1.9 ($\simeq$2.9 dB) and 50 ($\simeq$17 dB) to cover the specified temperature range. This dynamic range of 14.1 dB can easily be accommodated by a *PIN* diode attenuator, which is a current-driven device capable of more than 40 dB in linear dynamic range. The minimum loss factor (usually called insertion loss) of a *PIN* diode typically is about 2 dB. Thus, the values chosen for T_0, F_c, and T_N result in a range of values for L that is compatible with the capabilities of a *PIN* diode. Had we chosen T_0 to be exactly equal to $T'_A(\max) = 300$ K rather than 310 K, L would have had to have been infinite to produce null balancing.

Since the noise temperature seen by the input switch is always equal to T_0, the sensitivity is given by (6.75) with $T'_A = T_0$,

$$\Delta T = \frac{2(T_0 + T'_{REC})}{\sqrt{B\tau}}. \tag{6.83}$$

6-10.3 Pulsed Noise-Injection Method

Diode attenuators are most stable in their extreme ON and OFF states. When operated in only one or the other of these two states (by controlling the magnitude and polarity of the bias voltage), a *PIN* diode attenuator becomes an ON/OFF switch; in the ON position it causes minimum attenuation ($\simeq$2.0 dB), and in the OFF position it causes maximum attenuation (typically 60 dB). Use is made of this diode property in the configuration shown in Fig. 6.18 (Hardy et al., 1974), which basically is the same as that shown in Fig. 6.17 except that now the injected noise is generated in the form of narrow rectangular pulses rather than continuously. The feedback control circuit drives a voltage-controlled oscillator (VCO), which in turn drives a pulse generator. The output of the pulse generator consists of narrow rectangular pulses, each of length τ_p, with a repetition period $\tau_R = 1/f_R$, where f_R is the pulse repetition frequency (Fig. 6.19). When the diode switch is in the OFF position (no pulse), we have maximum attenuation which, in effect, masks the noise generated by the noise diode. The resultant value of T'_N is designated T'_{OFF}, and when the *PIN* diode is switched by a pulse to its ON position, we have minimum attenuation, or a large value of T'_N which we shall designate T'_{ON}. Thus, over a repetition period τ_R

$$T'_N = \begin{cases} T'_{ON} & \text{for } 0 \leq t \leq \tau_p, \\ T'_{OFF} & \text{for } \tau_p \leq t \leq \tau_R. \end{cases} \tag{6.84}$$

The pulse repetition frequency f_R should be much higher than f_s, the square-wave modulation frequency of the input switch, so that many pulses are

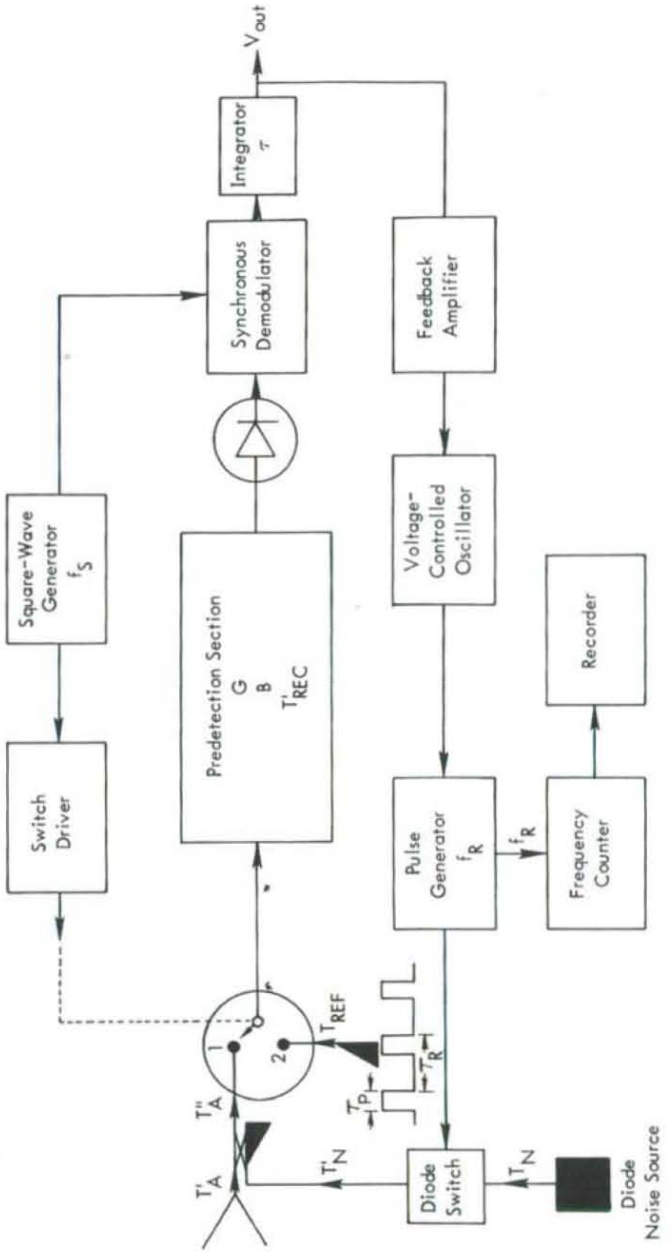

Fig. 6.18 Balanced Dicke radiometer, using pulsed noise-injection to maintain $T''_A = T_{REF}$. The output indicator of T'_A is the pulse repetition frequency f_R.

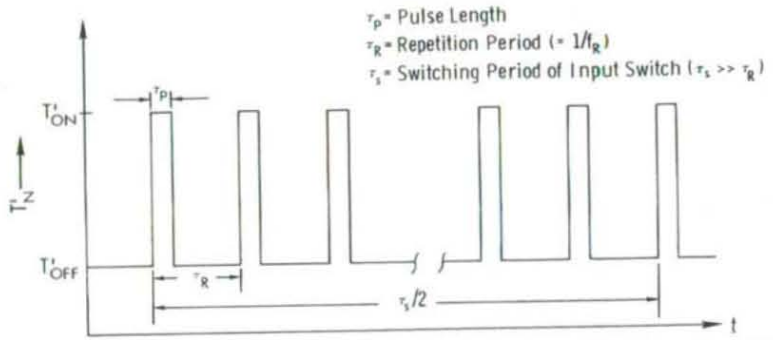

Fig. 6.19 Timing diagram showing the ON and OFF states of the noise temperature T'_N that is injected through the directional coupler of Fig. 6.18.

generated during the period $\tau_s/2$. The average value of T'_N is

$$\bar{T}'_N = \tau_p f_R T'_{ON} + (1 - \tau_p f_R) T'_{OFF}, \tag{6.85}$$

where $\tau_p f_R$ is the total time, during one second, that the diode switch is ON.

If τ_p is kept constant, f_R can be controlled by the feedback loop to provide the necessary value of $\bar{T}'_N$ to inject into the antenna port (via the directional coupler) so that a null condition always is maintained at the integrator output. The radiometer output indicator is a frequency counter that measures f_R, which is linearly related to T'_A by

$$f_R = \frac{(F_c T_0 - T'_{OFF}) - (F_c - 1) T'_A}{\tau_p (T'_{ON} - T'_{OFF})} \tag{6.86}$$

through the use of (6.78), (6.79), and (6.85). If during its OFF position, the attenuator loss factor is high enough to reduce the noise-diode contribution to a negligible value, then T'_{OFF} becomes approximately equal to T_0, and (6.86) reduces to

$$f_R = \frac{(F_c - 1)(T_0 - T'_A)}{\tau_p (T'_{ON} - T_0)}. \tag{6.87}$$

Since T_0 is known, it is sufficient to measure f_R at one value of a known noise temperature of a calibration source in order to determine the value of the quantity multiplying $T_0 - T'_A$ in (6.87). The radiometric sensitivity of this type of radiometer is given by (6.83).

The parameters of a 2.65-GHz pulsed noise-injection Dicke radiometer are listed in Table 6.2. The system was developed as a satellite prototype sensor for measuring the surface temperature of the ocean (Hardy et al., 1974).

TABLE 6.2
2.65-GHz Satellite Prototype Ocean-Temperature Sensing Radiometer Using Pulsed Noise-Injection Scheme[a]

Antenna:	
Antenna type	Multimode Pyramidal horn
Aperture size	35.6 cm × 35.6 cm
Beam efficiency	98%
Polarization	Circular
Radiometer:	
Center Frequency	2.65 GHz
Predetection bandwidth	100 MHz
Receiver noise temperature	60 K
Switching frequency	50 Hz
Diode excess noise	36 dB
Pulse width	40 μs
Pulse-generator frequency range	0–12 kHz
ΔT_{min} for 1-s integration time	0.15 K

[a]From Hardy et al. (1974).

6-10.4 Gain-Modulation Method

The balanced condition was realized in the methods considered thus far by adjusting the noise temperature of the reference channel to equal the noise temperature of the antenna channel, or vice versa, at the input switch. Another way to effect balance is by modulating the gain of the IF output voltage prior to the square-law detector. In the configuration shown in Fig. 6.20 (Orhaug and Waltman, 1962), the modulation consists of switching the IF output between a constant attenuator and a variable attenuator for the alternate half cycles of the input switch. The attenuator switch is driven by the switch-driver in synchronism with the input switch. The function of the feedback loop is to control the variable attenuator so that its output voltage (corresponding to the reference channel) is equal to the output voltage of the fixed attenuator (corresponding to the antenna channel). That is, if the loss factor of the variable attenuator, L_v, is adjusted to maintain the condition

$$\frac{1}{L_0}(T'_A + T'_{REC}) = \frac{1}{L_v}(T_{REF} + T'_{REC}), \tag{6.88}$$

then the dc value of the output voltage will be zero. The system is calibrated by relating the control voltage V_c to the noise temperature of a calibration noise source replacing the antenna. If the voltage V_c is scaled and linearized so that $V_c = 1/L_v$, then V_c becomes linearly related to T'_A:

$$V_c = \frac{1}{L_0(T_{REF} + T'_{REC})}(T'_A + T'_{REC}). \tag{6.89}$$

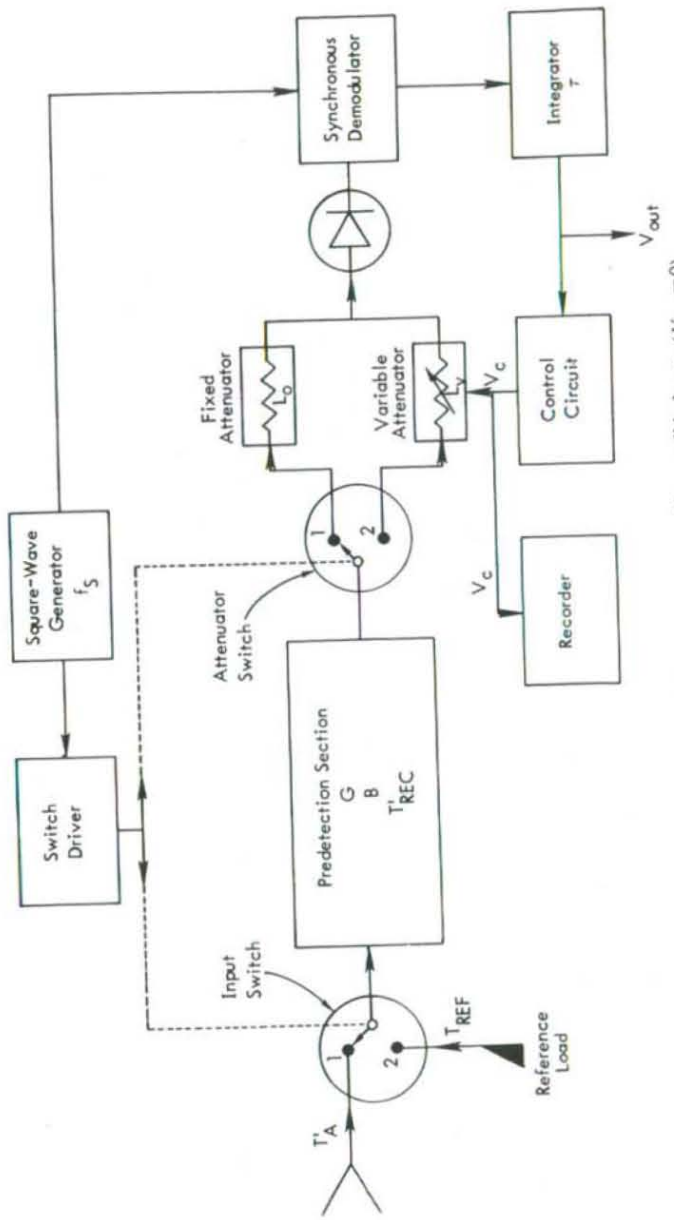

Fig. 6.20 Dicke radiometer using gain modulation of the IF output to achieve null balance ($V_{out} = 0$).

Conceptually, the gain modulation may be applied before or after the mixer, but in practice it is easier to control the loss factor (or gain) of a device operating in the IF frequency range than to control a microwave device.

One drawback of the gain-modulation technique is that slow variations in the receiver noise temperature T'_{REC} (between calibrations) result in a measurement error of the absolute value of T'_A. This is due to the dependence of V_c on T'_{REC}. In contrast, the techniques employing temperature control to balance the radiometer are insensitive to drifts in T'_{REC}. Another limitation of the gain-modulation technique pertains to the amplitude of the gain modulation, L_v/L_0. If this factor is large, the gain modulation is liable to produce excessive output fluctuations. Thus, for low-noise receivers (relatively small T'_{REC}), the gain-modulation method is useful over a narrow range of the difference $T'_{REC} - T'_A$.

6-11 AUTOMATIC-GAIN-CONTROL (AGC) TECHNIQUES

Automatic gain control (AGC) is a feedback technique used for stabilizing the gain of receiver systems. In continuous AGC, the output voltage of the receiver is compared with a reference voltage on a continuous basis, and the difference between the two voltages is used to adjust the gain of the receiver so that the output voltage is maintained at a constant level. Continuous AGC is inapplicable to radiometer receivers because the AGC action removes all variations, including those due to the signal (T'_A) that the radiometer is intended to measure. To eliminate the dependence of the AGC voltage on the antenna temperature, Seling (1964) introduced the *sampled*-AGC technique in which the detector output voltage is monitored by the AGC feedback circuit during only the half cycles (of the square-wave Dicke switching period) for which the Dicke switch is connected to the (constant-temperature) reference load. Successful operation of the sampled-AGC technique depends upon meeting certain constraints that dictate the choice of the AGC bandwidth, as discussed by Seling (1964).

The sampled-AGC technique shares a drawback with the gain-modulated radiometer (Section 6-10.4) in that slow variations in the receiver noise temperature (between calibrations) are compensated for as if they were gain variations, thereby introducing a bias error in the measurement accuracy of T'_A.

The sampled-AGC approach was extended by Hach (1966, 1968), who developed the *two-reference-temperature AGC radiometer* shown in Fig. 6.21. This radiometer has several attractive features: (1) insensitivity to system gain variations, (2) insensitivity to receiver noise-temperature variations, and (3) the ability to provide continuous calibration. Hach's concept was adopted by General Electric (1973) in the construction of the radiometer section of the RADSCAT system that was flown aboard the Skylab satellite in 1973. A list of the RADSCAT radiometer parameters is given in Table 6.3.

The discussion that follows is based on the papers by Hach (1966, 1968), to which the reader is referred for details. Other than differences in notation,

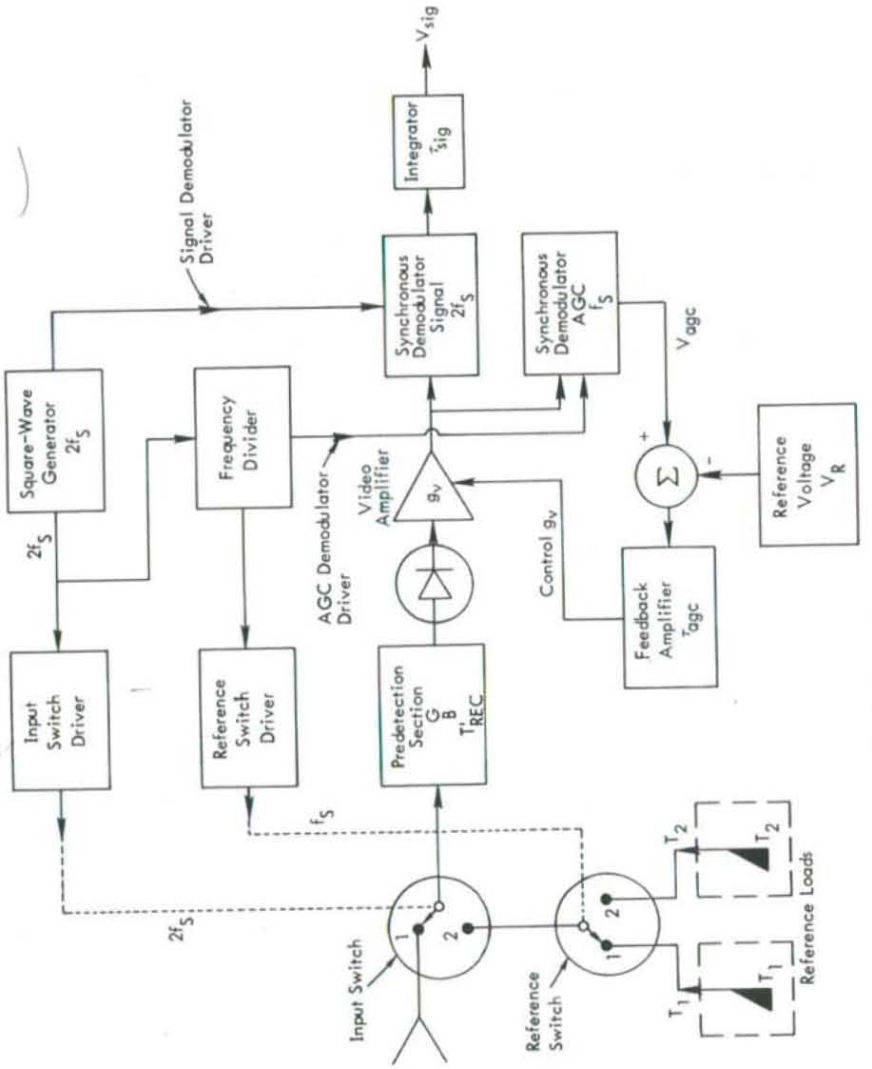

Fig. 6.21 Hach radiometer (block diagram).

TABLE 6.3
Radiometer Section of Skylab's RADSCAT[a]

Antenna:	
Antenna type	Parabolic reflector
Reflector diameter	114 cm
Half-power beamwidth	1.5°
Beam efficiency	90%
Antenna loss	0.3 dB
Polarization	Horizontal and vertical
Radiometer:	
Center frequency	13.9 GHz
Predetection half-power bandwidth	210 MHz
Receiver noise temperature	1195 K
Comparison temperatures	318 and 393 K
Switching frequency	996 Hz
Video amplifier gain	42 ± 4 dB
AGC integration time-constant	0.9 s
ΔT_{min} for integration time:	
32 ms	1.15 K
128 ms	0.6 K
256 ms	0.425 K

[a]General Electric Space Systems Division (1973).

the only notable difference is that we shall assume the switches to have such a short switching time constant, compared to the switching periods, that switching between ports may be assumed to be essentially instantaneous. Hach's treatment is more general in that it takes into account the effects of the nonzero switching time constant on the radiometer signals, although the final results are the same as those obtained assuming zero switching time constant.

The two-reference-temperature radiometer shown in Fig. 6.21 uses two RF switches: an input switch which connects the receiver to either the antenna port or to the reference port, and a reference switch which connects the input switch to one or the other of two reference noise sources (loads) with constant noise temperatures T_1 and T_2. The switching frequency of the input switch is $2f_s$, and it is exactly twice the switching frequency of the reference switch. Both switching waveforms are generated by the same square-wave generator of frequency $2f_s$, with the addition of a frequency divider prior to the reference-switch driver.

With reference to the switching sequences shown in Fig. 6.22(a) and (b), the output voltage of the square-law detector (Fig. 6.22(c)) is given by

$$V_d(t) = C_d G k B \begin{cases} (T_A' + T_{REC}') & \text{for } 0 \leq t \leq \frac{1}{4}\tau_s, \\ (T_2 + T_{REC}') & \text{for } \frac{1}{4}\tau_s \leq t \leq \frac{1}{2}\tau_s, \\ (T_A' + T_{REC}') & \text{for } \frac{1}{2}\tau_s \leq t \leq \frac{3}{4}\tau_s, \\ (T_1 + T_{REC}') & \text{for } \frac{3}{4}\tau_s \leq t \leq \tau_s, \end{cases} \tag{6.90}$$

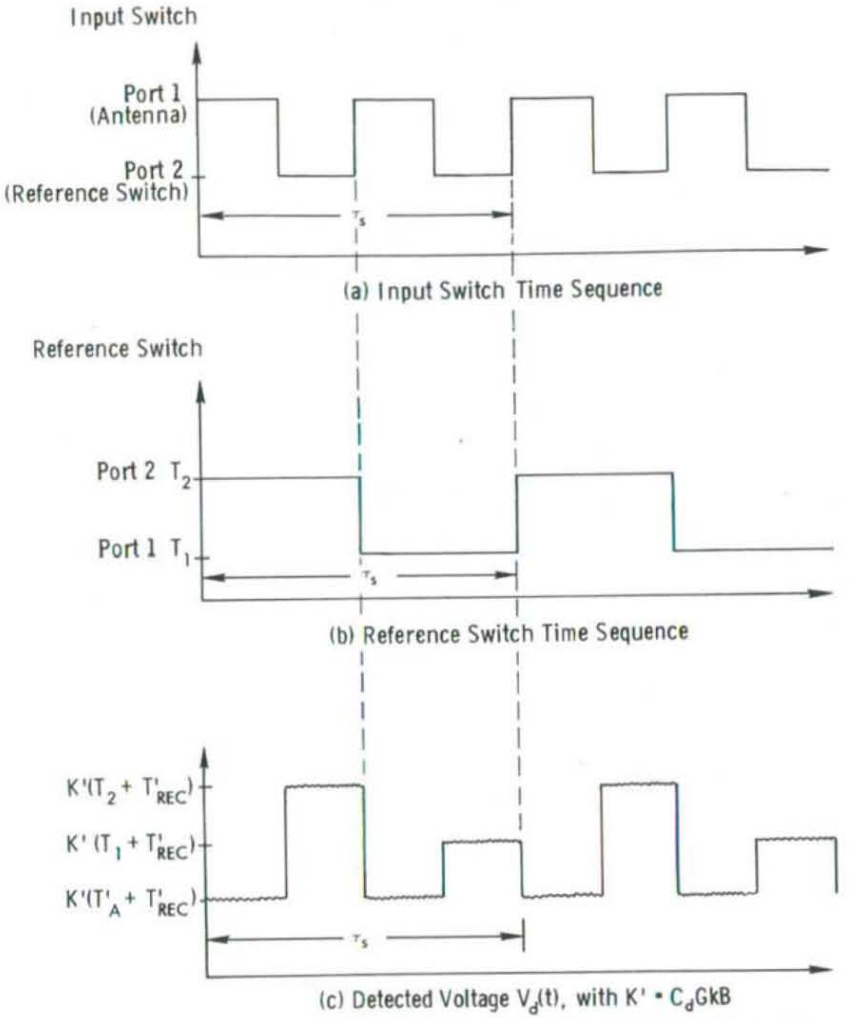

Fig. 6.22 Switching sequences of (a) input switch, (b) reference switch, and (c) square-law-detector output of Hach radiometer.

where τ_s $(=1/f_s)$ is the period of one switching cycle of the reference switch. The components due to noise and gain fluctuations have been ignored, since they will effectively be filtered out by the signal or AGC integrators.

The square-law detector is followed by an ac-coupled video amplifier with controllable voltage gain g_v and a rectangular passband that should extend from about $0.01f_s$ to $10f_s$ (Hach, 1968) in order to preserve the relative phase between the fundamental wave at f_s and the first harmonic at $2f_s$. The output voltage of the ac-coupled video amplifier is

$$V_v(t) = g_v\left[V_d(t) - \bar{V}_d\right]. \tag{6.91}$$

$\overline{V}_d$, the dc value of $V_d(t)$, is equal to one-quarter the sum of the four components given in (6.90), or

$$\overline{V}_d = K_0(2T'_A + T_1 + T_2 + 4T'_{REC}), \tag{6.92}$$

where

$$K_0 \triangleq C_d G k B/4. \tag{6.93}$$

Inserting (6.90) and (6.92) into (6.91) leads to

$$V_v(t) = K_0 g_v \begin{cases} (2T'_A - T_1 - T_2) & \text{for } 0 \leq t \leq \frac{1}{4}\tau_s, \\ (3T_2 - T_1 - 2T'_A) & \text{for } \frac{1}{4}\tau_s \leq t \leq \frac{1}{2}\tau_s, \\ (2T'_A - T_1 - T_2) & \text{for } \frac{1}{2}\tau_s \leq t \leq \frac{3}{4}\tau_s, \\ (3T_1 - T_2 - 2T'_A) & \text{for } \frac{3}{4}\tau_s \leq t \leq \tau_s. \end{cases} \tag{6.94}$$

$V_v(t)$ serves as the input waveform to each of two synchronous demodulators (detectors): the AGC demodulator and the signal demodulator. The AGC synchronous demodulator is followed by a low-pass filter (integrator) with integration time τ_{agc} (the reference voltage V_R of Fig. 6.21 may be ignored for the time being), and similarly, the signal demodulator is followed by a filter with integration time τ_{sig}. The integrators are, of course, used to filter out the noise and system-gain fluctuations, and therefore their bandwidths are of prime importance to the radiometric sensitivity ΔT, as discussed later. The total voltage gain of the AGC synchronous demodulator-integrator is designated g_{agc}, and g_{sig} is defined similarly for the signal branch.

The AGC demodulator-integrator branch demodulates $V_v(t)$ at the reference frequency f_s. The average value of its output voltage is

$$\overline{V}_{agc} = \frac{g_{agc}}{\tau_s}\left[\int_0^{\tau_s/2} V_v(t)\,dt - \int_{\tau_s/2}^{\tau} V_v(t)\,dt\right], \tag{6.95}$$

which, upon inserting (6.94), leads to

$$\overline{V}_{agc} = K_0 g_v g_{agc}(T_2 - T_1). \tag{6.96}$$

The signal demodulator-integrator branch performs a similar function, except that its reference frequency is $2f_s$. Hence, its output voltage is given by

$$\overline{V}_{sig} = \frac{g_{sig}}{\tau_s}\left[\int_0^{\frac{1}{4}\tau_s} V_v(t)\,dt - \int_{\frac{1}{4}\tau_s}^{\frac{1}{2}\tau_s} V_v(t)\,dt + \int_{\frac{1}{2}\tau_s}^{\frac{3}{4}\tau_s} V_v(t)\,dt - \int_{\frac{3}{4}\tau_s}^{\tau_s} V_v(t)\,dt\right], \tag{6.97}$$

which yields

$$\overline{V}_{sig} = K_0 g_v g_{sig}(2T'_A - T_1 - T_2). \tag{6.98}$$

Before we proceed further, it is worth noting the following observations:

1. Both output voltages, $\overline{V}_{agc}$ and $\overline{V}_{sig}$, are independent of the receiver noise temperature T'_{REC}. This is due to the ac coupling of the video amplifier.
2. Both output voltages are directly proportional to the factor $K_0 g_v$ ($= C_d G k B g_v/4$), which contains all the RF parameters that give rise to the system gain. Hence, the ratio V_{sig}/V_{agc} is independent of system gain variations.

The two-reference-temperature Dicke radiometer may be operated in either of two modes. The first mode consists of measuring $\overline{V}_{sig}$ and $\overline{V}_{agc}$ separately and then forming the ratio

$$\frac{\overline{V}_{sig}}{\overline{V}_{agc}} = \frac{g_{sig}}{g_{agc}}\,\frac{2T'_A - T_1 - T_2}{T_2 - T_1}, \tag{6.99}$$

from which T'_A can be determined. The measurement accuracy of T'_A depends on the stability of the reference temperatures T_1 and T_2, which, in practice, can be maintained constant to within a fraction of a kelvin. Since g_{sig} and g_{agc} are low-frequency parameters, they can be maintained at essentially constant levels. In this first mode, the gain of the video amplifier is kept constant also.

The second mode of operation uses the AGC output voltage $\overline{V}_{agc}$ to drive a feedback loop. Since $\overline{V}_{agc}$ is independent of T'_A and T'_{REC}, and since T_1 and T_2 are maintained constant, changes in $\overline{V}_{agc}$ are due to variations in the receiver parameters. Such changes can be compensated for by controlling the video-amplifier gain with a feedback loop. After experimentally measuring $\overline{V}_{agc}$ without feedback, the measured value (call it V_R) then is used to set the voltage level of a reference dc voltage source.

With $\overline{V}_{agc}$ maintained equal to V_R by the feedback loop, the ratio of (6.98) to (6.96) yields

$$\overline{V}_{sig} = \frac{V_R g_{sig}}{g_{agc}}\left(\frac{2T'_A - T_1 - T_2}{T_2 - T_1}\right), \tag{6.100}$$

from which the following expression for T'_A is obtained:

$$T'_A = \frac{1}{2}\left[\overline{V}_{sig}\left(\frac{g_{agc}}{V_R g_{sig}}\right)(T_2 - T_1) + (T_2 + T_1)\right]. \tag{6.101}$$

The radiometric sensitivity ΔT is given by (Hach, 1968)

$$\Delta T = \frac{1}{\sqrt{B\tau_{sig}}} \left\{ \left[1 + \left(\frac{1}{1+\tau_{agc}/\tau_{sig}} \right) \left(\frac{T_2 + T_1 - 2T'_A}{T_2 - T_1} \right)^2 \right] \times \left[(T_2 + T'_{REC})^2 + (T_1 + T'_{REC})^2 + 2(T'_A + T'_{REC})^2 \right] \right\}^{1/2} \tag{6.102}$$

where τ_{agc} and τ_{sig} are the integration times (not time constants) of the AGC and signal channels, respectively. For comparison purposes, the ratio of ΔT as given by (6.102) to ΔT of the balanced Dicke radiometer (Eq. (6.75)) is shown in Fig. 6.23 as a function of T'_A for several values of the ratio τ_{agc}/τ_{sig}. The values used for T_2, T_1, and T'_{REC} are 393, 318, and 1200 K, respectively (see Table 6.3).

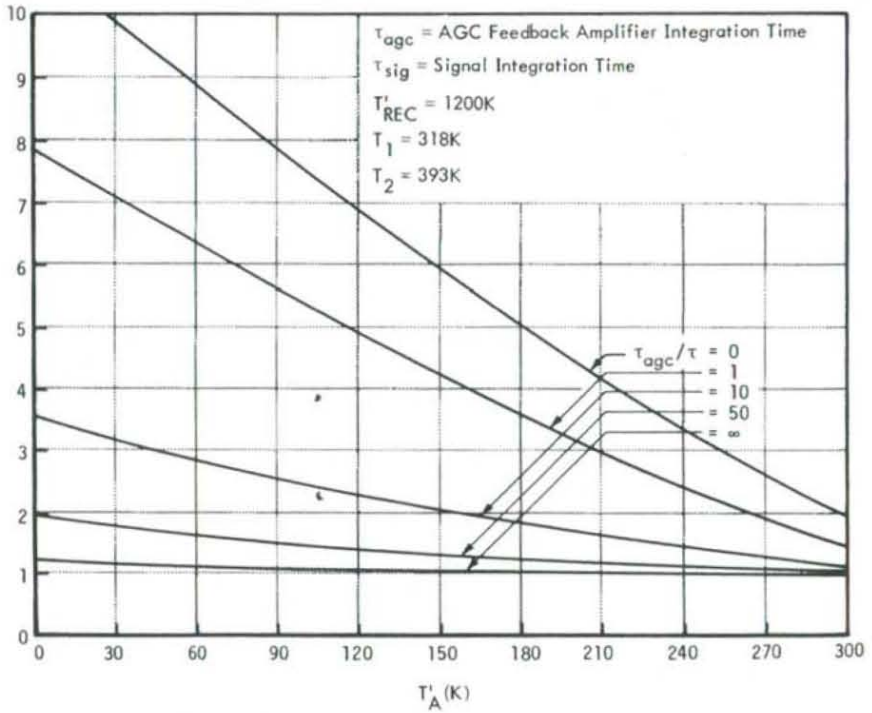

Fig. 6.23 Ratio of the radiometric resolution ΔT(Hach) as given by (6.102) to the radiometric resolution of the balanced Dicke radiometer, ΔT(Dicke), as given by (6.75), plotted as a function of T'_A for several values of τ_{agc}/τ_{sig}. Both types of radiometers are assumed to have the same bandwidth B and signal integration time τ_{sig} (or τ in (6.75)). The values used for T_1, T_2, and T'_{REC} are from Table 6.3.

6-12 NOISE-ADDING RADIOMETER

The noise-adding radiometer (Ohm and Snell, 1963; Batelaan et al., 1974) removes the effects of gain variations, but without the use of a Dicke switch. Square-wave noise is coupled into the receiver input from a noise diode driven by a constant-rate square-wave generator, as shown in Fig. 6.24. The output voltage of the square-law detector is synchronously detected (demodulated) at the same rate, and a voltage ratio Y is formed, whose average value is given by

$$\overline{Y} = \frac{\overline{V}_1}{\overline{V}_2 - \overline{V}_1} = \frac{T'_A + T'_{REC}}{T''_N}, \tag{6.103}$$

where $\overline{V}_1, \overline{V}_2$ = average square-law detector output voltage corresponding to the half cycle (of the switching period) during which the noise diode is OFF and ON, respectively,
T''_N = added noise to receiver input during the diode ON half cycle.

The ratio meter is followed by a low-pass filter to reduce noise fluctuations. For a unity-gain low-pass filter, we have

$$\overline{V}_{out} = \overline{Y} = (T'_A + T'_{REC})/T''_N. \tag{6.104}$$

The measurement accuracy of T'_A is independent of system gain variations, but it is linked directly to the stability of the receiver noise temperature T'_{REC} and to the excess noise temperature T''_N.

The theoretical sensitivity of the noise-adding radiometer is given by (Batelaan et al., 1974)

$$\Delta T = \frac{2(T'_A + T'_{REC})}{\sqrt{B\tau}} \left[1 + \frac{(T'_A + T'_{REC})}{T''_N} \right]. \tag{6.105}$$

The quantity multiplying the square bracket is recognized as twice the radiometric sensitivity of the ideal radiometer. Hence,

$$\Delta T(\text{noise-adding}) = 2\Delta T_{IDEAL} \left[1 + \frac{T_{SYS}}{T''_N} \right].$$

The absence of an input switch is an attractive feature of the noise-adding radiometer, particularly in low-noise receivers. A Dicke switch usually adds about 7–75 K to the receiver noise temperature T'_{REC}. In star-tracking and astronomical research, the brightness temperature of some targets may be only a few kelvins, which necessitates the use of low-noise receivers with noise temperatures of the order of a few tens of kelvins in order to achieve radiometric sensitivities of the order of 0.01–0.1 K. For such cases, the absence of an input switch becomes a significant factor.

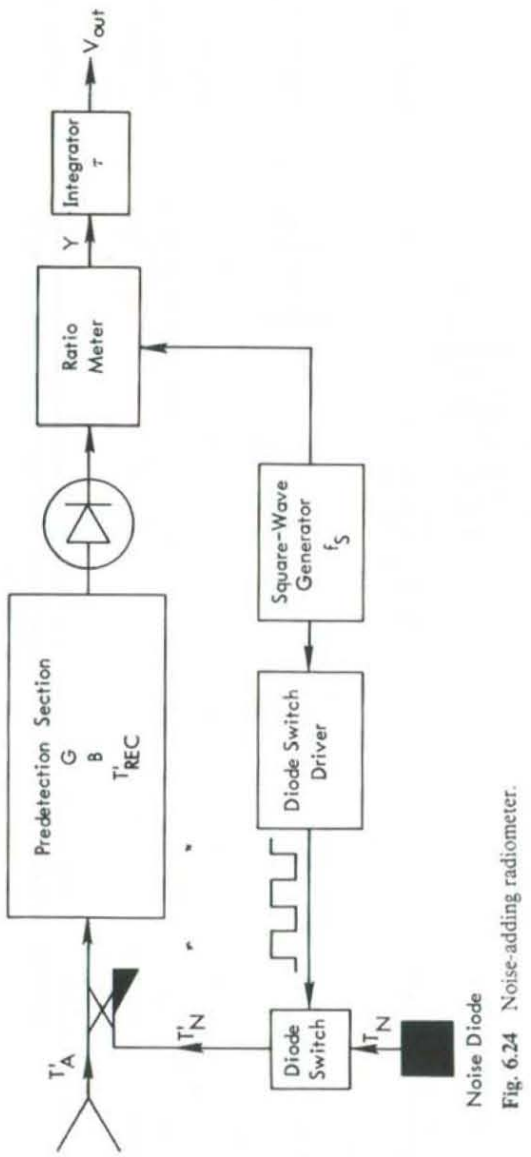

Fig. 6.24 Noise-adding radiometer.

6-13 OTHER TYPES OF RADIOMETERS

The radiometric techniques considered in the previous sections are those commonly used in microwave remote sensing. Other types of receivers also have been reported in the literature, primarily for use in radio astronomy. Among these are the interferometer receiver (Wesseling, 1967; Clark, 1968), the correlation receiver (Blum, 1959; Batchelor et al., 1968), and the Graham receiver (Graham, 1958), as well as receiver configurations that are hybrids of two or more techniques.

Most radiometer receivers use wide bandwidths and long integration times to achieve good radiometric resolutions. In some cases, however, the information being sought is contained in the spectral and/or temporal variation of the incoming radiation. Measurements of the emission spectra of spectral lines often require receiver systems with spectral resolutions of the order of 1–100 kHz. Such measurements usually are made using tunable spectrometers, multichannel spectrometers, or autocorrelation spectrometers (Price, 1976). Good temporal resolution is essential in observations of solar events, some of which are only a few milliseconds long, and in radio observations of pulsars. The emission from a pulsar consists of narrow pulses that occur at a regular interval, typically between 0.5 and 1.5 s (Manchester, 1973). The pulse width usually is of the order of 5 percent of the pulse repetition period, and the pulse substructure sometimes may be as short as 8 μs (Hankins, 1972). Techniques developed for observations of pulsars with high temporal and spectral resolutions are described by Huguenin (1976).

6-14 SUMMARY OF RADIOMETER PROPERTIES

For easy reference, Table 6.4 provides a summary of the input-output relationship and of the radiometric sensitivity for most of the receiver configurations discussed in the previous sections. The output indication I_{out} is related linearly to the antenna radiometric temperature T'_A through

$$I_{out} = a(T'_A + b), \tag{6.106}$$

where a and b are constants and I_{out} is either V_{out} (integrator output voltage), V_c (control voltage), or f_R (pulse-repetition frequency).

Since, in general, the radiometric sensitivity ΔT is a function of T'_A, Table 7.4 considers ΔT for each of two values of T'_A, namely, $T'_A = 0$ K and $T'_A = T_0$, where T_0 ($\simeq 310$ K) is the environmental temperature of the radiometer front end. In both cases, ΔT is normalized to ΔT_{IDEAL}, the sensitivity of the ideal total-power radiometer, which is given by (6.53),

$$\Delta T_{IDEAL} = \frac{T'_A + T'_{REC}}{\sqrt{B\tau}}. \tag{6.53}$$

6-15 PRACTICAL CONSIDERATIONS

Radiometer performance is measured in terms of measurement accuracy and precision, both of which are determined (in practice) by the RF portion of the radiometer. Although some mention of practical details was made occasionally in the preceding sections, most systems and devices were described in terms of their intended (ideal) functions, with little or no description of their operational characteristics. This section is intended to provide the reader with an overview of the factors that should be considered in the design of microwave radiometer systems.

Perhaps the single most important parameter that determines the performance (and/or cost) of a microwave radiometer is its frequency. Generally speaking, the noise performance and stability of microwave devices and systems decrease with increasing frequency, as does the number of available types of devices that can perform a certain function. For example, in present-day technology, a 100 K receiver noise temperature is fairly easy to achieve at 1 GHz using an uncooled field-effect-transistor (FET) RF amplifier. At 30 GHz, a 500-K receiver noise temperature is considered state-of-the-art (without cryogenic cooling), and the cost of such a receiver typically is an order of magnitude higher than that of the 1-GHz receiver. These figures soon will be out of date, however, because the field of microwave semiconductor and solid-state devices is moving at a tremendous rate, as illustrated by the example shown in Fig. 6.25. In 1968, solid-state amplifiers were limited to frequencies below 500 MHz and consisted primarily of bipolar transistor amplifiers. Most microwave receivers used traveling-wave-tube (TWT) amplifiers. The rapid development of the FET in the late sixties and early seventies brought about a revolution in microwave amplifiers; solid-state amplifiers began to and have continued to replace TWT amplifiers. In addition to the FET, several semiconductor devices also were developed in this timeperiod, including the tunnel, Gunn, and IMPATT diodes, among others. Kennedy (1978), the author of Fig. 6.25, projects the status of transistor-amplifier performance into the year 2000, at which time it is predicted (according to Fig. 6.25) that a similar performance will be attainable at 100 GHz to that attained at 0.1 GHz in 1968.

6-15.1 Dicke Input Switch

The purpose of the input switch is to switch the receiver periodically between the antenna and the reference load at a high enough rate that the system-gain remains essentially constant over a period of one cycle. In other words, in order to successfully subtract out system-gain variations in the synchronous demodulation, the switching rate f_s should be higher than the highest significant frequency in the system-gain variation spectrum. As was noted earlier, although no detailed studies have been conducted of the variation spectrum, its upper limit usually is assumed to be around 10 Hz. Another constraint on the lower limit of f_s is set by the effective bandwidth of the low-pass filter, B_{LF}. To

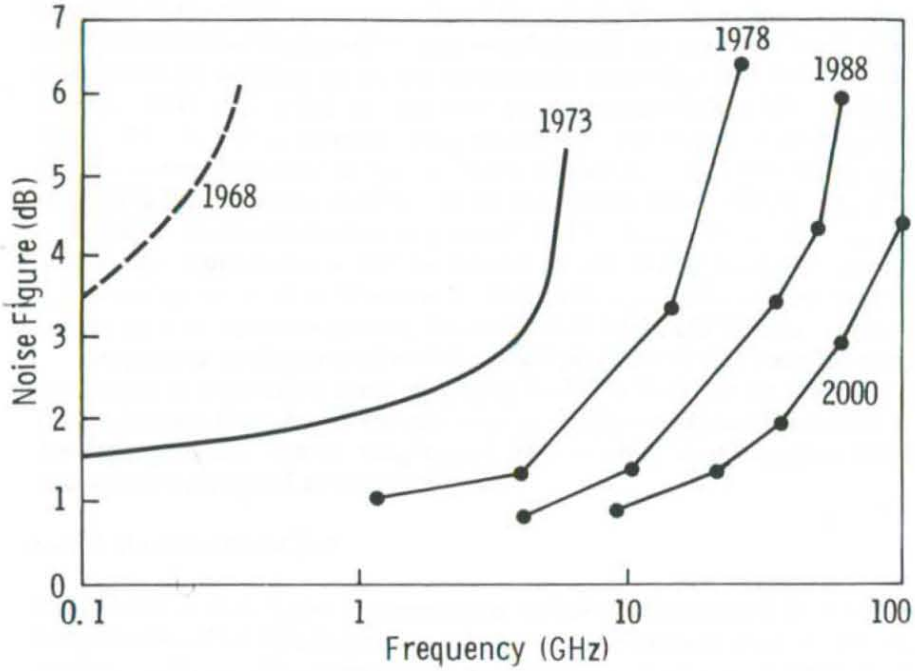

Fig. 6.25 Noise figure of narrow-band transistor amplifiers as a function of frequency and time (Kennedy, 1978).

satisfy the sampling theorem, we must have $f_s > 2B_{LF}$. Integration times τ $(=1/(2B_{LF}))$ used in ground-based radiometer systems typically are around 1 s, which corresponds to $B_{LF} = 0.5$ Hz, or $f_s > 1$ Hz. However, airborne and spaceborne imaging systems often use integration times as short as 30 ms, which means that $f_s > 2B_{LF} = 1/\tau \simeq 33$ Hz.

The upper limit of f_s usually is governed by the switching time τ_{sw}. To avoid the effects of switching time on the square-wave shape of the radiometer signal, it usually is recommended that

$$\frac{2\tau_{sw}}{\tau_s} < 10^{-2}, \tag{6.107}$$

where τ_s is the switching period. Electronically controlled microwave switches generally are one of two types: (1) semiconductor diode switches and (2) ferrite circulators (Table 6.5). The most commonly used diode switch is the *PIN* single-pole double-throw (SPDT) switch, whose switching-time is typically between 10 and 200 ns. Ferrite circulators are slower switching devices, with τ_{sw}-values in the 1–10-μs range. For $\tau_{sw} = 10$ μs, (6.107) is equivalent to $f_s < 500$ Hz. Most Dicke radiometers are operated at switching frequencies in the 10–1000-Hz range.

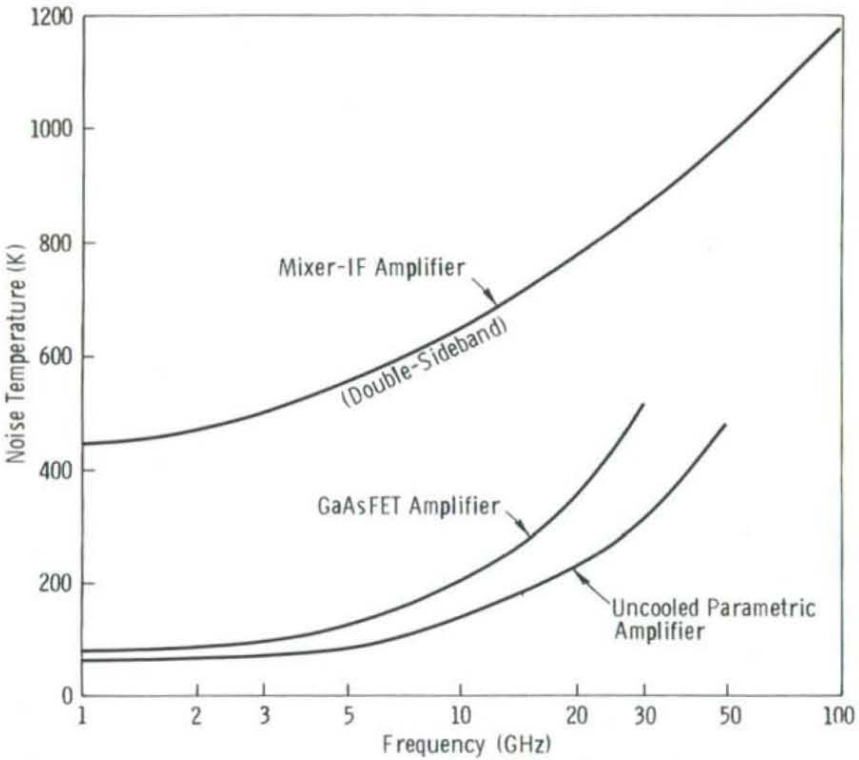

Fig. 6.26 Typical noise performance of commercially available parametric amplifiers, FET amplifiers, and mixer-preamplifier assemblies. Operating bandwidth is typically 10 percent of RF frequency for $f<20$ GHz, and between 0.1 and 2 GHz for $f>20$ GHz.

For state-of-the-art reviews, the reader is referred to the paper by Kennedy (1978), which provides a review of the development of microwave semiconductor and solid-state devices; to the paper by Sterzer (1978) on FET devices; and to the papers by Kerr (1975, 1979) on microwave mixers. Mixer design and noise performance at frequencies above 100 GHz are discussed by Held (1979).

6-15.3 Noise Sources and Reference Loads

Basically, there are two types of noise sources available for calibration and balancing and as reference sources: (1) passive sources and (2) active sources.

Passive Noise Sources

Any device or component that delivers noise power at a constant level without the use of external (electric) power may be defined as a passive noise source. The simplest passive noise source is a matched load. When maintained at a constant physical temperature T_p, it delivers an average noise power with an

equivalent noise temperature equal to its physical temperature. Matched loads are used as reference loads and usually are maintained at temperatures higher than the highest expected environmental temperature of the radiometer by enclosing them in a temperature-stabilized oven. To avoid temperature mismatches, it is sound engineering practice to include the entire front-end of the radiometer in a common temperature enclosure.

Matched loads also are used for calibration, whereby either the antenna is (physically) replaced by a load, or the radiometer is switched to a load via a calibration switch placed as close to the antenna as possible. Low noise-temperature values are obtained by immersing the load in a low-temperature medium such as liquid nitrogen or liquid helium, whose boiling temperatures are 77.4 and 4.2 K, respectively.

Active Noise Sources

Until the late 1960s, the gas-discharge tube was the most commonly used noise generator at frequencies above 1 GHz. Today, solid-state noise sources, primarily avalanche diodes, are available commercially up to 40 GHz.

The term commonly used to characterize the power delivered by a noise source is the *excess noise ratio*, ENR, which is defined as

$$\text{ENR} = \frac{P_n - P_0}{P_0} = \frac{\text{k}B(T_N - T_0)}{\text{k}BT_0}$$

$$= \frac{T_N}{T_0} - 1 \tag{6.110}$$

where T_N is the noise temperature of the source, and T_0 is its physical temperature. Often, ENR is expressed in dB,

$$\text{ENR(dB)} = 10 \log \text{ENR}. \tag{6.111}$$

Standard avalanche noise sources are available with excess-noise ratios of 35 dB at frequencies up to 12.4 GHz, and with lower levels at higher frequencies, typically 23 dB up to 40 GHz.

As was discussed earlier toward the end of Section 6-10.1, active noise sources may also be used to provide noise temperatures T_N that are lower than the ambient temperature T_0. Specifically, the COLDFET has been shown to have a noise temperature of 50 K at 1.4 GHz (Frater and Williams, 1981).

6-16 RADIOMETER CALIBRATION TECHNIQUES

Radiometer calibration may be divided into two steps. The first step involves relating the receiver output indication (voltage, count, deflection, etc.) to the noise temperature at the radiometer input. This usually is accomplished by

measuring the output indication as a function of the noise temperature T_{CAL} of a calibration source connected to the radiometer input (in place of the antenna). The resultant relationship between the output indicator and T_{CAL} provides the scale factors necessary for relating the output to the antenna temperature T_A' (when the radiometer receiver is connected to the antenna). We shall refer to this first step as *receiver calibration*.

The second step involves relating T_A' to the radiative properties of the scene under observation. T_A' consists of three components: (1) energy received through the antenna mainbeam, which is the quantity of interest; (2) energy received from directions outside the antenna mainbeam (sidelobe contributions); and (3) thermal energy emitted by the antenna structure itself. To evaluate the significance of the latter two components and to factor out (partially) their influence on T_A', it is necessary to know the radiative properties of the antenna with a high degree of accuracy. Standard test procedures have been defined for the measurement of antenna properties (IEEE, 1979), but for one of the properties of interest, namely the radiation efficiency η_l, the standard procedures do not provide (in practice) the level of accuracy that is desired for the application of radiometric corrections. Alternate measurement techniques that have been developed specifically for microwave radiometric applications are discussed in Section 6-16.3 under the heading "Antenna Calibration."

6-16.1 Receiver Calibration

Most radiometer receivers are linear systems in the sense that the output indication I_{out} is directly proportional to the antenna temperature T_A'. With reference to (6.106),

$$I_{out} = a(T_A' + b), \tag{6.106}$$

it is sufficient to measure I_{out} for each of two known values of T_A' to determine the constants a and b. For some radiometer configurations, the constant b is given in terms of known constant temperature(s); $b = -T_{REF} = -T_0$ for the three Dicke radiometer types given in Table 6.4, and $b = (T_2 - T_1)/2$ for the Hach radiometer, which uses two reference noise temperatures. In this case, one calibration measurement to determine the constant a is sufficient. In practice, however, it is advisable to calibrate the radiometer at more than one value of the input noise temperature, and at least one point should be for a c libration noise temperature lower than 100 K.

Figure 6.27 shows a calibration noise source placed at the radiometer input. Corresponding to measurements with calibration noise temperature T_{CAL}^h and T_{CAL}^c (where the superscripts h and c stand for hot and cold, respectively), the radiometer output indicator records values of

$$I_{out}^h = a(T_{CAL}^h + b), \tag{6.112a}$$

$$I_{out}^c = a(T_{CAL}^c + b). \tag{6.112b}$$

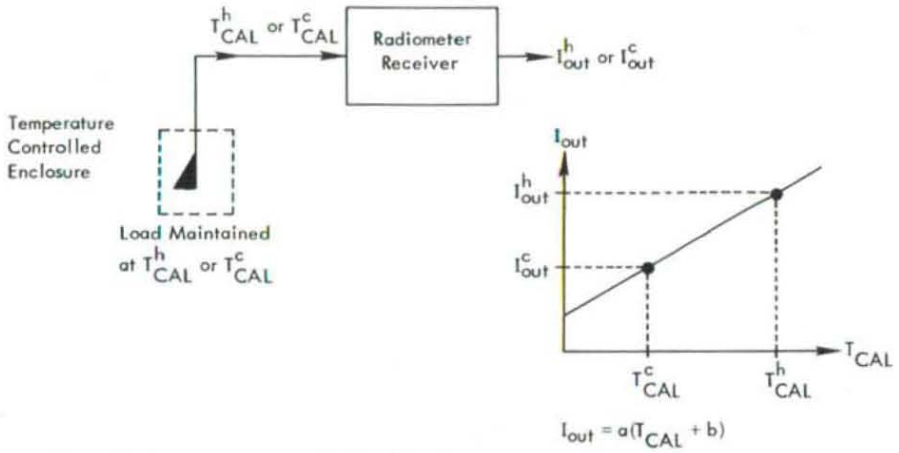

Fig. 6.27 Calibration of a reflection-free radiometer receiver.

The above two equations give the solutions

$$a = \frac{I_{out}^h - I_{out}^c}{T_{CAL}^h - T_{CAL}^c}, \tag{6.113a}$$

$$b = \frac{I_{out}^c T_{CAL}^h - I_{out}^h T_{CAL}^c}{I_{out}^h - I_{out}^c}. \tag{6.113b}$$

Three types of calibration noise sources have been used. The first type consists of a matched load (resistor) whose temperature may be held at a constant known value. A hot load usually is enclosed in a temperature-controlled oven, and a cold load usually is immersed in a Dewar flask containing a boiling cryogen. Liquid nitrogen (N_2), whose boiling temperature is 77.4 K at sea-level barometric pressure, is used commonly for this purpose.

The second type of calibration source consists of material with known emissivities, such as the highly absorbing, nonreflective materials used in anechoic chambers. These materials can be constructed to have emissivities close to unity, and therefore their brightness temperatures are approximately equal to their physical temperatures. Low brightness-temperature values are obtained by saturating the absorbing material in a boiling cryogen. The calibration procedure consists basically of observing the material with the antenna beam and then relating its emission to the noise temperature at the antenna terminals. The process involves the antenna properties, and therefore we defer discussing the details of the calibration procedure until the next section.

The above two receiver calibration methods usually are used to calibrate a radiometer before and/or after a measurement program only. If the matched-load method were to be used for periodic calibrations during an aircraft measurement mission, it would require the availability of a cryogen for the

duration of the flight, and, in spacecraft operations, refrigeration equipment would be needed to maintain the cryogenic fluid at the desired temperature. Radiometers employing balanced Dicke or Hach receiver configurations can be made sufficiently stable that calibration against external sources is needed only occasionally, thereby avoiding the cryogenic refrigeration problem. For example, according to the analysis reported by Blume (1977), the maximum calibration deviation (between calibrations) that was observed among 26 calibration measurements was 1.6 K, and the rms value of the deviation was 0.7 K. The calibration measurements were made over a 3.5-year period for a 2.65-GHz pulsed noise-injection Dicke radiometer (Fig. 6.18).

Satellite-borne radiometer systems use a third type of cold-calibration source, namely, outer space. When the antenna (or an auxiliary antenna) is pointed at cosmic space, it observes a brightness temperature of 2.7 K.

A fourth type of calibration noise source may be added to the above list, namely, the COLDFET circuit mentioned earlier in Section 6-10.1.

6-16.2 Effects of Impedance Mismatches

Throughout the foregoing discussion it was assumed that every RF component and transmission line contained in the radiometer front end was perfectly matched to whatever it was connected to. In other words, no reflections due to impedance mismatches existed. In practice, it may be possible to reduce reflections to small levels through the use of impedance-matching techniques, but they cannot always be eliminated altogether.

The effects of impedance mismatches on the radiometer measurement accuracy may be divided into two groups: (1) mismatches at points beyond the receiver input (Fig. 6.28) and (2) mismatches between the antenna (or calibration source) and the receiver input. For a reflection-free radiometer, the output indication I_{out} is linearly related to the input noise temperature T_{IN}, which represents the net power delivered to the receiver due to noise power supplied by the antenna (or calibration source) and the line in between. That is,

$$I_{out} = a_1 T_{IN} + b_1, \qquad (6.114)$$

where a_1 and b_1 are constants. Mismatched components give rise to reflection coefficients that end up modifying the values of a_1 and b_1. As long as the magnitudes and phases of these reflection coefficients remain constant, and as long as the noise temperatures of the components remain constant, the effects of mismatches may be factored out in the calibration process. The reflection coefficients of components are most susceptible to temperature variations. Therefore, not only is it important to maintain the environmental temperature of the radiometer front end at a constant value, but it is equally important that the absolute value of this temperature be the same (as close as possible) during the radiometer operating mode and during the calibration mode. That is, if a_1 and b_1 are maintained constant, I_{out} will be related accurately to T_{IN}.

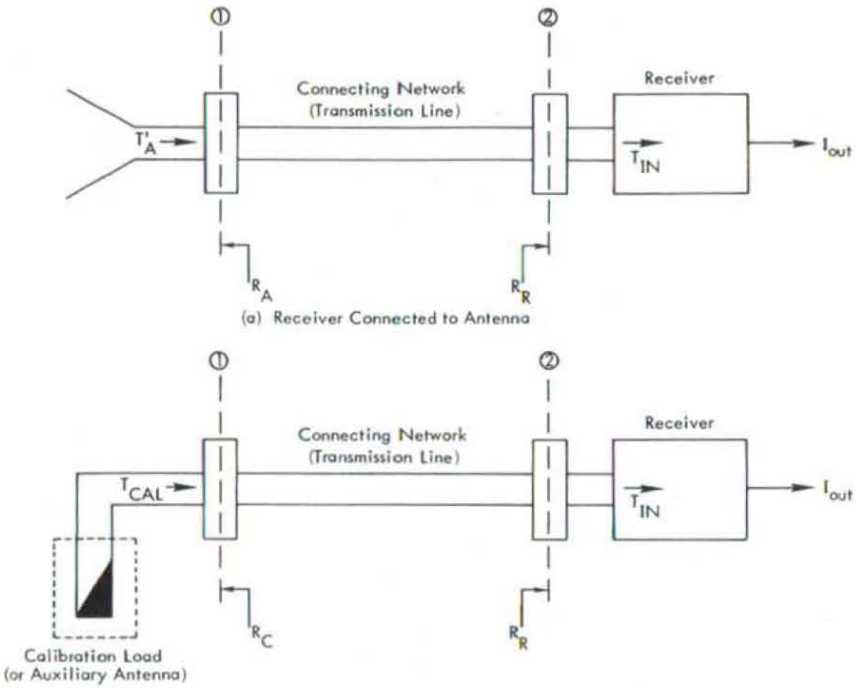

Fig. 6.28 Radiometer receiver connected to (a) antenna and (b) calibration source. The R's are voltage reflection coefficients looking into the indicated ports.

This brings us to the second step, namely, relating T_{IN} to the antenna temperature T'_A or to the noise temperature of the calibration source, T_{CAL}. If the voltage reflection coefficient as seen looking into the antenna, R_A, is equal to the voltage reflection coefficient (in magnitude and phase) as seen looking into the calibration load, R_C, the problem is an easy one. In this case, the calibration constants obtained by calibrating I_{out} against T_{CAL} will be the same as the constants in the relation between I_{out} and T'_A, assuming that the same line used to connect the antenna to the radiometer also is used during calibration. In the general case, however, $R_A \neq R_C$, which means that the relationship between I_{out} and T_{CAL} will not be exactly the same as the relationship between I_{out} and T'_A; therefore, if the calibration equation is used (without corrections) to predict T'_A-values, the predicted values may be in error. The magnitude of the error varies from values of the order of 1 K if $|R_C| < 0.05$ and $|R_A| < 0.05$ to much larger values if the magnitudes of R_C and R_A are larger and very different.

The effect of impedance mismatches may be accounted for by using the following procedure:

1. Develop a relationship between T_{IN} and T_{CAL} (Fig. 6.28) that incorporates reflections. The method is described below and results in a linear form

$$T_{IN} = a_2 T_{CAL} + b_2, \qquad (6.115a)$$

where a_2 and b_2 are constants that are given in terms of measurable quantities.

2. Develop a similar relationship between T_{IN} and T'_A:

$$T_{IN} = a_3 T'_A + b_3. \tag{6.115b}$$

3. Measure I^h_{out} and I^c_{out} corresponding to two known calibration temperatures T^h_{CAL} and T^c_{CAL}, respectively.
4. Using (6.115a), calculate T^h_{IN} and T^c_{IN}, and employ the form of (6.114) to determine the constants a_1 and b_1.
5. With a_1 and b_1 known, use (6.114) and (6.115b) to relate T'_A to I_{out}:

$$T'_A = \frac{I_{out} - a_1 b_3 - b_1}{a_1 a_3}. \tag{6.115c}$$

Steps (1) and (2), which are the keys to the above procedure, basically are the same; each involves the development of a relationship between the noise temperature of a noise generator (antenna or calibration source) and T_{IN}. Figure 6.29 shows a noise generator, with output noise temperature T_G, connected to the radiometer input via a lossy two-port network S. The network S may be a transmission line, a calibration switch, or any passive, linear, time-invariant network. It is characterized by a scattering matrix $\mathbf{S}$ given by

$$\mathbf{S} = \begin{bmatrix} S_{11} & S_{12} \\ S_{21} & S_{22} \end{bmatrix},$$

where the scattering coefficients S_{11} and S_{22} are related to the reflection properties of the network, and S_{12} and S_{21} are related to its transmission properties. Standard techniques for measuring the elements of $\mathbf{S}$ are described in Helszajn (1978). The network S is assumed to have a physical temperature T_0, and the voltage reflection coefficients as seen looking into the radiometer and into the generator are respectively R_R and R_G.

The effect of mismatches on receiver calibration has been treated by Wells et al. (1964), Miller et al. (1967), and Otoshi (1968), among others. Manipulation of Otoshi's expressions to suit the configuration shown in Fig. 6.29 can be shown to lead to the expression below for the noise temperature T_{IN} of the net power delivered to the receiver:

$$T_{IN} = \alpha_m \Upsilon T_G + \alpha_m (1 - \Upsilon) T_0 + (1 - \alpha_m) T_R, \tag{6.116}$$

where $\alpha_m \Upsilon T_G$ = net delivered noise temperature from generator,
$\alpha_m (1 - \Upsilon) T_0$ = net delivered noise temperature generated by lossy network S due to self-emission,
$(1 - \alpha_m) T_R$ = net delivered noise temperature generated by the receiver and then reflected back towards the receiver.

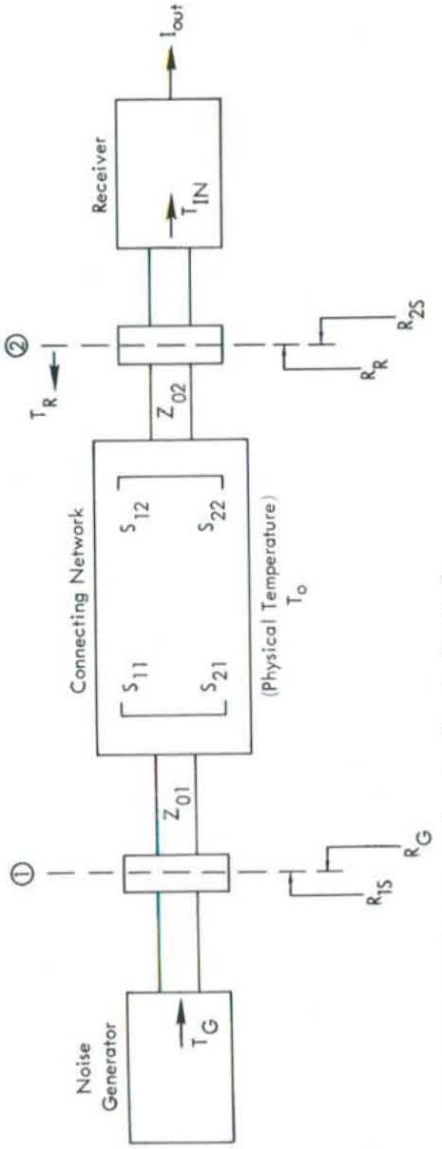

Fig. 6.29 Network representation of radiometer front end.

T_R is the noise temperature generated by the receiver in the direction of the generator, and it is not necessarily equal to the receiver input noise temperature T'_{REC}. Rather, T_R is the noise temperature of the power that would be absorbed by a matched load placed at the radiometer input. In practice, T_R can be either measured (by comparing the receiver output I_{out}, when a matched load is placed at the radiometer input, with the output when a short circuit is placed at the input) or estimated. The quantities α_m and Υ are known as the mismatch loss factor and the transmission factor, respectively, and are given by the expressions

$$\alpha_m = \frac{(1-|R_{2S}|^2)(1-|R_R|^2)}{|1-R_{2S}R_R|^2}, \tag{6.117}$$

$$\Upsilon = \frac{1}{L_S}\left[\frac{(1-|R_G|^2)(1-|S_{11}|^2)}{|1-S_{11}R_G|^2(1-|R_{2S}|^2)}\right], \tag{6.118}$$

where

$$R_{2S} = S_{22} + \frac{S_{21}S_{12}R_G}{1-S_{11}R_G}, \tag{6.119}$$

$$L_S = \frac{Z_{02}}{Z_{01}}\frac{(1-|S_{11}|^2)}{|S_{21}|^2}. \tag{6.120}$$

L_S is the loss factor of network S, and Z_{02} and Z_{01} are the characteristic impedances at ports 2 and 1, respectively. Usually, $Z_{01}=Z_{02}$. To compute α_m and Υ, it is necessary to know the magnitudes and phases of the voltage reflection coefficients R_R and R_G, and of the scattering coefficients of the network S. These quantities can be measured by a network analyzer.

Matched Case

If $Z_{01}=Z_{02}$ and $R_R=R_{2S}=R_G=0$,

$$\alpha_m = 1, \tag{6.121}$$

$$\Upsilon = \frac{1}{L_{S0}} \triangleq |S_{21}|^2, \tag{6.122}$$

where $|S_{21}|^2$ is the power transmission coefficient of the network. That is, L_{S0} is the loss factor under matched conditions, while L_S is the loss factor in the general case. For this matched case, (6.116) becomes

$$T_{IN}(\text{matched}) = \frac{1}{L_{S0}}T_G + \left(1-\frac{1}{L_{S0}}\right)T_0, \tag{6.123}$$

which is the familiar form (given by (6.80)) used for the noise temperature at the output of an attenuator whose input is fed by a matched noise generator.

Transmission-Line Case

If the network S is a uniform transmission line of length l, its scattering coefficients are given by

$$S_{11} = S_{22} = 0, \tag{6.124a}$$

$$S_{12} = S_{21} = e^{-\gamma l}, \tag{6.124b}$$

where $\gamma=\alpha+j\beta$ is the complex propagation factor of the line. Using (6.124), we obtain

$$L_S = e^{2\alpha l}, \tag{6.125}$$

$$\alpha_m = \frac{(1-|R_G|^2L_S^{-2})(1-|R_R|^2)}{|1-R_RR_Ge^{-2\gamma l}|^2}, \tag{6.126}$$

$$\Upsilon = \frac{1}{L_S}\left[\frac{(1-|R_G|^2)}{(1-|R_G|^2L_S^{-2})}\right]. \tag{6.127}$$

Error Bounds

In some cases the magnitudes of R_R and R_G are known, but their phase angles are not. It may be desirable to establish upper and lower bounds for T_{IN} on the basis of the magnitude information only.

The only place where phase angles play a role in the above expressions is in the denominator of α_m. With R_R and R_G defined by

$$R_R \triangleq |R_R|e^{j\phi_R} \tag{6.128a}$$

$$R_G \triangleq |R_G|e^{j\phi_G} \tag{6.128b}$$

we have

$$|1-R_RR_Ge^{-2\gamma l}|^2 = 1+|R_R|^2|R_G|^2L_S^{-2}-2|R_R||R_G|L_S^{-1}\cos\phi, \tag{6.129}$$

where

$$\phi = 2\beta l - \phi_R - \phi_G. \tag{6.130}$$

The following procedure leads to the determination of the upper and lower bounds, $T_{IN}(\max)$ and $T_{IN}(\min)$, with ϕ allowed to take any value in the range

$0 \leqslant \phi \leqslant \pi$:

1. Upon substituting (6.129) into (6.126) and then substituting (6.126) and (6.127) into (6.116), we obtain an expression for T_{IN} as a function of ϕ (as the only unknown quantity).
2. The values of ϕ for which T_{IN} is maximum or minimum may then be found by differentiating T_{IN} with respect to ϕ and equating the result to zero.
3. These values of ϕ then are used in the original expression for T_{IN} to determine $T_{IN}(\max)$ and $T_{IN}(\min)$.

In some cases, the above procedure is unnecessary because the desired values of ϕ for which T_{IN} is maximum or minimum can be deduced from the form of the T_{IN} expression. One such case is when T_R, the receiver noise temperature radiated towards the generator, is equal to T_0, the physical temperature of the transmission line. With $T_R = T_0$, (6.116) simplifies to

$$T_{IN} = T_0 - \alpha_m \Upsilon (T_0 - T_G). \tag{6.131}$$

Since T_G usually is smaller than T_0, $T_{IN} = T_{IN}(\max)$ when $\alpha_m = \alpha_m(\min)$, and vice versa for $T_{IN}(\min)$. With reference to (6.129) and (6.126),

$$\alpha_m(\max) = \alpha_m(\phi = 0), \tag{6.132a}$$

$$\alpha_m(\min) = \alpha_m(\phi = \pi). \tag{6.132b}$$

Comparison of (6.131) with the expression for $T_{IN}(\text{matched})$, given by (6.123), can be shown to lead to the conclusion

$$T_{IN}(\text{matched}) \leqslant T_{IN}(\min) \leqslant T_{IN}(\max),$$

where the equal signs apply when $|R_R| = |R_G| = 0$, or when $T_R = T_G = T_0$. Let us define the mismatch errors

$$\Delta_{min} = T_{IN}(\min) - T_{IN}(\text{matched}) \tag{6.133a}$$

and

$$\Delta_{max} = T_{IN}(\max) - T_{IN}(\text{matched}). \tag{6.133b}$$

If T_{IN} is computed using the expression for $T_{IN}(\text{matched})$, thereby ignoring mismatch errors, the value thus computed will be in error by at least Δ_{min} and by at most Δ_{max}.

To illustrate the significance of mismatch errors that are associated with radiometer calibration, let us consider the following examples.

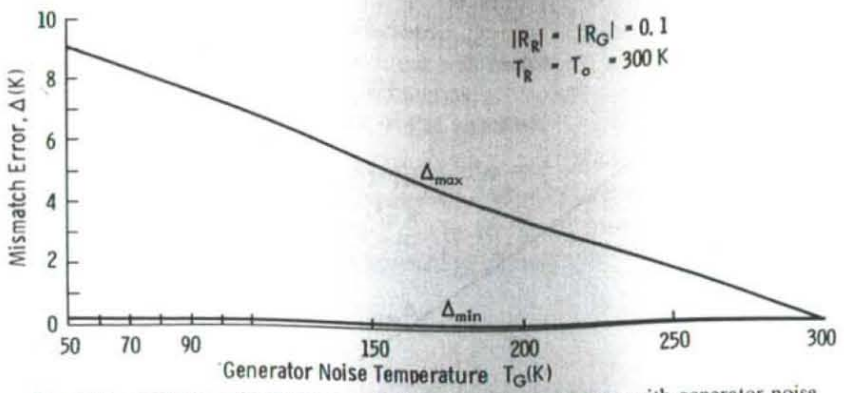

Fig. 6.30 Variation of maximum and minimum mismatch errors with generator noise temperature for $|R_R| = |R_G| = 0.1$.

Example 1:

$$T_R = T_0 = 300 \text{ K},$$
$$|R_R| = |R_G| = 0.1,$$
$$L_S = 1.05 \qquad (= 0.21 \text{ dB}).$$

Example 2: Same as Example 1, except $|R_R| = |R_G| = 0.2$.

Figures 6.30 and 6.31 pertain to Examples 1 and 2, respectively. Each figure shows plots of Δ_{min} and Δ_{max} as a function of T_G. As would be expected, the magnitudes of Δ_{min} and Δ_{max} are larger for Example 2 than for Example 1 due to the larger reflection coefficients. Also, for a given T_G, the difference between Δ_{max} and Δ_{min} is larger for Example 2.

When reflections exist, T_{IN} consists of contributions from three sources of noise energy: (1) the generator at the input, (2) the lossy transmission line, and (3) the receiver noise (T_R) emitted in the direction of the generator. If $R_G = 0$, the last term would not contribute to T_{IN}. In the above examples, $T_R = T_0 = 300$ K. When T_G also is equal to 300 K, the entire system becomes thermally balanced, and therefore, insensitive to reflections. This results in $T_{IN}(\text{matched}) = T_{IN}(\max) = T_{IN}(\min) = 300$ K, or $\Delta_{min} = \Delta_{max} = 0$. The mismatch errors are directly proportional to the difference $T_0 - T_G$, and therefore, they are most important when the generator noise temperature T_G is very different from T_0, as illustrated in Figs. 6.30 and 6.31. This points out an added advantage of radiometer configurations that inject noise into the line connecting the antenna to the receiver (Fig. 6.17) to raise the antenna temperature to the temperature of the reference load, which usually is maintained at the temperature T_0. Thus, use of the noise-injection scheme results in improved measurement precision (by eliminating the effects of system gain fluctuations) as well as improved measurement accuracy. These conclusions hinge on the assumption that $T_R = T_0$. In practice, this is a reasonable assumption because most radiometers employ

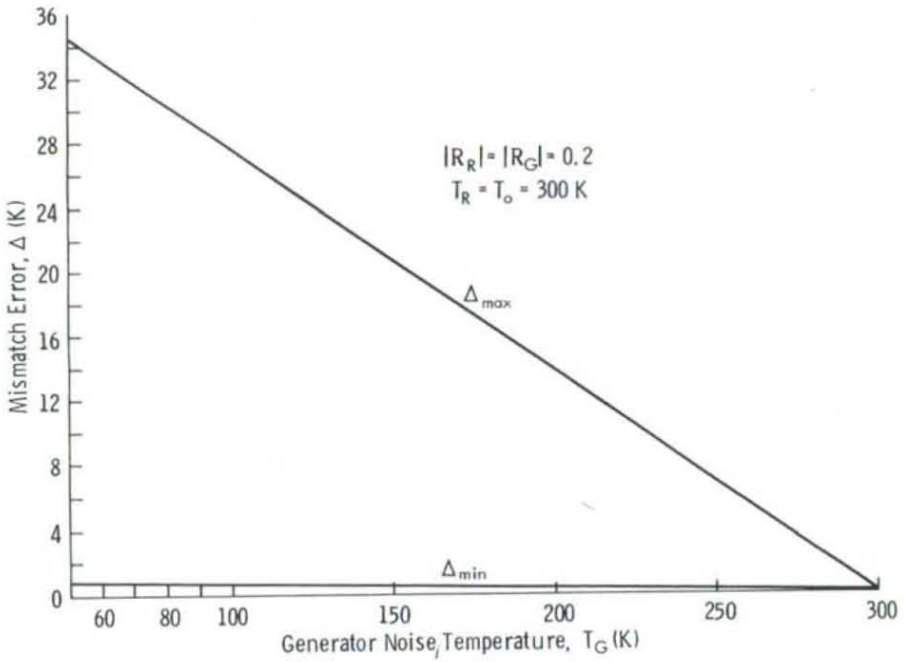

Fig. 6.31 Variation of maximum and minimum mismatch errors with generator noise temperature for $|R_R|=|R_G|=0.2$.

isolators somewhere between the antenna and the receiver. An isolator acts as a low-loss attenuator for propagation in one direction and as a high-loss attenuator for propagation in the opposite direction. When placed with its low-loss propagation direction lying in the direction of the receiver, an isolator attenuates energy emitted by the receiver towards the antenna. Thus, in the direction of the antenna, an isolator exhibits a high loss factor, and therefore emits energy characterized by a noise temperature equal to the isolator's physical temperature, T_0. Hence, when an isolator is used, $T_R = T_0$.

6-16.3 Antenna Calibration

In the preceding material, we discussed calibration methods for transforming the radiometer output indicator to an antenna temperature T_A', where T_A' represents the noise power delivered by the antenna. Now, we shall discuss a second transformation, namely that between T_A' and $\overline{T}_{ML}$, the main-lobe apparent temperature of the scene observed by the antenna. To that end, use will be made of (4.62):

$$T_A' = \eta_l \eta_M \overline{T}_{ML} + \eta_l (1-\eta_M) \overline{T}_{SL} + (1-\eta_l) T_0, \tag{4.62}$$

where η_l = antenna radiation efficiency
$= 1/L_a$, where L_a = antenna loss factor,
η_M = antenna main-beam efficiency,
T_0 = physical temperature of the antenna.

$\overline{T}_{ML}$ and $\overline{T}_{SL}$ were defined as the main-lobe and side-lobe contributions, and are given by (4.56) and (4.59), respectively. With T_A' measured by the radiometer, the objective is the estimate $\overline{T}_{ML}$. In the ideal case of a lossless antenna ($\eta_l = 1$) with a radiation pattern consisting of only one main lobe ($\eta_M = 1$), the above expression reduces to

$$T_A' = \overline{T}_{ML}.$$

In the real case, however, exact determination of $\overline{T}_{ML}$ necessitates that η_l, η_M, and $\overline{T}_{SL}$ be known. Techniques for measuring the antenna parameters η_l and η_M are discussed below, but $\overline{T}_{SL}$ is not a measurable quantity, nor is it a constant, since it depends on the distribution of radiation incident upon the antenna from directions outside the main lobe. As was discussed in Section 4-6.4, the magnitude of the error associated with the estimated value of $\overline{T}_{ML}$ due to the lack of knowledge of $\overline{T}_{SL}$ is a function of η_M only. Therefore, in order to minimize this source of error, whose magnitude is shown in Fig. 4.11 for several values of η_M, it is essential that the radiometer antenna be characterized by a main-beam efficiency that is as close to unity as possible. High main-beam efficiency is achieved by suppressing the side lobes of the radiation pattern, which is accomplished by properly tapering the aperture distribution, as discussed in Chapter 3. A higher main-beam efficiency, however, means a wider main beam, or equivalently, a lower aperture efficiency. The tradeoff between main-beam efficiency η_M and aperture efficiency η_a is shown in Fig. 6.32. For radiometric remote sensing, this is equivalent to a tradeoff between radiometric resolution and angular (or spatial) resolution.

η_M and η_l were defined in Chapter 3 as

$$\eta_M = \frac{\iint_{\text{main lobe}} F_n(\theta,\phi)\, d\Omega}{\iint_{4\pi} F_n(\theta,\phi)\, d\Omega}, \tag{6.134}$$

$$\eta_l = \frac{G_0}{D_0} = \frac{4\pi G_0}{\iint_{4\pi} F_n(\theta,\phi)\, d\Omega}, \tag{6.135}$$

where $F_n(\theta,\phi)$ = normalized radiation pattern,
G_0 = maximum power gain,
D_0 = maximum directivity.

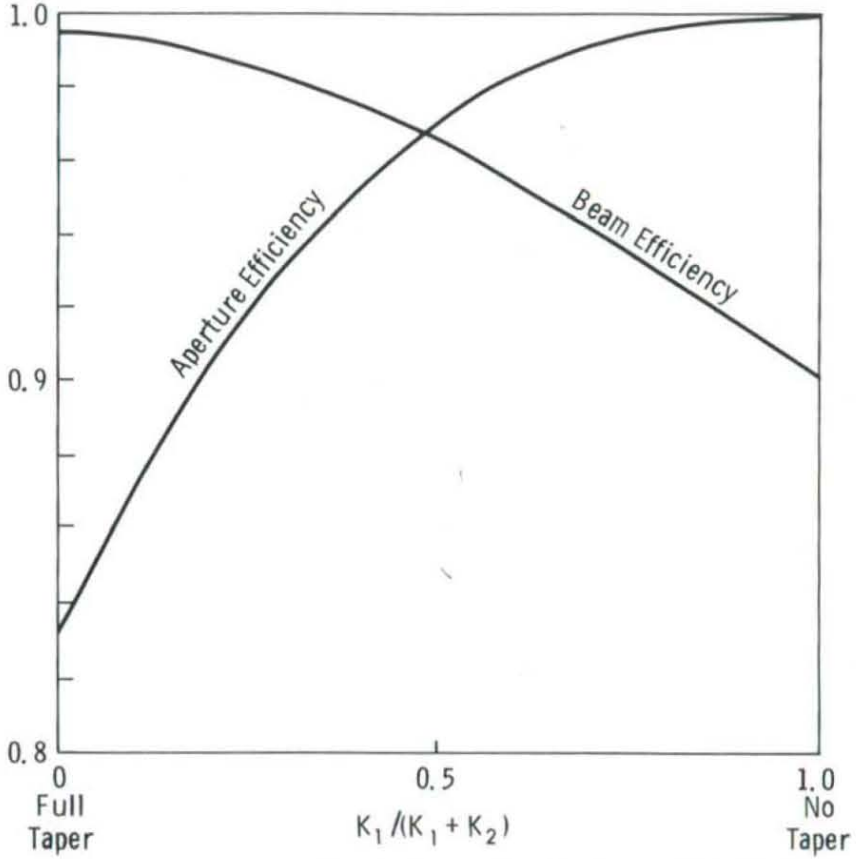

Fig. 6.32 Beam and aperture efficiencies for a one-dimensional aperture as a function of taper (after Nash, © 1964 IEEE). The aperture distribution is $E_a(x_a)=K_1+K_2(1-x_1^2)$, where $x_1=2x_a/l$ and l is the aperture length.

If the radiation pattern $F_n(\theta,\phi)$ is accurately known for all directions (θ,ϕ) over 4π solid angle, the determination of η_M becomes a straightforward task. Similarly, η_l also can be determined provided G_0 is known. In practice, G_0 is one of the easiest antenna parameters to measure. The problem with the above method is one of accuracy and cost; if the denominator in (6.134) and (6.135) is in error by only 1 percent, it is liable to result in an error of several kelvins in the estimated value of $\overline{T}_{ML}$, and in order to have good accuracy it is necessary to measure the complete two-dimensional variation of $F_n(\theta,\phi)$ with a measurement sensitivity of at least -60 dB relative to the peak value of $F_n(\theta,\phi)$, which is likely to be a costly operation. Alternative, and perhaps more accurate, methods developed for measuring η_l are described next. Once η_l has been determined, η_M can be easily computed from

$$\eta_M=\frac{\eta_l}{4\pi G_0}\iint_{\text{main lobe}}F_n(\theta,\phi)\,d\Omega. \tag{6.136}$$

As was mentioned earlier, G_0 is an easily measurable quantity, and so is $F_n(\theta,\phi)$ over the narrow angular range covered by the mainlobe. In some cases, it is difficult to define exactly the extent of the main lobe, and so η_M is quoted as the main-beam efficiency for a certain angular range (such as within two half-power beamwidths of the main-beam center) or for a range of $F_n(\theta,\phi)$ relative to the maximum (such as down to the -20-dB level).

6-16.4 Cryoload Technique

The aperture of the antenna shown in Fig. 6.33 is placed directly over a box containing microwave-absorbing material. The porous absorbing material is saturated with liquid nitrogen as described by Hardy (1973). The absorbing material is characterized by a very small reflection coefficient (Fig. 6.34) and therefore acts like a perfect absorber (emitter) with a brightness temperature equal to its physical temperature.

With the antenna aperture viewing an essentially constant brightness temperature distribution T_B, (from all directions), the antenna temperature T_A' measured by a microwave radiometer is given by

$$T_A'=\eta_l T_B+(1-\eta_l)T_0, \tag{6.137}$$

where η_l is the radiation efficiency of the antenna and T_0 is its physical

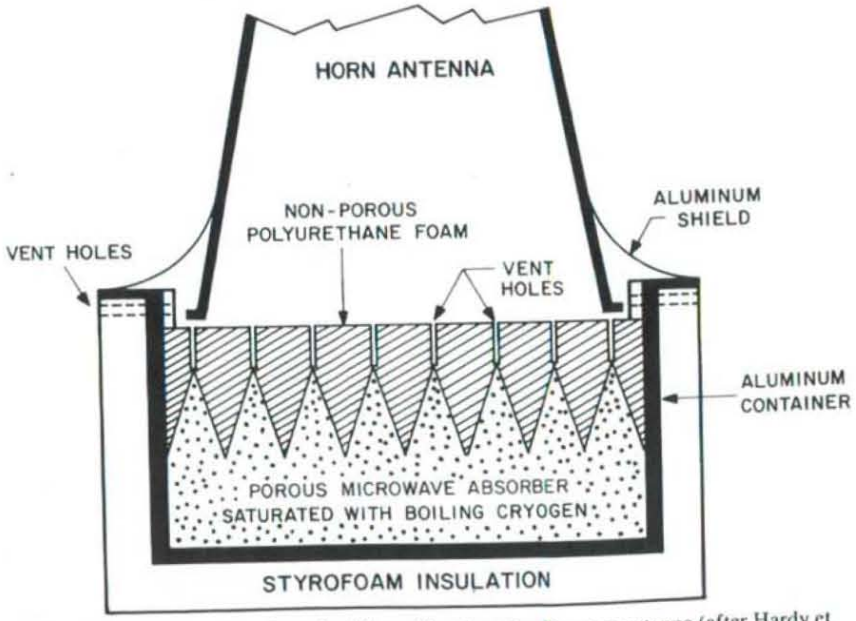

Fig. 6.33 Construction of cryoload for calibration of radiometer antenna (after Hardy et al., © 1974 IEEE).

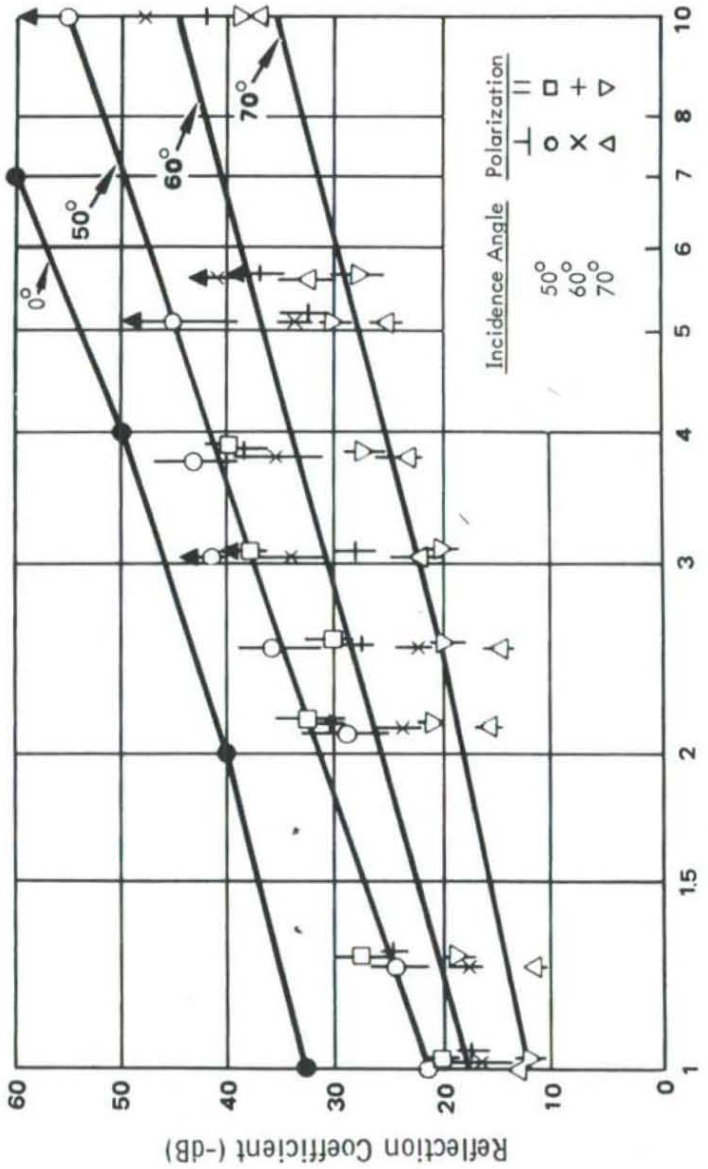

Fig. 6.34 Characteristics of RF absorbers (after Emerson, © 1973 IEEE).

temperature. Solving for η_l, we have

$$\eta_l = \frac{T_0 - T_A'}{T_0 - T_B}, \tag{6.138}$$

where in this case $T_B = 77.36$ K.

The cryoload calibration technique has several attractive features: it is accurate, repeatable, and relatively inexpensive. According to Hardy et al. (1974), who used the cryoload technique to calibrate a 2.65-GHz radiometer, absolute accuracy of about ± 0.1 percent was achieved, and according to Blume (1977) the calibration repeatability had an rms value of 0.7 K and an average deviation of 0.03 K. A slightly modified version of the above technique also was used to calibrate a small-aperture (10-cm × 10-cm) horn antenna at 86.1 GHz (Ulich, 1977).

To date, the use of the cyroload calibration technique has been limited to relatively small antenna apertures (of the order of 1 m per side). For large antennas, the *bucket* technique has proved useful.

6-16.5 Bucket Technique

The antenna shown in Fig. 6.35 is placed inside a large metal bucket whose dimensions are sufficiently large that it can be safely assumed that there is no mutual coupling between the antenna and the bucket. The indicated dimensions are those of the New Mexico State University antenna calibration bucket, which was constructed on a mountain to avoid emissions from the surrounding terrain (Carver, 1975). With the antenna main beam pointed in the zenith direction, the antenna temperature T_A' measured by the radiometer is given by

$$T_A' = \eta_l T_A + (1 - \eta_l) T_0, \tag{6.139}$$

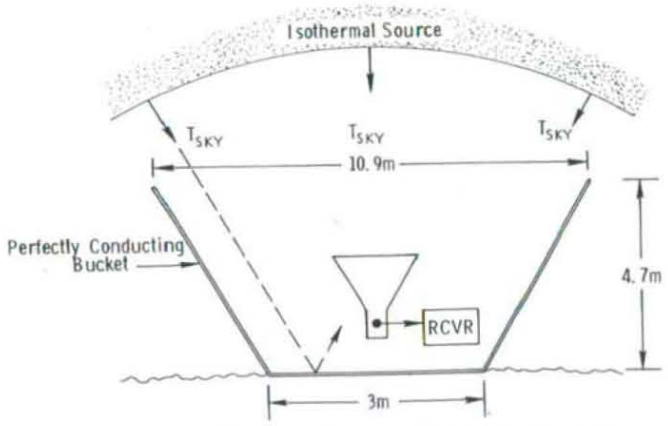

Fig. 6.35 The bucket method for measuring the radiation efficiency of an antenna (after Carver, 1975).

here T_A is the antenna temperature for a lossless antenna and is equal to the tegrated brightness temperature of the sky (see (4.53)),

$$T_A = \frac{\iint_{4\pi} T_{SKY}(\theta,\phi) F_n(\theta,\phi)\, d\Omega}{\iint_{4\pi} F_n(\theta,\phi)\, d\Omega} \tag{6.140}$$

he surface of the perfectly reflecting metal bucket has an emissivity of zero. lence, the radiation received by the antenna is due entirely to atmospheric mission, the major portion of which is received directly from above and the est of which is received through the side lobes after being reflected by ne bucket walls. Assuming that $T_{SKY}(\theta,\phi)$ is approximately constant over the ngular range subtended by the main lobe and the first few significant side obes, (6.140) reduces to

$$T_A = T_{SKY}(\theta = 0°).$$

Using values of meteorological parameters provided by a weather station ocated next to the bucket, $T_{SKY}(\theta=0°)$ could be calculated using the atmospheric-emission formulas given in Chapter 5. With T_A computed, and T_0 and T_A' measured, η_l is determined from (6.139).

6-17 IMAGING CONSIDERATIONS

According to Slater (1980), "the limit of resolution of an optical system is reached when, according to a given criterion, the system can just separate the elements of a well-defined test object, such as a double star in astronomy, the line of a grating in microscopy, and the bars of a bar target in photography." Several standard methods are used for measuring the resolving power of optical systems (Slater, 1980), but no equivalent methods or standard targets have been adopted for microwave systems.

The most frequently used definition for the spatial resolution of a microwave radiometer is given in terms of the *instantaneous field of view* (IFOV) corresponding to the half-power beamwidths. The IFOV defines the area on the ground covered by the antenna main beam. For the configuration shown in Fig. 6.36, the spatial resolutions Δx and Δy are given by

$$\Delta x = \beta_x h, \tag{6.141a}$$

$$\Delta y = \beta_y h, \tag{6.141b}$$

where h is the height of the antenna platform, and β_x and β_y are the half-power beamwidths in the x- and y-directions, respectively. Most microwave radiometric systems use antennas with circularly symmetric patterns, i.e., $\beta_x = \beta_y \triangleq \beta$.

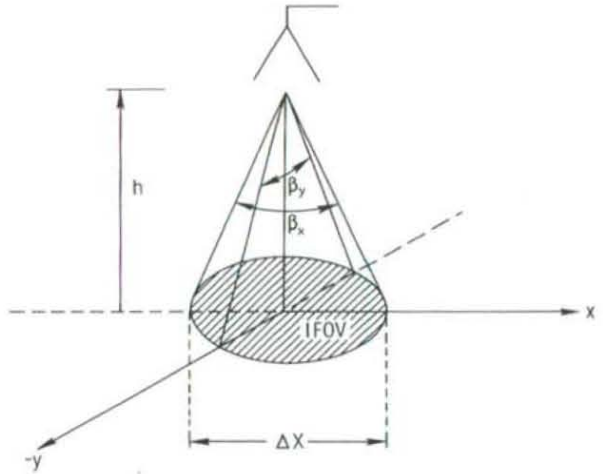

Fig. 6.36 The Instantaneous Field of View (IFOV) for a nadir-pointing antenna with beamwidths β_x and β_y. The antenna platform is at a height h above the ground.

As was discussed in Chapter 3,

$$\beta = k\frac{\lambda}{l}, \qquad \text{radians}, \tag{6.142}$$

where l is the length (and width) of a square aperture or the diameter of a circular aperture, and k is a constant for a given antenna configuration. Usually k is between 0.88 (for a uniformly illuminated aperture) and about 2 (for steeply tapered illuminations) (see Tables 3.1 and 3.2); for calculation purposes, a value of $k=1.5$ is appropriate for antennas with high main-beam efficiency.

6-17.1 Scanning Configurations

Radiometric imaging of a scene of interest is accomplished by scanning the main beam of the antenna; for a moving platform, scanning in the cross-track dimension is sufficient to produce an image. Both mechanical and electronic (beam-steering) scanning techniques are used in microwave radiometry. In mechanical scanning, the direction of the antenna beam is changed by mechanical rotation or angular movement of the radiating aperture of the antenna system. Examples are shown in Fig. 6.37; they include (a) the simple configuration in which the entire antenna structure is made to scan in angle, (b) a second configuration where scanning is achieved by rotating a reflector (mirror) back and forth while maintaining the antenna in a fixed position, and (c) a parabolic torus configuration consisting of a fixed reflector and a spun feed.

Phased-array antennas are used to steer the direction of the antenna beam electronically, without the involvement of mechanical motion in the scanning

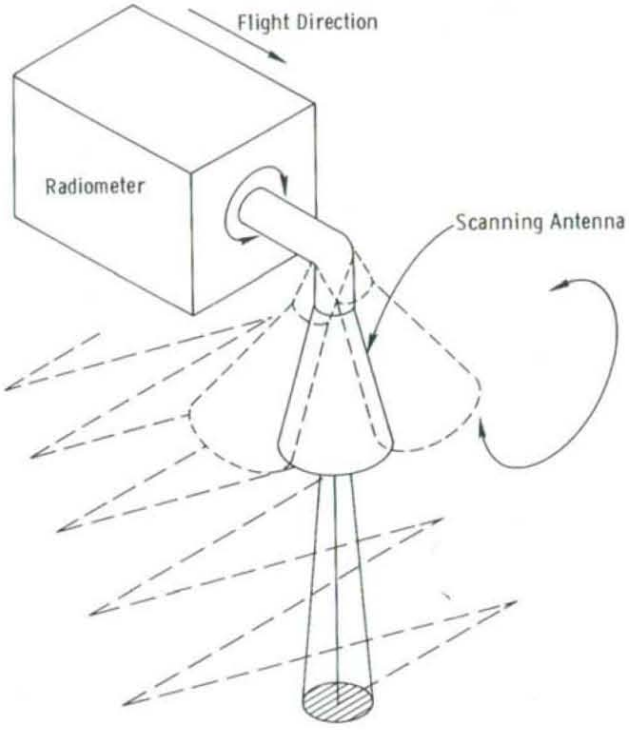

(a)

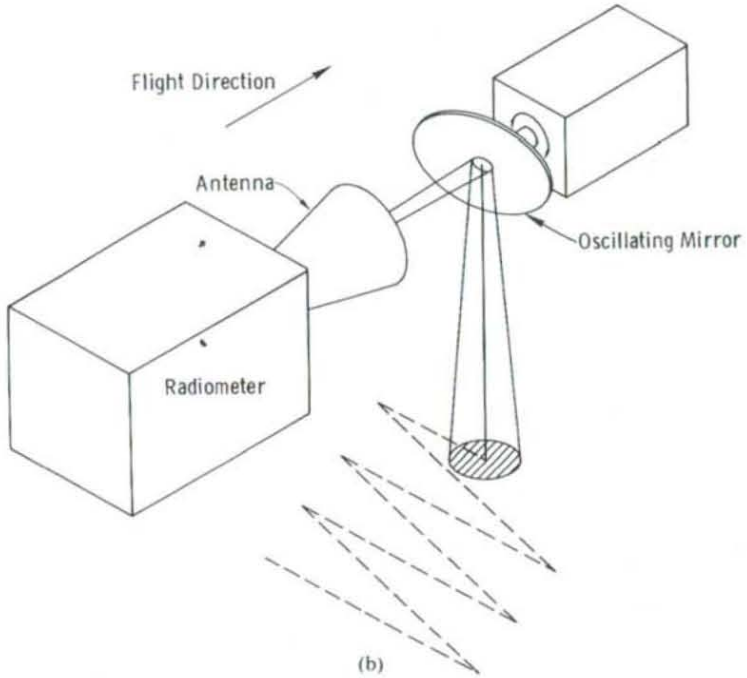

(b)

Fig. 6.37 Mechanical scanning configurations: (a) scanning antenna; (b) fixed antenna and oscillating reflector; (c) fixed parabolic reflector and oscillating antenna feed.

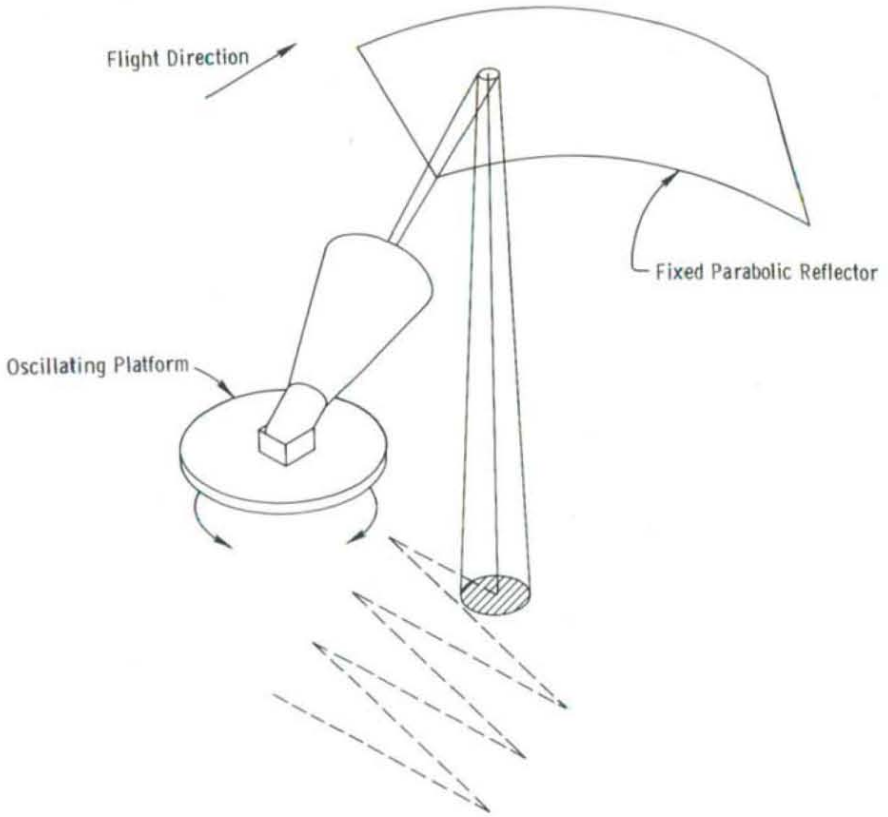

(c)

Fig. 6.37 (*continued*)

process (see Section 3.20). If the antenna is to scan in only one direction, it is sufficient to control the relative phase in one dimension, as illustrated in Fig. 6.38. Another advantage over mechanically scanned antennas is the high scanning-speed capability of phased arrays. Electronic beam steering has some drawbacks, however: phased arrays are more complex, more expensive, heavier and lossier than single-antenna structures of comparable size. The highe antenna losses of phased arrays are due to the phase shifters that are used t control the phase of each individual feed line. Usually ferrite or *PIN* diod phase shifters are used.

Among the scanning microwave radiometer systems that have been flow on the Nimbus satellite series, the 19.35-GHz (Nimbus 5) and 37-GHz (Nimbu 6) electrically scanning microwave radiometers (ESMRs) employed phase array antennas, while the Nimbus 6 scanning microwave spectrometer (SCAM and the Nimbus 7 scanning multichannel microwave radiometer (SMMI employed mechanically scanned antenna configurations.

Figure 6.39 illustrates the two most commonly used viewing configur tions. In the first configuration (Fig. 6.39(a)) the antenna beam scans in

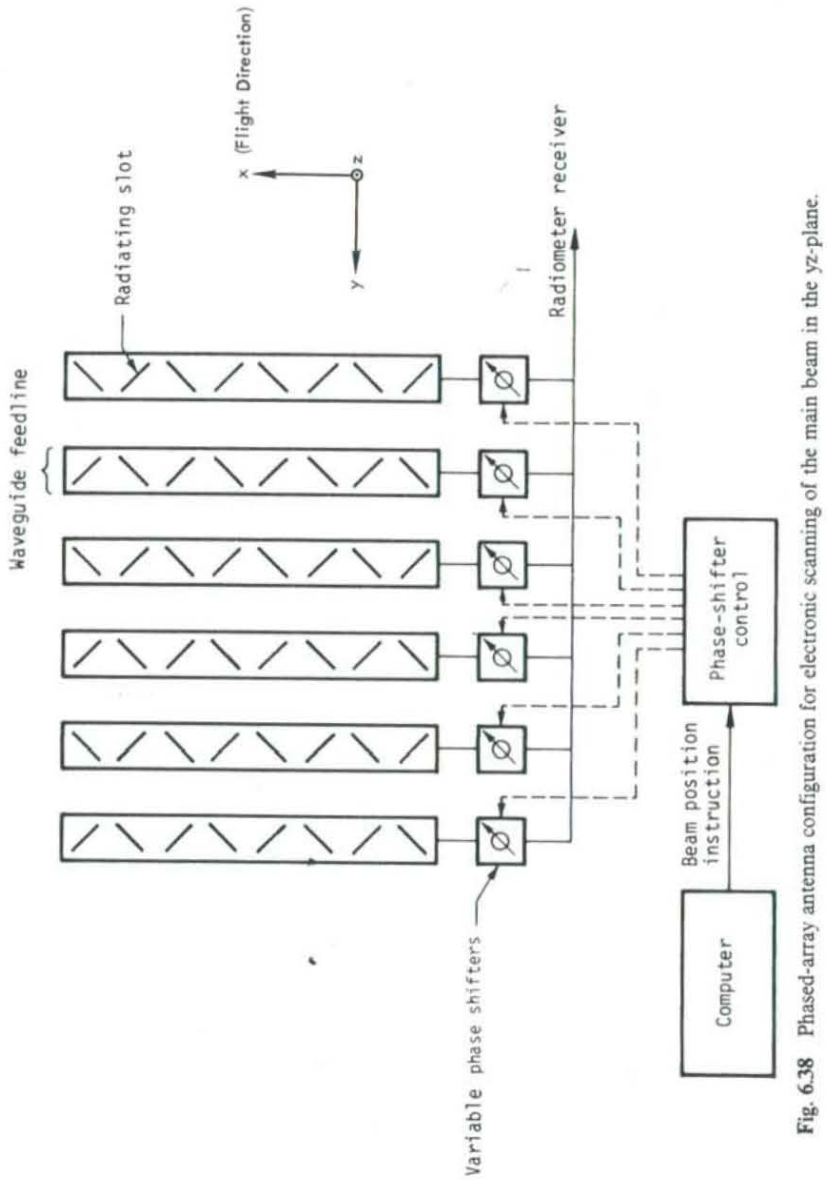

Fig. 6.38 Phased-array antenna configuration for electronic scanning of the main beam in the yz-plane.

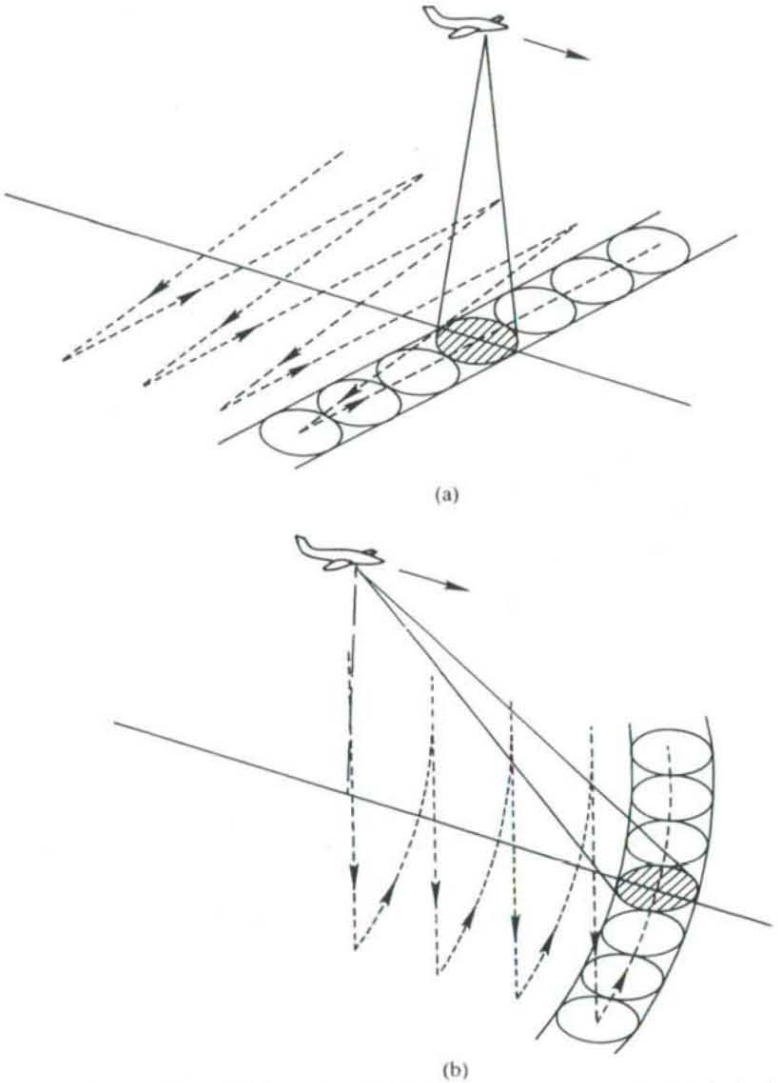

Fig. 6.39 Radiometric imaging by zigzag scanning: (a) cross-track scanning in the plane normal to the direction of flight; (b) conical scanning.

plane that is approximately perpendicular to the direction of motion. The angle of incidence varies between $\theta = 0°$ for the nadir beam and $\theta = \theta_s$ at the edge of the scanline. Also, the shape of the IFOV changes from a circle (for a circular antenna pattern) at nadir to an ellipse with its long axis in the y-direction. For some antenna scanning configurations, the direction of the polarization vector also is a function of the beam position within the scanline.

The major advantage of the viewing configuration shown in Fig. 6.39(b) is that the angle of incidence remains approximately constant as the beam scans

in azimuth along a conical surface ahead of the radiometer platform. An example of a conical scan system is the 37-GHz ESMR, which scans in azimuth $\pm 35°$ about the forward direction at a constant tilt angle of 45° with respect to the direction of motion. With the earth's curvature taken into account, the angle of incidence at the earth's surface varies between 49.6° for the beam position corresponding to an azimuth angle of zero and 50.8° at the edge of the scanline; in other words, the angle of incidence essentially would be constant across the image generated by such a scanning arrangement.

6-17.2 Radiometer Uncertainty Principle

We pointed out in preceding sections that, for a given integration time τ, there is a tradeoff between spectral resolution (the predetection bandwidth B) and the radiometric resolution ΔT. For most radiometer systems, ΔT may be expressed in the general form

$$\Delta T = \frac{M}{\sqrt{B\tau}}, \tag{6.143}$$

where the radiometer figure of merit M is a constant for a given receiver configuration. For a stationary radiometer (with respect to the scene), there are no fundamental constraints imposed on how long τ may be. The situation is different for a moving platform.

To relate the parameters of a scanning system to τ, consider the simple case shown in Fig. 6.40. The platform is at a height h above the ground and is moving with a speed u in the x-direction. The radiometer antenna scans between $+\theta_s$ ($+y$-direction) and $-\theta_s$ ($-y$-direction) in a direction transverse to the flight direction. The forward motion of the platform provides a line-by-line scanning format. The time it takes to travel through one nadir beamwidth in the longitudinal (forward) direction is given by

$$t_1 = \frac{\Delta x}{u} = \frac{\beta h}{u}. \tag{6.144}$$

Ignoring the reset time involved in steering the beam from the end of one scanline ($\theta = \theta_s$) to start a new scanline, and assuming that one transverse scan is completed per beamwidth of forward motion (i.e., in time t_1), the angular scanning rate is

$$\omega = \frac{2\theta_s}{t_1}, \qquad \text{rad s}^{-1}. \tag{6.145}$$

If we assume further that the antenna beamwidth remains constant as the beam is made to scan between $-\theta_s$ and $+\theta_s$ (which is valid only if the scanning is mechanical or if the effective aperture remains constant), then the time it takes to scan through one beamwidth in the transverse direction is

$$\tau_d = \frac{\beta}{\omega} = \frac{t_1 \beta}{2\theta_s}. \tag{6.146}$$

This time τ_d is called the *dwell time* because it is equal to the time that a point on the ground is observed by the antenna beam. Using (6.144), τ_d can be expressed in terms of the spatial resolution Δx:

$$\tau_d = \frac{(\Delta x)^2}{2u\theta_s h}, \tag{6.147}$$

where θ_s is in radians.

Now let us suppose that the radiometer beam crosses over a sharp boundary (in either direction) between two areas of very different emission characteristics. If the radiometer integration time τ is much smaller than τ_d, it will take the radiometer output approximately τ_d seconds to make the transition between the two levels corresponding to the two dissimilar areas. If, on the other hand, $\tau \gg \tau_d$, it will take the radiometer much longer than τ_d seconds to register the change due to the sharp boundary, which is equivalent to having an

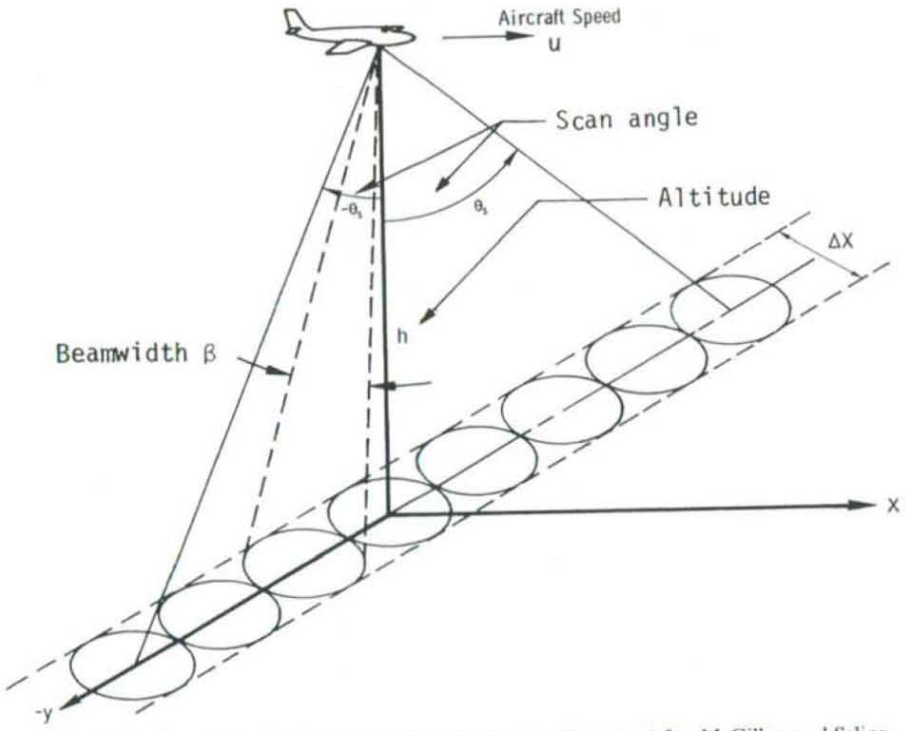

Fig. 6.40 Geometry of airborne scanning microwave radiometer (after McGillem and Seling, © 1963 IEEE).

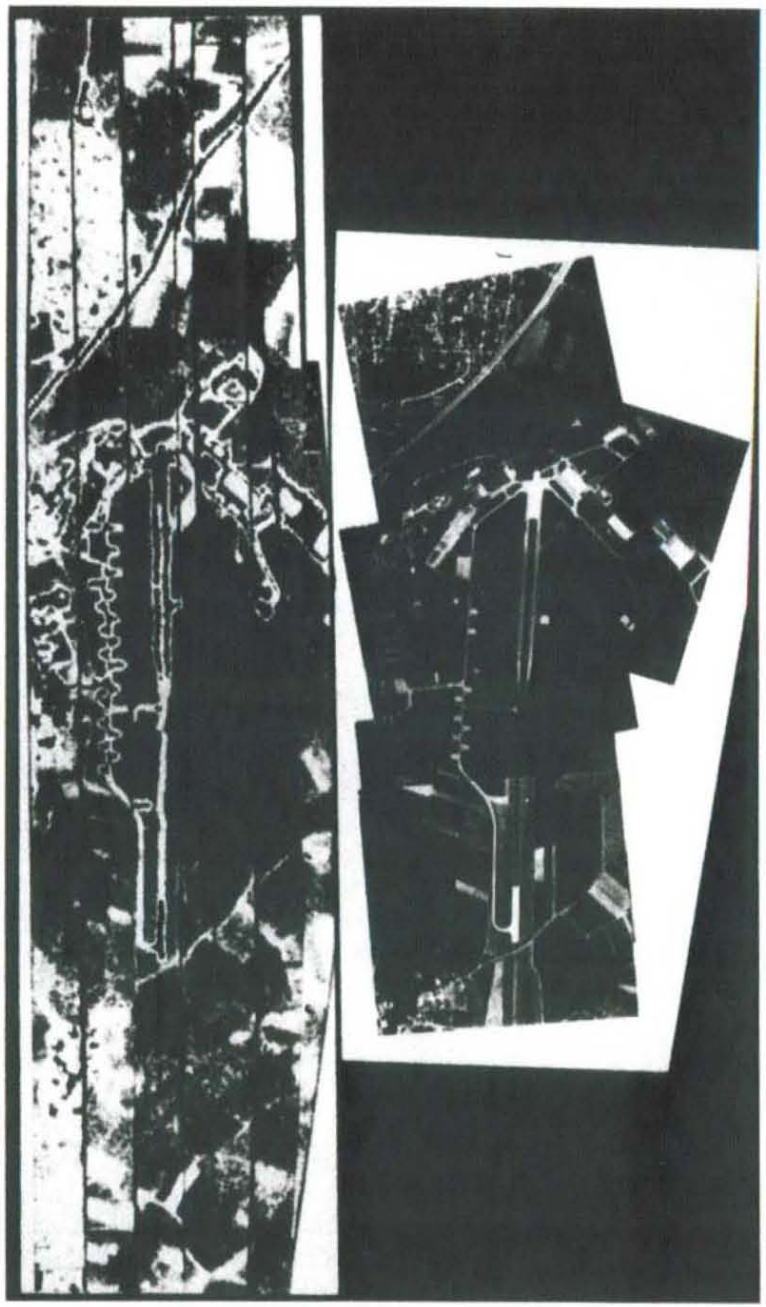

Fig. 6.41 Top image is a 32-GHz radiometric recording of the photomosaic shown below it. The radiometric image was obtained by a low-flying aircraft from a height of 700 m above the ground (photo courtesy of A. Sieber, DFVLR).

effective spatial resolution that is much larger than Δx. Hence, from the standpoint of radiometric resolution it is desirable to have τ as long as possible, and from the standpoint of spatial resolution it is desirable to have $\tau \ll \tau_d$. The optimum choice is dependent upon the nature of the application for which the radiometer is used and on other system parameters. In the general case, however, a compromise solution is to set

$$\tau = \tau_d. \tag{6.148}$$

For $\tau = \tau_d$, inserting (6.147) into (6.143) leads to

$$\Delta T \cdot \Delta x \cdot B^{1/2} = M(2u\theta_s h)^{1/2}. \tag{6.149}$$

The above expression may be termed the *radiometer uncertainty equation*. It states that for given radiometer configuration (i.e., M), flight parameters (h and u), and angular scan range ($2\theta_s$), the product of the radiometric uncertainty ΔT, the spatial uncertainty Δx, and the square root of the spectral uncertainty ($B^{1/2}$) is a constant. Similar expressions may be developed for more complex scanning configurations, but the basic idea remains the same, namely, that the three types of resolutions (uncertainties) are interrelated, and therefore improving one of them is likely to degrade one or both of the other two (unless the flight parameters and/or the scanning configuration is changed).

We close this chapter with an example of a radiometric image consisting of several parallel strips mosaicked together, as shown in the top part of Fig. 6.41. Below the radiometric image is a photograph of the imaged scene, which includes agricultural fields, a residential area, and several streets. The images were recorded by a 32-GHz imaging radiometer flying at a height of 700 m above an area near Oberpfaffenhofen, Federal Republic of Germany.

PROBLEMS

6.1. Consider an antenna connected to a receiver system consisting of a transmission line having a loss factor of 1.5 dB; an RF amplifier with a noise figure of 7 dB and a gain of 20 dB, followed by a mixer-preamplifier with a noise figure of 8 dB and conversion gain of 6 dB; and finally, an IF amplifier with a noise figure of 6 dB and gain of 40 dB. The entire receiver is maintained at an environmental temperature of 290 K.

(a) Find the overall noise figure and effective noise temperature of the receiver system.

(b) Find the overall noise figure and effective noise temperature of the receiver system with RF amplifier and transmission line interchanged.

6.2. The receiver of Problem 6.1(a) is connected to an antenna with a radiation efficiency of 0.9. If the calculated antenna temperature of the scene under observation is $T_A = 100$ K, and if the antenna physical temperature is 290 K, what is the system noise temperature at the antenna terminals?

6.3. In a superheterodyne receiver with local oscillator frequency f_{LO} and IF bandwidth B centered at f_{IF}, the IF output spectrum corresponds to two RF spectral bands centered at f_1 and f_2 where

$$f_1 \pm \frac{B}{2} = f_{LO} - f_{IF} \pm \frac{B}{2},$$

$$f_2 \pm \frac{B}{2} = f_{LO} + f_{IF} \pm \frac{B}{2}.$$

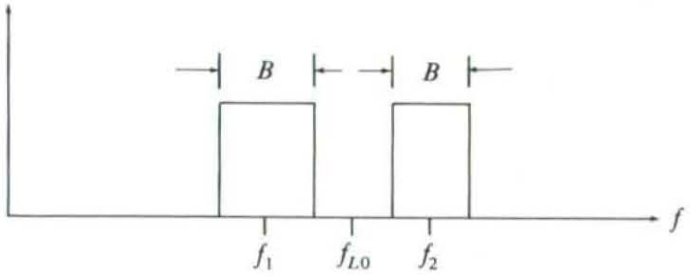

If an RF amplifier is used (ahead of the mixer) whose passband allows only one of the two RF bands to reach the mixer input, the system is referred to as a single-sideband receiver. On the other hand, if the mixer input contains both RF bands (centered at f_1 and f_2), the IF output will include input signals and noise from a total RF bandwidth of $2B$. This latter situation, which is known as double-sideband reception, exists if no RF amplifier (or RF filter) is used or if the RF amplifier passband extends from below $f_1 - B/2$ to above $f_2 + B/2$, thereby amplifying both RF bands.

If F_{SSB} is the single-sideband noise figure of a mixer-preamplifier assembly, show that for the double-sideband receiver, the double-sideband noise figure F_{DSB} of the mixer-preamplifier is given by

$$F_{DSB} = \tfrac{1}{2}(F_{SSB} + 1)$$

and that the corresponding equivalent noise temperatures are related by

$$T_{DSB} = \tfrac{1}{2} T_{SSB}.$$

6.4. Verify the result given by (6.60).

6.5. The pulsed noise-injection radiometer of Fig. 6.18 drives the *PIN* diode with 40-μs pulses at a pulse repetition frequency f_R. The noise diode has an "excess noise ratio" of 23 dB, and the loss factor of the *PIN* diode is 2 dB in the ON state and 60 dB in the OFF state. The directional coupler has a 20-dB coupling factor ($F_c = 100$), and the entire radiometer is enclosed in a chamber maintained at 320 K. What should the range of f_R be in order to maintain the balanced condition over the range $50\ \text{K} \leq T_A' \leq 300$ K?

6.6. A 1-GHz balanced Dicke radiometer with a 100-MHz bandwidth is to be flown on a satellite at an altitude of 600 km and with an average speed of 7.5 km s^{-1}. The radiometer uses a 10-m-diameter antenna, and the receiver is characterized by $T_{REC}' = 1000$ K and $T_{REF} = T_0 = 300$ K. The radiometer integration time is chosen to be equal to 0.1 of the dwell time of the antenna beam for a point on the ground. If the antenna is fixed so that its main beam is always pointed in the nadir direction, what will ΔT be?

6.7. Suppose the antenna of Problem 6.6 is made to scan between $-20°$ and $+20°$ relative to nadir in the plane orthogonal to the flight direction. What is ΔT?

6.8. Verify that (6.95) leads to (6.96) and (6.97) leads to (6.98).

6.9 Repeat the computations leading to Fig. 6.31 for $L_S = 0.5$ dB and $|R_R| = |R_G| = 0.2$.

References

Batchelor, R. A., J. W. Brooks, and B. F. C. Cooper (1968), Eleven-Centimeter Broadband Correlation Radiometers, *IEEE Trans. Antennas and Prop.*, AP-16, pp. 228–234.

Batelaan, Paul E., Richard M. Goldstein, and Charles T. Stelzried (1974), Improved Noise-Adding Radiometer for Microwave Receivers, NASA Tech. Brief 73-10345, Jet Propulsion Laboratory, Pasadena, California.

Blum, E. J. (1959), Sensibilitè des Radiotelescopes et Rècepteurs à Correlation, *Ann. Astrophys.*, 22, pp. 140–163.

Blume, H. J. C. (1977), Noise Calibration Repeatability of an Airborne Third-Generation Radiometer, *IEEE Trans. Micro. Theory and Tech.*, MTT-25, pp. 852–855.

Cardiasmenos, A. G. (1980), Practical MIC's Ready for Millimeter Receivers, *Micro. Sys. News*, 10, No. 8, pp. 37–51.

Carver, K. R. (1975), Antenna and Radome Loss Measurements for MFMR and PMIS, Phys. Sci. Lab. Tech. Rept. PA00817, New Mexico State University, Las Cruces.

Clark, B. G. (1968), Radio Interferometers of Intermediate Type, *IEEE Trans. Antennas and Prop.*, AP-16, pp. 143–144.

Colvin, R. S. (1961), A Study of Radio Astronomy Receivers, Stanford Elec. Lab., Radio Sci. Lab., Sci. Rept. 18, Stanford, California.

Dicke, R. H. (1946), The Measurement of Thermal Radiation at Microwave Frequencies, *Rev. Sci. Instr.*, 17, pp. 268–275.

Emerson, W. H. (1973), Electromagnetic Wave Absorbers and Anechoic Chambers through the Years, *IEEE Trans. Antennas and Prop.*, AP-21, pp. 484–489.

Evans, G. and C. W. McLeish (1977), *RF Radiometer Handbook*, Artech House, Inc., Dedham, Massachusetts, Appendix A.

Frater, R. H. and D. R. Williams (1981), An Active "Cold" Noise Source, *IEEE Trans. on Micro. Theory and Tech.*, MTT-29, pp. 344–347.

General Electric Space Systems Div. (1973), S-193 Microwave Radiometer/Scatterometer/Altimeter Calibration Data Report, Flight Hardware, 1A, Valley Forge, Pennsylvania.

Goggins, William B. Jr. (1967), A Microwave Feedback Radiometer, *IEEE Trans. on Aerospace and Elec. Sys.*, AES-3, No. 1, pp. 83–90.

Graham, M. H. (1958), Radiometer Circuits, *Proc. IRE*, 46, pp. 1966.

Hach, Johann-Peter (1966), Proposal for a Continuously Calibrated Radiometer, *IEEE Proceedings Letters*, 54, pp. 2015–2016.

Hach, Johann-Peter (1968), A Very Sensitive Airborne Microwave Radiometer Using Two Reference Temperatures, *IEEE Trans. Micro. Theory and Tech.*, MTT-16, 9, pp. 629–636.

Hankins, T. H. (1972), Short-Timescale Structure in Two Pulsars, *Astrophys. J.*, 177, pp. 211–215.

Hardy, W. N. (1973), Precision Temperature Reference for Microwave Radiometry, *IEEE Trans. Micro. Theory and Tech.*, MTT-21, pp. 149–150.

Hardy, W. N., K. W. Gray, and A. W. Love (1974), An S-Band Radiometer Design with High Absolute Precision, *IEEE Trans. Micro. Theory and Tech.*, MTT-22, pp. 382–390.

Held, D. N. (1979), An Approach to Optimal Mixer Design at Millimeter and Submillimeter Wavelengths, *IEEE MTT-S Int. Micro. Symp. Digest*, pp. 25–27.

Helszajn, J. (1978), *Passive and Active Microwave Circuits*, John Wiley and Sons, New York, Chapter 1.

Hersman, M. S. and G. A. Poe (1981), Sensitivity of the Total Power Radiometer with Periodic Absolute Calibration, *IEEE Trans. Micro. Theory and Tech.*, MTT-29, pp. 32–40.

Huguenin, G. R. (1976), Pulsar Observing Techniques, in *Astrophysics*, 12, Part C., M. L. Meeks, ed., Academic Press, New York, Section 4.5.

IEEE (1979), *Standard Test Procedures for Antennas*, IEEE Press, New York.

Kennedy, W. K. (1978), M. W. Semiconductor Solid State Components, *Microwave J.*, 21, No. 11, pp. 66–69.

Kerr, A. R. (1975), Low-Noise Room-Temperature and Cryogenic Mixers for 80–120 GHz, *IEEE Trans. Micro. Theory and Tech.*, MTT-23, pp. 781–787.

Kerr, A. R. (1979), Noise and Loss in Balanced and Subharmonically Pumped Mixers: Part I—Theory, Part II—Application, *IEEE Trans. Micro. Theory and Tech.*, MTT-27, pp. 938–950.

Machin, K. E., M. Ryle, and D. D. Vonberg (1952), The Design of an Equipment for Measuring Small Radio-Frequency Noise Powers, *Proc. IEE* (London), 99, pp. 127–134.

Manchester, R. N. (1973), The Properties of Pulsars, *Proc. IEEE*, 61, pp. 1205–1211.

McGillem, C. D., and T. V. Seling (1963), Influence of System Parameters on Airborne Microwave Radiometer Design, *IEEE Trans. Military Elec.*, pp. 296–302.

Miller, C. K. S., W. C. Daywitt, and M. G. Arthur (1967), Noise Standards, Measurements, and Receiver Noise Definitions, *Proc. IEEE*, 55, pp. 865–877.

NASA, *Nimbus 5 User's Guide* (1972), The Electrically Scanning Microwave Radiometer (ESMR) Experiment, NASA Goddard Space Flight Center, Greenbelt, Maryland.

NASA, *Nimbus 6 User's Guide* (1975), The Electrically Scanning Microwave Radiometer (ESMR) Experiment, NASA Goddard Space Flight Center, Greenbelt, Maryland.

Nash, R. T. (1964), Beam Efficiency Limitations of Large Antennas, *IEEE Trans. Antennas and Prop.*, AP-12, pp. 918–923.

Nyquist, H. (1928), Thermal Agitation of Electric Charge in Conductors, *Phys. Rev.*, 32, pp. 110–113.

Ohm, E. A., and W. W. Snell (1963), A Radiometer for a Space Communications Receiver, *Bell Sys. Tech. J.*, 42, pp. 2047–2080.

Orhaug, T., and W. Waltman (1962), A Switched Load Radiometer, *Publ. Natl. Radio Astron. Obs.*, 1, pp. 179–204.

Otoshi, T. Y. (1968), The Effect of Mismatched Components on Microwave Noise-Temperature Calibrations, *IEEE Trans. Micro. Theory and Tech.*, MTT-16, pp. 675–686.

Price, R. M. (1976), Radiometers Fundamentals, in *Astrophys., Part B: Radio Telescopes*, M. L. Meeks, ed., Academic Press, New York, Section 3.1.

Seling, Theodore V. (1964), The Application of Automatic Gain Control to Microwave Radiometers, *IEEE Trans. Antennas and Prop.*, AP-12, pp. 636–639.

Slater, P. N. (1980), *Remote Sensing, Optics and Optical Systems*, Addison-Wesley, Reading, Massachusetts, p. 326.

Steinberg, J. L. (1952), Les Rècepteurs de Bruits Radioèlectriques, *Onde Elec.*, 32, pp. 519–526.

Sterzer, F. (1978), GaAs Field Effect Transistors, *Microwave J.*, 21, No. 11, pp. 73–77.

Tiuri, M. G. (1964), Radio Astronomy Receivers, *IEEE Trans. Antennas & Prop.*, AP-12, pp. 930–938. See also Tiuri, M. E. (1966), Radio-Telescope Receivers, in *Radio Astronomy*, J. D. Kraus, ed., McGraw-Hill Book Company, New York, Chapter 7.

Ulich, B. L. (1977), A Radiometric Antenna Gain Calibration Method, *IEEE Trans. Antennas and Prop.*, AP-21, pp. 484–489.

Wells, J. S., W. C. Daywitt, and C. K. S. Miller (1964), Measurement of Effective Temperatures of Microwave Noise Sources, *IEEE Trans. Instr. and Measurement*, IM-13, pp. 17–28.

Wesseling, K. H. (1967), A Single-Sideband, Double-Sideband Interferometer Receiver for Radio Astronomy, *IEEE Trans. Antennas and Prop.*, AP-15, pp. 332–333.

Yaroshenko, V. (1964), Influence of the Fluctuating Factor of Amplification on the Measurement of Weak Noiselike Signals, *Radiotechnica*, 7, pp. 749–751.